To the Graduate Council:

I am submitting a dissertation written by James R. Cox entitled "NMR Studies of Aminoglycoside Antibiotics Bound to An Aminoglycoside Antibiotic 3′-Phosphotransferase". I have examined the final copy of this dissertation for form and content and recommend that it be accepted in partial fulfillment of the requirements for the degree of Doctor of Philosophy, with a major in Biochemistry.

Engin Serpersu

Engin H. Serpersu, Major Professor

We have read this dissertation
and recommend its acceptance:

Elizabeth Howell

Barry D. Bruce

David C. Baker

Accepted for the Council:

Carolyn Minkel

Associate Vice Chancellor and
Dean of The Graduate School

NMR STUDIES OF AMINOGLYCOSIDE ANTIBIOTICS BOUND TO AN AMINOGLYCOSIDE ANTIBIOTIC 3′-PHOSPHOTRANSFERASE

A Dissertation
Presented for the
Doctor of Philosophy
Degree
The University of Tennessee, Knoxville

James Richard Cox
August, 1997

DEDICATION

This dissertation is dedicated to my grandparents

Juanita and Buddy Henderson

who let me use their bathroom as my chemistry lab and took

me fishing when I was a young boy

and

to my parents

Joe and Carol Cox

who gave me a wonderful life and loved me unconditionally

and

to my wife

Amy Lynne Cox

without her love and support I would have never realized my dream

ACKNOWLEDGMENTS

I would like to express my deepest gratitude to my major professor, Dr. Engin H. Serpersu. He always answered my many questions with a smile on his face, which made for an excellent learning atmosphere in the laboratory. I consider him a friend and I feel lucky to have had Dr. Serpersu as my advisor over the last four years. I would also like to thank Drs. Elizabeth Howell, Barry Bruce, and David Baker for serving on my dissertation and preliminary exam committees.

My friends from the lab deserve special recognition. The friendship and special sense of humors displayed by Enrico DiGiammarino, John Lamerdin, Ayca Akal, Mike Mohler, Dr. Kamesh Pappu, and Dr. Baburaj Kunnumal made the lab a special and fun place to work. Amy and I want to especially thank Enrico and Mary DiGiammarino for their friendship.

My friends who were in the Department of Chemistry at Murray State University with Amy and me should also be recognized. Our time together was special on a personal and professional level. I also owe a special thanks to Mrs. Amber Howard, my High School AP chemistry teacher, for making her chemistry class the hardest class I ever had to take.

Finally, I want to thank my family for their love and support. In particular, I want to thank Amy and Murphy for making every day something special.

Abstract

Bacterial resistance to antibiotics is currently at a crisis level and has been declared a public health emergency. The once seemingly formidable array of effective antibiotics is declining, thus making previously treatable infections life-threatening. One of the most alarming examples of antibiotic resistance is that in Gram-positive cocci, which are responsible for a large fraction of hospital-acquired infections. Enterococcal and staphylococcal infections are typically treated through the administration of aminoglycoside antibiotics, which are a class of aminocyclitol antibiotics that bind to the bacterial 30S ribosomal subunit. They interfere with normal protein biosynthesis which ultimately leads to cell death. Bacteria have responded to the evolutionary pressure brought about by the use of these drugs by expressing an array of enzymes which covalently modify aminoglycosides, thereby rendering them inoffensive. These modifying enzymes can be classified as *O*-phosphotransferases (APH), *O*-nucleotidyltransferases, and *N*-acetyltransferases. The 3′-phosphotransferases are widely distributed in pathogenic bacteria, and at least seven different isozymes have been identified.

One particular enterococcal 3′-phosphotransferase, APH(3′)-IIIa, has the broadest substrate specificity of all the isozymes. Recently, this enzyme has been overexpressed and characterized as an ATP-dependent aminoglycoside kinase. A variety of NMR experiments were performed to determine the arrangement and conformation of APH(3′)-IIIa-bound aminoglycosides.

The complete one-dimensional ^1H assignments of various aminoglycosides were made through the use of various homo- and heteronuclear two-dimensional NMR methods. The complete ^1H NMR assignments were necessary for studies to determine the bound conformations of aminoglycosides.

The ^{15}N resonances of butirosin A and ribostamycin were assigned, and the pK_a values of the amino groups of amikacin, butirosin A, and ribostamycin were determined by ^{15}N NMR spectroscopy. The N-3 amino group of butirosin A and amikacin have lowered pK_a values, which are attributed to the (*S*)-4-amino-2-hydroxybutyryl group (AHB) group of the antibiotics, while the N-1 amino group of ribostamycin has a perturbed pK_a (much lower pK_a) which is attributed to charge repulsion with another amino group at N-3.

β,γ-Bidentate CrATP, a stable exchange-inert metal-nucleotide analog, was used as a paramagnetic probe to determine the arrangement of amikacin and butirosin A in their respective Enzyme•CrATP•Antibiotic complexes. The paramagnetic effects of Cr^{3+} on the longitudinal relaxation rates ($1/T_{1p}$) of the ^1H nuclei of amikacin and butirosin A were examined to determine the distances between enzyme-bound CrATP and various protons of these aminoglycoside antibiotics in the ternary APH(3')-IIIa•CrATP•Antibiotic complexes. From these distances, models were constructed that represent possible enzyme-bound arrangements and conformations for these aminoglycosides. These models show that amikacin and butirosin A adopt different arrangements at the active site of APH(3′)-IIIa. The results for butirosin A suggest that the 2,6-diamino-2,6-dideoxy-

D-glucose and D-xylose rings are in a stacking arrangement.

The NMR method of transferred nuclear Overhauser effect spectroscopy (TRNOESY) was used to detect intra- and inter-ring TRNOEs for amikacin, butirosin A and ribostamycin in their respective ternary complexes with APH(3′)-IIIa and ATP. NOE-derived distance restraints were used in energy minimization and dynamics routines to yield enzyme-bound structures for butirosin A and ribostamycin. The results for butirosin A suggest that the 2,6-diamino-2,6-dideoxy-D-glucose and D-xylose rings have restricted motions and are in a stacking arrangement. Two major conformers of enzyme-bound ribostamycin resulted from the energy minimization/molecular dynamics calculations. One of the conformers is similar to the structure of APH(3′)-IIIa-bound butirosin A with the primed ring (ring A) and the double-primed ring (ring C) in a stacking arrangement. The other conformer is similar to the structure of paromomycin bound to ribosomal RNA (rRNA), that represents the A-site of the small ribosomal subunit, where rings A and C are in a bisecting arrangement. The TRNOESY data for amikacin suggest that the 6-amino-6-deoxy-D-glucose ring is flexible when the antibiotic is bound to APH(3′)-IIIa.

This work is significant in that it demonstrates that aminoglycosides can use a similar conformation to bind both protein- and RNA-based targets. Additionally, this work provides insight into the geometrical and electrostatic nature of aminoglycoside antibiotics bound to a modifying enzyme and will provide a basis for the design of inhibitors of APH(3′)-IIIa.

TABLE OF CONTENTS

LIST OF TABLES

LIST OF FIGURES

LIST OF ABBREVIATIONS

Ala	Alanine (A)
ADP	Adenosine 5′-diphosphate
AHB	(*S*)-4-amino-2-hydroxybutyryl
AMBER	Assisted model building and energy refinement
AMP	Adenosine 5′-monophosphate
APH	Aminoglycoside Phosphotransferase
Arg	Arginine (R)
Asn	Asparagine (N)
Asp	Aspartate (D)
ATP	Adenosine 5′-triphosphate
Ax	Axial
cAMP	Cyclic adenosine 5′-monophosphate
cAPK	cAMP-dependent protein kinase
COSY	Correlated spectroscopy
Cdk2	Cyclin-dependent kinase 2
DOS	Deoxystreptamine
DSS	Sodium 2,2-dimethyl-2-silapentane-5-sulfonic acid
DTT	Dithiothreitol
EDTA	Ethylenediaminetetraacetic acid
E_{pot}	Potential energy function

Eq	Equatorial
Erk2	Microtubule-associated protein kinase 2
Gly	Glycine (G)
His	Histidine (H)
HOHAHA	Homonuclear Hartmann-Hahn spectroscopy
HSQC	Homonuclear single quantum coherence
IRK	Human insulin receptor kinase
IPTG	Isopropyl 1-thio-β-D-galactopyranoside
ISPA	Isolated spin pair approximation
Leu	Leucine (L)
LDH	Lactate dehydrogenase
LFSE	Ligand field stabilization energy
MD	Molecular dynamics
Me	Metal
MES	2-(*N*-morpholino)ethanesulfonic acid
NADPH	Nicotinamide adenine dinucleotide phosphate, reduced form
NMR	Nuclear Magnetic Resonance
NOE	Nuclear Overhauser effect
NOESY	Nuclear Overhauser effect spectroscopy
PEP	Phophoenolpyruvate
Phe	Phenylalanine (F)
PK	Pyruvate kinase

PMSF	Phenylmethylsulfonyl fluoride
ppm	Parts per million
rRNA	Ribosomal ribonucleic acid
tRNA	Transfer ribonucleic acid
SDS-PAGE	Sodium dodecyl sulfate-polyacrylamide gel electrophoresis
Ser	Serine (S)
TPPI	Time-proportional phase increment
TRNOE	Transferred nuclear Overhauser effect
TRNOESY	Transferred nuclear Overhauser effect spectroscopy
Tris	Tris(hydroxymethyl)aminoethane

NOMENCLATURE

B	Zero-field splitting parameter
B_0	Static magnetic field
B_1	The radio-frequency magnetic field
b	Bound
δ	Parts per million
ε	Enhancement factor
f	Free
$f(\tau_c)$	Correlation function
p	Normalizing factor
q	Stoichiometry
r	Distance between two nuclei
τ_c	Dipolar correlation time
τ_M	Lifetime of a paramagnetic complex
τ_v	Time constant that modulates B
T	Total
T	Temperature
T_1	Spin-lattice relaxation time
ω	Angular precession frequency
ω_I	Nuclear precession frequency
ω_s	Electron precession frequency

Chapter I

Introduction

In the 1940s and early 1950s, antibiotics such as penicillin, chloramphenicol, tetracycline, and erythromycin, were introduced for the treatment of common microbial infections. Streptomycin, an aminoglycoside antibiotic introduced after penicillin, made a tremendous contribution in saving lives from tuberculosis and serious bacterial infections (Schatz *et al.*, 1944).

In only a few years, staphylococci and Gram-negative organisms resistant to most of the common antibiotics appeared in hospital patients. This was quite surprising to bacterial geneticists because they believed that antibiotic resistance occurring during normal therapeutic usage was unlikely because the mutation frequency to create resistance was low (Davies, 1994). The ability of bacteria to collect and exchange genetic information was unexpected. In fact, the ability of different species to exchange genetic material has enabled bacterial species to gain resistance mechanisms that has already evolved in other species.

Even before penicillin was put into clinical practice, researchers identified a bacterial enzyme that could catalyze the hydrolysis of the β-lactam ring (Abraham & Chain, 1940) and eliminate penicillin's antibacterial activity. It was feared that this enzyme might hamper penicillin therapy. Unfortunately, this has turned out to be the case. Hydrolysis of the β-lactam ring is the most prevalent mechanism for the inactivation of the penicillins.

Neomycin, an aminoglycoside discovered shortly after streptomycin, saw limited use because of its toxicity, even though it is a highly potent drug. In the late 1950s, when resistance to existing antibiotics was discovered in hospital patients, Umezawa and coworkers (Umezawa & Kondo, 1982) discovered kanamycin, an aminoglycoside antibiotic which has fewer toxic side effects. In general, aminoglycosides produce serious side effects such as oto- and nephrotoxicity (Mingeot-Leclercq *et al.*, 1995). Kanamycin was used as an agent for the treatment of infections with resistant staphylococci and streptomycin-resistant tuberculosis. It was later used against infections caused by Gram-negative bacteria. However, due to the extensive use of the antibiotic, kanamycin-resistant strains were isolated in 1965. This led Umezawa (Umezawa *et al.*, 1967) to investigate the biochemical mechanisms behind the modification of aminoglycoside antibiotics. Gentamicin was discovered in 1963 (Weinstein *et al.*, 1963), which led to an increase in the use of aminoglycosides in the treatment of hospital-acquired infections. Gentamicin was found to be active against strains resistant to kanamycin. Subsequently, the appearance in hospitals of resistant strains diminished the efficacy of this antibiotic. Semisynthetic aminoglycosides, most notable amikacin (Kawaguchi *et al.*, 1972), were designed to overcome the problem of resistance. As a result, amikacin is still a clinically useful drug even though some resistant strains do exist (Tolmasky *et al.*, 1988).

The extensive use of antibiotics over many years has put tremendous pressure on bacteria. In turn, they have responded to the evolutionary pressure by

producing a variety of gene products that can lead to the detoxification of these drugs (Chu *et al.*, 1996). The current state of antibiotic resistance seems somewhat bleak. Bacterial resistance to antibiotics is currently at a crisis level and has been declared a public health emergency (Kunin, 1993; Berkleman & Hughes, 1993). As with the cephalosporin and penicillin antibiotics, the widespread use of semisynthetic and naturally occurring aminoglycoside antibiotics over many years has led to the emergence of resistant strains of bacteria (Davies, 1994).

Inactive antibiotics can be produced by three major mechanisms: covalent modification, restricted access to its target, and alteration of the antibiotic target site (Neu, 1992). The best examples of enzymatic modification is the action of β-lactamases and the aminoglycoside-modifying enzymes. Unlike the β-lactams, where hydrolysis of the four-membered ring renders the antibiotics inoffensive, aminoglycoside antibiotics are inactivated by three types of modification. These modifying enzymes can be classified as *O*-phosphotransferases (APH), *O*-nucleotidyltransferases, and *N*-acetyltransferases (Shaw *et al.*, 1993). Each type of modifying enzyme has many isoforms; therefore, as many as 40 different genes involved in microbial resistance to aminoglycoside antibiotics have been identified. It seems that different proteins within the same family of enzymes may show as much as 44% homology. In addition, point mutations in the aminoglycoside resistance genes rarely leads to altered substrate specificities, although a few examples have been reported (Kocabiyik & Perlin, 1992). This is not the case with the β-lactamases, where point mutations in an existing gene frequently produce an

enzyme that can be used to modify substrate specificity and detoxify new β-lactam antibiotics (Bryan & Godfrey, 1991).

The chemical modification of aminoglycoside antibiotics disrupts their function as bactericidal agents. Aminoglycosides enter bacterial cells by moving across the cytoplasmic membrane in response to an internally negative electrical potential (Bryan, 1989). There is not an universally accepted theory for the inhibition of bacterial cell growth by aminoglycosides that can explain all of the reported physiological effects (Davies, 1991). For the most part, aminoglycoside antibiotics exert their toxic effect through the disruption of bacterial protein synthesis (Tanaka, 1982). They inhibit the bacterial 30S ribosome initiation complex formation, release fMet-$tRNA_F$ from the 70S initiation complex, and prevent the dissociation of free ribosomes into 30S and 50S subunits by IF-3. In addition, these drugs can cause codon misreading, interfere with aminoacyl-tRNA binding, and inhibit translocation of peptidyl-tRNA (Davies *et al.*, 1965; Misumi *et al.*, 1978). In addition to disrupting bacterial protein synthesis, aminoglycosides have been implicated in causing cellular membrane damage (Martin & Beveridge, 1986).

Ribosomal RNA (rRNA) plays a vital role in the selection of transfer RNAs (tRNA) and in the formation of peptide bonds by ribosomes (Noller, 1991). The accuracy of translation depends on specific interactions between the tRNA anticodons and the messenger RNA (mRNA) codons. The interaction between codon and anticodon occurs in the decoding region of the 30S ribosomal subunit, which is formed by two short conserved sequences near the 3′ end of the 16S

rRNA. These sequences define a portion of the A and P sites, which contain the aminoacyl-tRNA and peptidyl-tRNA, respectively. Studies have shown that aminoglycoside antibiotics bind to the A site (Purohit & Stern, 1994). Subsequent experiments have shown that specific bases of the rRNA are involved in the interaction with aminoglycosides (Recht *et al.*, 1996). The structures of the aminoglycosides paromomycin (Fourmy *et al.*, 1996) and tobramycin (Jiang *et al.*, 1997), complexed to RNA, have recently been solved by NMR and modeling methods. The models derived from these studies provide insight into how modification of aminoglycosides disrupts their interaction with bacterial rRNA, and are thus detoxified.

Aminoglycosides have historically been used against staphylococcal and enterococcal infections. Both bacterial strains have gained resistance through the production of aminoglycoside-modifying enzymes. Staphylococci and enterococci are intrinsically resistant to low levels of aminoglycosides and β-lactams. However, a combination of both antibiotics results in a synergistic killing of the cells (Moellering, 1991). The dissemination of aminoglycoside resistance in enterococci and staphylococci has seriously affected the use of aminoglycoside/β-lactam synergism as a treatment for these types of infections (Shlaes *et al.*, 1993). This is especially troubling because *Enterococcus faecalis* accounts for 90% and *E. faecium* for 5% of cases around the world of endocarditis and urinary tract, intra-abdominal, wound, and pelvic infections (Neu, 1992). In addition, throughout the entire nation, 25% of enterococcal species possess a high-level of aminoglycoside-

modifying enzymes that confer resistance (Schaberg *et al.*, 1991). Unfortunately, the percentage of resistant isolates is even higher in other countries (Moellering, 1991). *Klebsiella pneumoniae*, which have caused hospital outbreaks of wound infection and septicemia, also contain genes that code for aminoglycoside-modifying enzymes. Another example of bacteria that have obtained aminoglycoside-modifying enzymes is *Serratia marcescens*, which is a common cause of hospital-acquired wound, urinary tract, pulmonary, and bacteremic infections.

Phosphorylation is perhaps the most important and prevalent chemical reaction found in biological systems. Pathogenic bacteria have utilized phosphorylation to detoxify aminoglycoside antibiotics with the expression of five different positional *O*-phosphotransferases. The aminoglycoside 3′-phospho-transferases are widely distributed in pathogenic bacteria, and at least seven different isozymes have been identified (Shaw *et al.*, 1993). These enzymes, found in many pathogenic bacteria, catalyze the phosphorylation of many aminoglycosides at the 3′and/or 5″-OH group and have essentially eliminated the clinical utility of formerly useful aminoglycosides.

One particular enterococcal 3′/5″-phosphotransferase, APH(3′)-IIIa, has the broadest substrate specificity of all the isozymes. Wright and coworkers recently overexpressed and characterized APH(3′)-IIIa as an ATP-dependent aminoglycoside kinase (McKay *et al.*, 1994). APH(3′)-IIIa can exist as a monomer of 264 amino acids (31 kDa) or a dimer of 528 amino acids (62 kDa). Both forms are catalytically indistinguishable and show K_m values in the low micromolar range and k_{cat} values of

1-4 s^{-1} for good substrates such as kanamycin and neomycin.

APH(3′)-IIIa regiospecifically phosphorylates 4,6-disubstituted aminoglycosides such as kanamycin and amikacin at the 3′-OH group of the 6-amino-6-deoxy-D-glucose ring. Lividomycin, a 4,5-disubstituted aminoglycoside, does not have a 3′-OH group, but can be phosphorylated at the 5″-OH group of the ribose ring. Other 4,5-disubstituted aminoglycosides such as butirosin A, ribostamycin, and neomycin B, can be phosphorylated at both the 3′- and 5″-hydroxyl groups (Thompson *et al.*, 1996a). The initial phosphotransfer is favored at the 3′-OH group of butirosin A and at the 5″-OH group of neomycin B.

A wealth of kinetic evidence based on product and dead-end inhibition (McKay & Wright, 1995), along with viscosity and solvent isotope effects (McKay & Wright, 1996), support a Theorell-Chance mechanism for APH(3′)-IIIa. Additionally, positional isotope experiments were consistent with a direct attack of the reactive hydroxyl group of the aminoglycoside on the γ-phosphate of ATP (Thompson *et al.*, 1996b). Therefore, the mechanism of APH(3′)-IIIa involves the initial binding of ATP, a fast step involving the association of the aminoglycoside and the dissociation of phosphorylated product, followed by the slow release of ADP.

The crystal structure of APH(3′)-IIIa (with bound Mg^{2+}-ADP) has recently been determined (Hon *et al.*, 1997). X-ray structures for other 3′-phospho-transferases have not been solved. This demonstrates the need for structural information on APH(3′)-IIIa-bound aminoglycosides. Information on enzyme-

bound antibiotics will complement any X-ray studies and can serve to explain how APH(3′)-IIIa modifies both 4,5- and 4,6-disubstituted aminoglycoside antibiotics and the regioselectivity unique to both types of antibiotics.

The ultimate goal in studying the interactions of aminoglycoside antibiotics with phosphorylating enzymes is to provide a basis for rational drug design to produce enzyme inhibitors. Gaining a knowledge of the geometrical and electrostatic attributes of enzyme-bound substrates is essential in the design of non-aminoglycoside inhibitors, which may be the key to recapturing the effectiveness of aminoglycoside antibiotics.

Structure-based drug design has made a huge leap in the past few years with advances in molecular structure determination and computational resources. Structure-based drug design has its foundation in the design of molecules that interact with biochemical targets whose structures are known. For example, DOCK (Kuntz *et al.*, 1994) is a program which uses spheres complementary to the receptor molecular surface to create a space-filling image of the receptor binding site. Databases of molecules are searched for candidates that complement the structure of the receptor. DOCK has been very successful in finding novel, micromolar inhibitors for several receptors of therapeutic interest (Kuntz *et al.*, 1994). GRID, a program that determines possible interaction sites between probes with various functional group characteristics and a protein surface, was used to find inhibitors of influenza virus replication (von Itzstein *et al.*, 1993).

Recently, drug discovery programs have been developed that are based on

structural characteristics of known ligands. An excellent example is CAVEAT, a set of programs that originated out of the laboratory of Paul A. Bartlett at the University of California at Berkeley (Lauri & Bartlett, 1994). CAVEAT can be used to generate potential inhibitors of APH(3′)-IIIa if structural information on enzyme-bound aminoglycosides is available.

Chapter II

^{1}H and ^{15}N Spectroscopy of Aminoglycoside Antibiotics

A. Introduction

One of the largest groups of aminoglycoside antibiotics are those in which the aglycone is 2-deoxystreptamine (2-DOS). The structure of these aminocyclitol antibiotics are interesting in that the free cyclitol (2-DOS ring) is optically inactive (Hooper, 1982). Substitution of this ring on one side of the plane of symmetry yields an optically active drug. Generally, these aminoglycosides are 4,5- or 4,6-disubstituted at the 2-DOS ring and are pseudotri-, tetra-, or pentasaccharides (Rinehart & Shield, 1980). The substituents on the 2-DOS ring are numbered 1 to 6 and this ring is labeled the unprimed ring or ring B. The sugar ring, attached by a glycosidic linkage to the 4-position of the 2-DOS ring, is labeled as the primed (′) ring or ring A. The sugar ring, attached by a glycosidic linkage to the 5- or 6-position of the 2-DOS ring, is labeled as the double primed (″) ring or ring C. Some aminocyclitols, such as butirosin A and amikacin, have a 2-DOS ring that is modified at N-1 with a (*S*)-4-amino-2-hydroxybutyryl (AHB) group, which is denoted with a triple prime (‴) or D.

There are approximately 50 different aminoglycosides that have been characterized and tested for antibacterial effects. However, only a fraction of these are substrates for APH(3′)-IIIa. The structures of 4,6- and 4,5-disubstituted

aminoglycosides, that are substrates for APH(3′)-IIIa, are presented in Figure II-1 and II-2, respectively.

The conformations of carbohydrate and carbohydrate-like molecules has become an important question in modern structural biology (Bush, 1992). The structures that carbohydrates adopt in solution and bound to their biological targets have received tremendous attention because they can be a basis for a rational drug design program (Scheffler *et al.*, 1995). Nuclear magnetic resonance (NMR) spectroscopy has emerged as the one of most powerful tools in elucidating structural characteristics of carbohydrates and their complexes (van Halbeek, 1994).

Before aminoglycoside antibiotics can be used in structural studies with APH(3′)-IIIa, the one-dimensional ^{1}H assignments of various aminoglycosides need to be made. Therefore, the proton assignments of kanamycin A, kanamycin B, and butirosin A were made at pH 6.5 through the use of two-dimensional homo- and heteronuclear NMR methods. The proton assignments of kanamycin A and kanamycin B were made previously through the use of 1D NMR methods (at an unspecified pH) (Lemieux & Bock, 1979) and at a high pH value (Eneva & Spassov, 1991). These assignments are not useful for structural studies where a more physiological pH is necessary. Since the aminoglycoside chemical shifts can be pH sensitive, direct comparison with the previous studies is not feasible.

The ^{1}H assignments of other aminoglycosides, such as tobramycin (Szilágyi, 1987), amikacin (Anderson *et al.*, 1988), neomycin B (Reid & Gajjar, 1987), and apramycin (Szilágyi & Pusztahelyi, 1992), have also been made through the use of

two-dimensional NMR methods. A comparison of the results from these studies with our results, demonstrate that even small structural changes in aminoglycosides can lead to much different one-dimensional and two-dimensional NMR spectra.

Since aminoglycoside antibiotics are highly polar and have the possibility to be positively charged, the driving force for complexation between APH(3′)-IIIa and aminoglycosides may be electrostatic. Electrostatic interactions in neamine and kanamycin A phosphorylation has recently been demonstrated with 3′-phosphotransferases, type Ia and IIa (Roestamadji *et al.*, 1995), and suggested in the type IIIa enzyme (McKay *et al.*, 1996). Additionally, studies with tobramycin (3′-deoxykanamycin B) (Dorman *et al.*, 1976) and neomycin B (Botto & Coxon, 1983) revealed that both have one amino group with an unusually low pK_a value. Both of these aminoglycosides have amino groups at N-1 and N-3 of the 2-DOS ring and charge repulsion is believed to account for the low pK_a values of 6.2 (N-1) for tobramycin and 5.7 (N-3) for neomycin B. Therefore, it was necessary to assign the ^{15}N resonances of butirosin A and ribostamycin and to calculate the pK_a values for the amino groups of amikacin, butirosin A, and ribostamycin. The ^{15}N resonances of amikacin, at pH 5.40, have been previously assigned (Schanck *et al.*, 1992). Amikacin, butirosin A, and ribostamycin were chosen for the ^{15}N NMR studies because they were used in structural studies described in later chapters.

B. Experimental Procedures

1. Materials and Sample Preparation

Kanamycin A, kanamycin B, butirosin A, and ribostamycin were obtained as sulfate salts and amikacin as the free base from Sigma Chemical Co. $CaCl_2$ and ATP were also from Sigma. $Ba(OH)_2 \cdot 8H_2O$ was obtained from Johnson-Matthey Electronics and $^{15}NH_4Cl$ (5 atom %) was from Icon Isotopes. ^2H_2O (99.9 and 99.96 atom %) was from MSD Isotopes. Solutions for ^1H NMR spectroscopy were prepared by dissolving the sulfate salts or free base directly in 99.9% ^2H_2O. Sample concentrations were 100 mM (pH 6.5) in all experiments except for NOESY (^1H-^1H nuclear Overhauser and exchange spectroscopy) experiments in which the sample concentrations were 10 mM at pH 6.5.

Solutions for the ^{15}N NMR spectroscopy were prepared by dissolving amikacin directly in 85:15 (v/v) H_2O:^2H_2O to a concentration of 0.8 M. Butirosin A (or ribostamycin) and $Ba(OH)_2 \cdot 8H_2O$ were dissolved in 85:15 (v/v) H_2O:^2H_2O to concentrations of 0.5 M. $BaSO_4$ was removed by centrifugation for 10 min at 5,000*g*.

APH(3′)-IIIa used in these studies was purified as described in the "Experimental Procedures" section of Chapter V. The overexpression system was provided by Dr. Gerard D. Wright of the Department of Biochemistry, McMaster University (Hamilton, Ontario, Canada).

2. NMR Spectroscopy to Make the ^1H NMR Assignments

All NMR spectra were obtained on a wide-bore Bruker AMX 400 MHZ spectrometer at operating at 27 °C. One-dimensional data sets were collected over a spectral width of 6024 Hz with an acquisition time of 2.72 s and a delay of 0.5 s. 16k-32k data points of 8-16 transients were collected. All ^1H chemical shifts were referenced to 2,2-dimethyl-2-sila-pentane-5-sulfonate (DSS).

Two-dimensional ^1H-^1H COSY, ^1H-^1H NOESY, and ^1H-^1H HOHAHA (homonuclear Hartmann-Hahn spectroscopy) (Davis & Bax, 1985; Bax & Davis, 1985) data sets were collected in the phase-sensitive mode using the time-proportional phase increment method (Marion & Wütrich, 1983). The transmitter offset was placed on the H^2HO resonance, which was irradiated during the relaxation delay of 2.0 s to suppress the water signal. 201-423 FIDs of 2k data sets were collected in the HOHAHA experiments. The spectral width was 2809 Hz and 32-112 scans per FID were acquired. The HOHAHA pulse program (Braunschweiler & Ernst, 1983) contained a MLEV 17 spin lock pulse (Bax & Davis, 1985) which was preceded and followed by two 2.5 ms trim pulses. Mixing times of 14.7 ms to 85.8 ms (including trim pulses) were employed. Mixing times of 300, 400, and 500 ms were used in the solution NOESY experiments. The data were zero filled to 1k points (0.5k in NOESY experiments) in t_1 and were multiplied by sine (COSY) and sine^2 (HOHAHA, NOESY) window functions in both dimensions before Fourier transformation. A 2k x (202-248 FIDs) data matrix was acquired for ^1H-^{13}C COSY experiments (Bax, 1983; Wilde & Bolton, 1984). Proton decoupling

was achieved with the WALTZ 16 sequence (Shaka *et al.*, 1983) and 80-96 transients were obtained for each value of t_1. The data were zero filled to 512 points in t_1 and Gaussian multiplication was used in both dimensions.

3. NMR Spectroscopy to Make the ^{15}N NMR Assignments and pK_a Determinations

^1H-decoupled one-dimensional ^{15}N NMR spectra were recorded as a function of pH for amikacin, butirosin A, and ribostamycin at 40.54 MHZ on a Bruker AMX-400 wide bore spectrometer at 27°C using a 5 mm inverse broadband probe. Acquisition parameters included a spectral width of 8196.7 Hz, a 90° pulse width of 17 μs, and an acquisition time of 0.5 s. A total of 32k data points of 2000-8000 FIDs were collected. Before Fourier transformation, 10 Hz line broadening was applied. All ^{15}N chemical shifts were referenced to $^{15}NH_4Cl$. The $^{15}NH_4Cl$ (5% enriched) solution was 1 M prepared in 85:15 (v/v) H_2O:^2H_2O. The pK_a values of the amino groups of amikacin, butirosin A, and ribostamycin were determined by fitting the data to a modified Hill equation (Markley, 1975) using the program P-Fit.

The ^{15}N assignments of butirosin A and ribostamycin, at pH 1.0, were made through the use of two-dimensional ^1H-^1H COSY and ^1H-^{15}N HSQC experiments. The antibiotic samples (0.5 M in 85:15 (v/v) H_2O:^2H_2O) were adjusted to pH 1.0 and used in the two-dimensional experiments. The COSY data sets were collected in the phase-sensitive mode using the time-proportional phase increment method (Marion & Wütrich, 1983). The transmitter offset was placed on the H^2HO resonance, which was irradiated with a low power pulse during a relaxation delay of 1.8 s to suppress

the water signal. A total of 256 FIDs of 2k data were collected with a total of 32 scans per FID with a spectral width of 3205 Hz. The data were zero filled to 1k points in t_1 and multiplied by the sine-window function in both dimensions before Fourier transformation. An $^{1}H-^{15}N$ HSQC experiment was performed at the National NMR Facility at Madison, Wisconsin (NMRFAM) on a Bruker 500 MHZ spectrometer. 16 transients of 1k data points, with 32 increments, were collected over a spectral width of 8333 Hz and 333 Hz in t_2 and t_1, respectively. Before Fourier transformation, the data were multiplied with shifted sine^2 and sine-window functions in t_2 and t_1, respectively.

4. ^{15}N NMR Spectroscopy of Butirosin A Upon Titration with APH(3')-IIIa

Butirosin A was desalted as described above and used to make three different samples for ^{15}N NMR spectroscopy. APH(3')-IIIa was lyophilized and resuspended in 85:15 (v/v) H_2O:^2H_2O to make a 5 mM solution and used to make the following samples. One sample contained 300 mM butirosin A, 2 mM ATP, and 2 mM $CaCl_2$ in 85:15 (v/v) H_2O:^2H_2O. Another sample contained 300 mM butirosin A, 200 μM APH(3')-IIIa, 2 mM ATP, and 2 mM $CaCl_2$ in 85:15 (v/v) H_2O:^2H_2O. The final sample contained 300 mM butirosin A, 1000 μM APH(3')-IIIa, 10 mM ATP, and 10 mM $CaCl_2$ in 85:15 (v/v) H_2O:^2H_2O. The pH of the three samples were 8.15 $\pm$ 0.01 as read directly from the pH meter. ^{1}H-decoupled one-dimensional ^{15}N NMR spectra were recorded (8,000-12,000 scans) as described above.

C. Results and Discussion

1. ^1H Assignments of Kanamycin A, Kanamycin B, and Butirosin A

The primed ring (ring A) is 6-amino-6-deoxy-D-glucose in kanamycin A and 2,6-diamino-2,6-dideoxy-D-glucose in kanamycin B and butirosin A. The double primed ring (ring C) is 3-amino-3-deoxy-D-glucose in kanamycin A and kanamycin B and D-xylose in butirosin A. The unprimed ring (ring B) in kanamycin A and kanamycin B is 2-DOS. The unprimed ring in butirosin A is 2-DOS modified at N-1 with a (*S*)-4-amino-2-hydroxybutyryl (AHB) group, which is denoted with a triple prime (or D).

The complete proton assignments of kanamycin A, kanamycin B, and butirosin A, at pH 6.5, are presented in Tables II-1*, II-2, and II-3, respectively. The assignment strategy used to make the proton assignments of the three antibiotics is described below and demonstrated with two-dimensional NMR spectra of kanamycin A. The ^1H assignments of ribostamycin were made in a similar manner as part of a Threshold Program research project and are not reported in this chapter.

The assignment of the anomeric protons and 2-DOS methylene protons was straightforward based on their chemical shift and/or coupling constants. Previous studies with kanamycin A (Lemieux *et al.*, 1973), and other 4,6-disubstituted aminoglycosides (Anderson *et al.*, 1988), have established that H-1′ resonates

---

*All tables and figures may be found in the appendices.

downfield of H-1″. The anomeric protons of butirosin A can be assigned based on the fact that one of the peaks is a singlet, which suggests that there is negligible coupling of one of the anomeric protons to a vicinal proton. This suggests that this resonance is H-1″ because it is *trans* to H-2″, which can produce a negligible coupling constant (J≈0) when the dihedral angle between the two protons is ≈ 90° (Figure II-3A) (Lemieux & Lown, 1963). There is a *cis* relationship between H-1′ and H-2′ and the observed $^{3}J_{1'-2'}$ value is 3.7 Hz, which is in the range expected for this type of relationship. The methylene protons (H-2) in the 2-DOS ring were assigned based on the knowledge that an equatorial proton in a rigid six-membered ring is deshielded and will resonate 0.1-0.7 ppm downfield of the axial proton (Silverstein & Bassler, 1991). This small difference is due to circulating σ electrons in C-C bonds of the 2-DOS ring. The axial and equatorial protons of C-2 are oriented similarly with respect to C1-C2 and C2-C3, but the equatorial proton is within the deshielding cone of the C1-C6 and C3-C4 bonds (Figure II-3B).

^{1}H-^{1}H COSY and ^{1}H-^{13}C COSY experiments were employed to assign additional proton resonances in kanamycin A. Cross-peaks in a ^{1}H-^{1}H COSY spectrum result from a magnetization transfer between vicinal (3-bond connectivity) or geminal (2-bond connectivity) protons. Cross-peaks in a ^{1}H-^{13}C COSY experiment result from magnetization transfer between a ^{13}C atom and any covalently attached proton. The ^{13}C assignments of kanamycin have been previously assigned at pH 3.6 and 9.6 (Lemieux & Koto, 1973). Since the ^{13}C resonances are sensitive to pH, the relative positions of the resonances may be

slightly different at pH 6.5. Therefore, the previously reported ^{13}C assignments were only used to corroborate proton assignments made through two-dimensional homonuclear ^{1}H NMR experiments described below.

The ^{1}H-^{1}H COSY (Figure II-4) spectrum of kanamycin A allowed assignment of the H-2″, H-3, and H-1 resonances, which were confirmed in the ^{1}H-^{13}C COSY spectrum (Figure II-5). The ^{1}H-^{1}H COSY spectrum also allowed assignment of H-2′, which was ambiguous in the ^{1}H-^{13}C COSY spectrum. The ^{1}H-^{1}H COSY and ^{1}H-^{13}C COSY spectra are quite crowded between 3 and 4 ppm. Also, C-3′ and C-5″ share a common ^{13}C resonance at 50 ppm and C-2′ and C-4′ share a common ^{13}C resonance at 48 ppm in the ^{1}H-^{13}C COSY spectrum. Therefore, HOHAHA spectra of kanamycin A were obtained to avoid ambiguities. HOHAHA experiments allow magnetization diffusion through isotropic mixing, and cross-peaks can be assigned based on their appearance as the mixing time of the experiment is increased (Hicks *et al.*, 1994).

HOHAHA experiments were performed with five different mixing times ranging from 14.7 ms to 77.7 ms. Figure II-6 shows an expanded view of the ^{1}H-^{1}H COSY spectrum and two ^{1}H-^{1}H HOHAHA spectra which resolved the ambiguities and permitted the complete proton assignments to be made. Panel A of this figure shows a portion of the ^{1}H-^{1}H COSY spectrum with the two cross-peaks involving the anomeric protons marked. Panel B of Figure II-6 show an expanded view of a HOHAHA experiment with a mixing time of 45.4 ms. In panel B it is evident that a strong cross peak for H1′-H3′ (bottom row, e) has already formed

while a weaker cross peak for H1′-H4′ (bottom row, f) is barely visible with the 45.4 ms mixing time. Assignment of H-3′ in this experiment clears up the ambiguity between H-3′ and H-5″ in the ^{1}H- ^{13}C COSY experiment. In panel C (61.6 ms mixing time), additional cross-peaks are visible. The cross-peak labeled i (bottom row) was assigned to H1′-H5′ because it is more fully formed. The remaining two cross-peaks (bottom row, j) were assigned to H1′-H6′. The H1′-H6′ cross-peaks at 3.10 ppm were more fully formed in the HOHAHA experiment with a mixing time of 77.7 ms. The same strategy was employed to assign the protons of the 2-DOS ring and ring C of kanamycin A, as well as the protons of the other two antibiotics.

Two-dimensional ^{1}H-^{1}H NOESY spectra were useful in confirming the proton assignments, especially in the 2-DOS ring. Strong NOEs across the glycosidic bonds provided key landmarks on this ring which aided in the interpretation of the HOHAHA experiments, where the magnetization can diffuse both ways around the cyclitol ring. In a NOESY experiment, a cross-peak is observed for a proton pair when the two protons are approximately 4 Å away from each other, either in a through-bond or through-space relationship.

The results from NOESY experiments can yield qualitative or quantitative information about the conformation of molecule. The results from the NOESY studies with kanamycin A and kanamycin B suggest that rings A, B, and C adopt the chair conformations presented in Figure II-1. Besides NOEs across the α-glycosidic bonds (H1′-H4 and H1″-H6), no inter-ring NOEs were observed in the

kanamycins. The results from the NOESY experiments with butirosin A also suggest that ring A and B adopt the chair conformations presented in Figure II-2. In butirosin A, NOE cross peaks were detected between H-1′ and H-4 across the α-glycosidic linkage and between H-1″ and H-5 across the β-glycosidic linkage. A NOE was also observed between H-1 of ring B and H-2‴ of the AHB chain. The most interesting observation was the detection of a strong NOE cross-peak between H-5′ and H-5″. This suggests that, in solution, the xylose ring faces the 2,6-diamino-2,6-dideoxy-D-glucose ring to bring these protons near each other.

2. ^{15}N NMR Studies of Amikacin, Butirosin A, and Ribostamycin

The ^{15}N resonances for amikacin at pH 5.40 have been previously assigned (Schanck *et al.*, 1992) and the ^{15}N assignments of butirosin A and ribostamycin were made in this study at pH 1.0 where the ammonium protons were easily visible in the ^{1}H NMR spectrum of the aminoglycosides. The ^{1}H-^{1}H COSY experiment allowed the assignment of amine protons based on connectivity with vicinal carbon-bound protons. ^{1}H-^{15}N HSQC (Heteronuclear Single Quantum Coherence) experiments allowed the ^{15}N assignments to be made based on connectivity of the nitrogen-bound protons assigned in the COSY experiment. The ^{15}N assignments of butirosin A, at pH 5.90, and ribostamycin, at pH 6.30, are given in Table II-4. The reporting of the chemical shifts at these pH values allows a more direct comparison of the previously reported ^{15}N chemical shifts of amikacin (Schanck *et al.*, 1992).

One-dimensional ^{1}H-decoupled ^{15}N NMR spectra of butirosin A (Figure II-7)

and amikacin (Figure II-8) are shown to demonstrate the changes of ^{15}N chemical shifts with pH of a 4,5- and 4,6-disubstituted aminoglycoside. The complete pH dependence of the ^{15}N chemical shifts of butirosin A and amikacin is shown in Figure II-9 and Figure II-10, respectively. A similar curve was generated for ribostamycin. The pK_as calculated from the titration curves are presented in Table II-5. The amide proton at N-1 in amikacin and butirosin A did not titrate over the pH values used in this study.

As seen in Table II-5, the amino groups at N-3 of amikacin and butirosin A have lowered pK_a values, and the amino group at N-1 of ribostamycin has a perturbed pK_a, but not to the extent of those mentioned above for tobramycin and neomycin B. There have been no previous reports of the pK_a values for the amino groups of aminoglycosides that have the 2-DOS ring modified at N-1 with the AHB chain. The partial positively charged amide nitrogen (N-1) of the AHB chain may serve to slightly perturb the pK_a value of the amino groups at N-3 of amikacin and butirosin A, through a charge repulsion phenomenon. As in a peptide bond, the amide bond in the AHB chain is a partial double bond due to resonance. Therefore, N-1 has a partial positive charge which may affect the protonation state of N-3 (Figure II-3C). On the other hand, the low pK_a value for the amino group at N-1 in ribostamycin is also probably due to charge repulsion with the amino group at N-3.

3. ^{15}N NMR Studies of APH(3′)-IIIa-bound Butirosin A

The one-dimensional ^{15}N NMR spectrum for butirosin A, in the presence of 1 mM APH(3′)-IIIa (pH 8.15), was very similar to the ^{15}N NMR spectrum of butirosin A (pH 8.20) presented in Figure II-7. There was not a significant difference in the ^{15}N chemical shift values in these two one-dimensional spectra. Since ^{15}N chemical shifts are very sensitive to their environment (Blomberg & Rüterjans, 1983), this suggests that the solution pK_a values presented in Table II-5 for butirosin A are not significantly different when the antibiotic is bound to the enzyme.

An interesting observation was made in the ^{15}N NMR experiments for the butirosin A samples that contained APH(3′)-IIIa. The ^{15}N resonances for N-6′ and N-4‴ became somewhat sharper in the presence of the enzyme. This suggests that the amino (ammonium) group at these two positions may interact with the enzyme. In fact, previous studies have shown that the 6′-amino group of the aminoglycosides is important in substrate binding (McKay *et al.*, 1996). Although this was an informative experiment, the calculation of the relaxation rates ($1/T_1$) of the ^{15}N nuclei for free and enzyme-bound antibiotics would provide a more quantitative description of the molecular tumbling of the aminoglycosides (Mason, 1996). However, this would certainly require ^{15}N-labeled aminoglycosides, which are not available at this time.

Chapter III

The Interaction of CrATP and RhATP with APH(3′)-IIIa

A. Introduction

Many enzyme-catalyzed reactions that occur in living systems require ATP as a substrate. Generally, ATP can be hydrolyzed to produce energy to drive a disfavored chemical reaction or it can transfer a phosphate group to another substrate. In the first case, nucleophilic water attacks the electrophilic phosphorus of the γ-phosphoryl group of ATP. In ATP-dependent phosphoryl transfer reactions, dissociative and associative (in-line or adjacent) mechanisms are theoretically possible. The associative mechanisms generally require nucleophilic attack of an oxyanion on the γ-phosphorus. In fact, a wealth of evidence suggests that enzyme-catalyzed phosphorylation reactions follow an in-line associative mechanism, where the nucleophile enters opposite the leaving group (Fersht, 1985).

The electrophilic nature of the γ-phosphate of ATP is an important requirement for ATP-utilizing reactions. ATP coordinates Mg^{2+} in living cells, and it is this complex that participates in the reactions mentioned above. The Mg^{2+} acts as an "electon sink" and enhances the electrophilicity of the γ-phosphorus when it forms a coordination complex with ATP^{4-} (Mildvan, 1979). Mg^{2+} forms a tight complex (K_d = 14 μM) with ATP when it forms a bidentate complex, $MgATP^{2-}$, where a γ- and β-oxygen of ATP are involved in the complex. Chelates of Mg^{2+}

equilibrate very rapidly in solution with exchange rates on the order of 10^3 to 10^5 s^{-1} (Cleland & Mildvan, 1979).

Other metal complexes of ATP are possible where ligand exchange can be very slow. Kinetically inert complexes of ATP were first utilized, around the same time, by the laboratories of Mildvan and Cleland (Foster & Mildvan, 1972; DePamphilis & Cleland, 1973). These first inert complexes of ATP were based on the coordination of Cr^{3+} and Co^{3+}.

Over a thousand complexes involving Cr^{3+} are known. With few exceptions, all of these complexes are six-coordinate and octahedral. Cr^{3+} is a redox-stable metal ion and can form a variety of complexes with nucleotides. Water and/or ammonia ligands usually occupy the coordination positions not taken by the nucleotide. Cr^{3+} is a paramagnetic metal ion with three unpaired electrons in its outer shell (d^3 species). This allows its ATP complexes to act as paramagnetic probes in the active site of ATP-utilizing enzymes. For example, β,γ-bidentate CrATP ($Cr(H_2O)_4ATP$) is very stable and has been very useful in the study of several kinases (Dunaway-Mariano & Cleland, 1980a; Wolkers *et al.*, 1991; Gregory & Serpersu, 1993).

Co^{3+} is a diamagnetic metal ion because it has no unpaired electrons in its outer shell (low-spin d^6 species) and all of its complexes are octahedral. The Co^{3+} ion has a high affinity for N donors such as NH_3, ethylenediaminetetraacetic acid (EDTA), and NCS^- (Cotton *et al.*, 1987). The aqua Co^{3+}-nucleotide complexes are redox unstable, while the tri- and tetraamine complexes can be quite stable. This

makes ATP complexes of Co^{3+} unsuitable mimics of the normal aqua Mg^{2+}-ATP complex.

Since a diamagnetic metal-ATP analog would also be useful as an enzyme active site probe, RhATP complexes were developed (Lin *et al.*, 1984; Lu *et al.*, 1988). Rh^{3+} is a diamagnetic metal ion since it has no unpaired electrons in its outer shell (low-spin d^6 species). Unlike Co^{3+}, Rh^{3+} can form stable aqua ATP complexes and they can be used to study enzymes that use MgATP. The complexes of Rh^{3+} and Cr^{3+}, with ATP, can be β, γ-bidentate or α, β, γ-tridentate, which is similar to the complexes of Mg^{2+} and ATP (Pecoraro *et al.*, 1984). Like CrATP, β, γ-bidentate RhATP has been used to probe the mechanism of various kinases (Lu *et al.*, 1993; Pappu *et al.*, 1994).

The usefulness of complexes in which ATP is coordinated to Cr^{3+}, Co^{3+}, and Rh^{3+} partly relies on the fact that these metal ions are exchange-inert. The rate of water ligand exchange in aqua complexes of these metal ions are on the order of 10^{-4} s^{-1} for Cr^{3+} and Co^{3+}, and 10^{-8} s^{-1} for Rh^{3+} (Mønsted & Mønsted, 1989). All three metal ions form octahedral complexes with ATP. In octahedral complexes, each of the six ligands contributes one electron pair to the coordinate covalent bond. Six pairs of electrons occupy six equivalent hybrid orbitals of the central ion. An *s*, two *d*, and three *p* orbitals of the central ion are available for the construction of the hybrid orbitals. For "outer orbital" complexes, the six pairs of electrons are distributed over sp^3d^2, where the *d* orbitals having the same principal quantum number (n) as the *s* and *p* orbitals are used to make the hybrid orbitals. For "inner

orbital" complexes, the electrons are distributed over d^2sp^3, where the *d* orbitals having a principal quantum number one lower (n-1) than the s and p orbitals are used to make the hybrid orbitals (Gliemann & Schläfer, 1969).

According to Taube (Taube, 1952), outer orbital transition metal complexes are labile, while d^3 (Cr^{3+}) as well as low-spin d^6 (Co^{3+} and Rh^{3+}) inner orbital complexes are inert to ligand exchange.

The ligand field theory provides the best explanation for the behavior of these transition metal complexes. The term "ligand field theory" refers to an entire body of theoretical ideas used to understand the bonding and associated electronic properties of complexes and other compounds formed by transition elements. The bonding in transition metal complexes is fundamentally the same as that for main group elements. All of the usual forms of the valence bond theory that are applied to the main group elements can successfully be applied to transition elements. In general, there is one major thing that sets the study of the electronic structures of transition metal compounds apart from other compounds. The presence of partially filled *d* and *f* orbitals in transition metals leads to experimental observations not possible in other cases: paramagnetism, visible absorption spectra, and irregular variations in thermodynamic and structural properties.

A convenient and accurate way of viewing the relationship between electron configuration and the lability of a complex is a consideration of ligand field stabilization energy (LFSE). Simply stated, LFSE is the "extra" energy provided to a ligand field due to the assymetrical nature of d orbital splittings. As an example,

inert complexes formed from d^3 and low-spin d^6 ions have very high LFSEs (Douglas, 1983).

There are two different mechanisms that account for the substitution of ligands in octahedral complexes. A dissociative mechanism involves the prior departure of the leaving ligand followed by attack of the entering ligand on the resulting five-coordinate species. An associative path involves the attack of the entering ligand, to form a seven-coordinate species, followed by the departure of the leaving ligand. Ligand field calculations suggest that there would be a large loss in LFSE for d^3 and low-spin d^6 complexes in going from six- to either a five- or seven-coordinate species (Douglas, 1983). Therefore, a great deal of stabilization is lost by these complexes while forming the intermediate(s) necessary for ligand exchange. This results in exchange-inert Cr^{3+}- and Rh^{3+}-based ATP complexes.

CrATP (β, γ-bidentate $Cr(H_2O)_4ATP$) and RhATP (β, γ-bidentate $Rh(H_2O)_4ATP$) are exchange-inert metal-ATP analogs used in this research. The electron configuration of CrATP shows that Cr^{3+} has three unpaired electrons; therefore, CrATP is a paramagnetic metal-ATP analog. This makes CrATP a potentially useful probe of the microenvironment present at the active site of ATP-utilizing enzymes. The measurement of relaxation rates of magnetic nuclei is an important part of nuclear magnetic resonance (NMR) spectroscopy. In the presence of paramagnetic species (like CrATP), NMR techniques can be used to derive thermodynamic, structural, and kinetic information about enzyme complexes (Mildvan & Engle, 1972). In fact, the measurement of the longitudinal relaxation

rates ($1/T_1$) of water protons, in the coordination sphere of a paramagnetic ion, allows the calculation of the dissociation constants of binary and ternary complexes of an enzyme with a paramagnetic species, along with the stoichiometry of binding (Mildvan & Cohn, 1963; Mildvan & Cohn, 1966; Reuben & Cohn, 1970). A brief discussion of the concept of relaxation is necessary to define relaxation rates and the experimental parameters derived from these rates.

Any atom that has an odd number of protons or neutrons in its nucleus will have a net magnetic moment and behave as if it was spinning about an axis. Since the nuclei are positively charged, these spinning nuclei act like tiny magnets and can interact with an externally applied magnetic field (B_0). In the absence of a strong external magnetic field, the nuclear spins of magnetic nuclei are oriented randomly. However, when placed in an external magnetic field, a spinning nucleus can orient so that its own tiny magnetic field is aligned with (parallel) or against (antiparallel) the external field. These two possible orientations (spin states) do not have the same energy. The parallel spin state is lower in energy than the antiparallel spin state. The equilibrium alignment can be changed to a population of excited states (spin flip) by applying radio frequency (RF) pulses (B_1) to the sample of nuclei. Neighboring magnetic nuclei in motion (the lattice) can produce oscillating fields with the same frequency (Larmor frequency) and phase as the excited nucleus. Energy may pass from the excited spins to the lattice, so that nuclei can return to the lower spin state and be available for another spin excitation by B_1. This process is called spin-lattice relaxation. It can be defined more rigorously as any process that

returns the spin distribution to its equilibrium state. It is a first-order process with rate constant $1/T_1$, where T_1 is called the spin-lattice or longitudinal relaxation time.

The modulation of the magnetic interaction between a proton and its magnetic environment is due to the periodic interruption by molecular tumbling, a high frequency process for small molecules ($\sim 10^{11}\ s^{-1}$). In aqueous solution, the relaxation rates of water protons and other small molecules are small ($\leq 1\ s^{-1}$). This is because protons are weak magnets and there is a large difference in the tumbling frequency of small molecules and the Larmor precession frequency of protons. This results in an inefficient transfer of magnetic energy between protons and the lattice (Mildvan & Engle, 1972). When small molecules are bound to macromolecules, their interaction with the lattice is affected by the slower tumbling of the large molecule ($\sim 10^{8}\ s^{-1}$) or by the rate of exchange into a different magnetic environment provided by the macromolecule ($\leq 10^{9}\ s^{-1}$). Both of these are processes with lower frequencies closer to that of the precession frequency of protons. Therefore, there is a more efficient transfer of magnetic energy which translates into greater relaxation rates.

Paramagnetic species contain unpaired electrons, which have magnetic moments three orders of magnitude greater than protons. Therefore, an unpaired electron is a much stronger magnet than a proton. Accordingly, paramagnetic species can greatly increase the relaxation rate of coordinated ligands and nearby nuclei. The paramagnetic contribution to the longitudinal relaxation rate is defined in Equation III-1 (Figure 1). In this equation, $(1/T_1)$ is the measured relaxation rate

in the presence of the paramagnetic species and $(1/T_1)_o$ is the measured relaxation rate in the absence of the paramagnetic species.

The relaxation rate of ligands coordinated to paramagnetic ions depends on the rate of exchange of magnetic energy between the ligands and the unpaired electrons. This energy can be exchanged between protons and unpaired electrons through chemical bonds (hyperfine interaction) and through space (dipolar interaction). The dipolar interaction is a sum of three processes: tumbling, ligand exchange, and electron spin relaxation. Relaxation through chemical bonds is modulated by ligand exchange and electron spin relaxation. When the paramagnetic species has a slow electron spin relaxation rate (such as Cr^{3+} species), tumbling dominates the dipolar process in small complexes and determines the relaxation rate. When the tumbling of the paramagnetic species is slowed by immobilization on a macromolecule, slower processes with frequencies closer to the Larmor frequency of the proton can dominate. These processes such as hindered rotation, electron spin relaxation, and ligand exchange can enhance the relaxation rate (Mildvan & Engle, 1972).

The experimentally determined value of the observed enhancement of the relaxation rate of water protons is the enhancement factor (ε^*). The enhancement factor is defined as the ratio of the paramagnetic contribution to the relaxation rate of the ligand in the presence of the macromolecule to that in the absence of the macromolecule (Equation III-2, Figure III-1). The asterisk denotes the presence of a macromolecule and p = [paramagnetic species]/[relaxing ligand]. The normalizing

factor (p) allows the definition of enhancement to be generalized to all ligands under various conditions.

B. Experimental Procedures

1. Materials

Amikacin, butirosin A, and ATP, Dowex-50W cation-exchange resin, Sephadex G-10, NADPH, the dicyclohexylammonium salt of phosphoenolpyruvate (PEP) and 2-(morpholino)ethanesulfonic acid (MES) were obtained from Sigma Chemical Co. Deuterated Tris (Tris-d_{11}) was from Isotec, ^2H_2O (99.9 and 99.96 atom %), deuterium chloride, and sodium deuteroxide (both 99.9 atom %) were from MSD Isotopes. Pyruvate kinase (PK) and lactate dehydrogenase (LDH) were obtained from Boehringer Mannheim. $CrCl_3$ was from Morton Thiokol and $RhCl_3$ was obtained from Aldrich Chemical Co. All other chemicals used were of the highest grade commercially available. The concentration of ATP solutions were determined spectrophotometrically using an extinction coefficient of ε_{260} = 15,400 $M^{-1}cm^{-1}$.

APH(3′)-IIIa used in these studies was provided by Dr. Gerard D. Wright of the Department of Biochemistry, McMaster University (Hamilton, Ontario, Canada). The overexpression and purification of the enzyme has been described previously (McKay *et al.*, 1994).

2. Preparation of CrATP

The preparation of β, γ-bidentate CrATP was carried out as previously described (Dunaway-Mariano & Cleland, 1980b). A 10-mL solution of 20 mM ATP was mixed with 10 mL of a 20 mM $CrCl_3 \bullet 6H_2O$ solution and the pH of the resulting mixture was adjusted to 3.0. The sample was heated at 75-80 °C in a water bath for 10 min and then cooled on ice until the temperature of the solution was 4 °C. A 0.5 x 10 cm column of Dowex-50W cation-exchange resin (2% crosslinking) was treated with 0.1 N HCl and then washed with sufficient deionized H_2O to bring the pH of the effluent to approximately 6.0. The solution was applied to the Dowex column and washed with deionized H_2O to separate CrATP from unreacted ATP and $Cr(H_2O)_6^{3+}$. ATP does not bind to the column, so it washes through with deionized H_2O and the $Cr(H_2O)_6^{3+}$ remains at the top of the resin where it is tightly bound. The $Cr(H_2O)_6^{3+}$ layer was removed with a pasteur pipette and put into a waste beaker and set aside. The bright green band that had migrated one-third the length of the column (with ~150 mL deionized H_2O) was collected with a pasteur pipette and loaded onto another Dowex-50W column (1 x 1 cm). This column had been pretreated with 6 N HCl and then washed with deionized H_2O to bring the effluent back up to pH 6.0. CrATP was eluted from this column with a 0.3 M aniline mobile phase. Fractions of 1 mL were collected and the presence of CrATP was indicated by its characteristic green color. Fractions containing CrATP were pooled and the aniline was removed by extraction with diethyl ether in a separatory funnel. The residual ether was removed by passing a stream of nitrogen gas over the CrATP

solution. The pH of the solution was adjusted 5.0. The concentration of CrATP was determined spectrophotometrically at 427 nm (ε = 30 M^{-1} cm^{-1}), 606 nm (ε = 25 M^{-1} cm^{-1}), and 260 nm (ε = 15,400 M^{-1} cm^{-1}). The values obtained at these wavelengths were averaged to give an initial concentration. The CrATP solution was diluted to give a final concentration of 5-10 mM and stored at 4 °C for a maximum of 5 days.

3. Preparation of RhATP

The first step in RhATP synthesis involves the preparation of $[Rh(H_2O)_6](ClO_4)_3$, which has been described by Jørgensen (1956). $RhCl_3$ (0.30 g) was added to approximately 30 mL of 5 M $HClO_4$ and the mixture was boiled and stirred until the $RhCl_3$ dissolved. A clear dark brown solution resulted which was allowed to cool and the pH was adjusted to 3.0 with KOH. This produced solid $KClO_4$, which was removed upon filtration. The $[Rh(H_2O)_6](ClO_4)_3$ filtrate was collected and brought up to a volume of 50 mL, which made the concentration of $[Rh(H_2O)_6](ClO_4)_3$ approximately 20 mM. The remaining procedures used to make RhATP were adapted from Lin *et al.* (1984). The 50-mL solution of $[Rh(H_2O)_6](ClO_4)_3$ was added to 50 mL of a 20 mM ATP solution and the pH was adjusted to pH 3.0. This sample was heated at 80 °C for 2 min, allowed to cool, and the pH was adjusted to 2.0 with HCl. The sample was loaded on a 1.5 x 40 cm column of Dowex-50W cation exchange resin (4 °C, 2% cross-linking) and RhATP was eluted using deionized H_2O. The RhATP was in a broad yellow band which

was collected in 10 mL fractions. A mixture of β, γ-bidentate RhATP, α, β, γ-tridentate RhATP, and AMP elute from the column in the yellow band. Fractions containing the RhATP isomers and AMP were collected (A_{260} > 0.7) and concentrated under a vacuum (at 25 °C) to a volume of 3 mL. This sample was loaded on a 1.5 x 100 cm G-10 Sephadex gel-filtration column equilibrated at 4 °C. AMP was separated from the RhATP isomers by eluting with 10 mM MES at pH 5.5. Fractions containing the RhATP isomers were identified spectrophotometrically, by the absorption of RhATP in the visible spectrum (ε_{327} = 72 M^{-1} cm^{-1}; ε_{415} = 62 M^{-1} cm^{-1}), combined, and stored at 4 °C (no longer than 10 days). The isomer ratio (bidentate:tridentate) was typically 1:1.

4. Inhibition and Inactivation Studies

The inhibition of APH(3′)-IIIa activity by CrATP and RhATP was measured by following the oxidation of NADH at 340 nm in a coupled enzyme assay system. This was accomplished by coupling the release of ADP (from kanamycin phosphorylation) to a pyruvate kinase/lactate dehydrogenase reaction system. The reaction mixture contained 100 mM KCl, 50 mM MES (pH 6.5), 2 mM PEP (cyclohexylammonium salt), 0.2 mM NADH, 0.25 mM kanamycin A, 90 Units of pyruvate kinase and 55 Units of lactate dehydrogenase. All reaction mixtures contained 30 μg/mL APH(3′)-IIIa and ATP concentrations ranged from 0.03 to 0.50 mM. The CrATP or RhATP concentrations used were 0, 0.05, 0.20, and 0.40 mM and the concentration of $MgCl_2$ in each assay was 1 mM greater than the ATP

concentration. Rate measurements were carried out by monitoring the loss of absorbance at 340 nm on a Beckman DU-70 spectrophotometer at 25 °C. Double-reciprocal plots of velocity vs. [MgATP] (1/v vs. 1/[MgATP]) were obtained with the various CrATP/RhATP concentrations and each line was fit by a linear regression analysis. For both analogs, the slope of each line was plotted against [MeATP] and the $K_{i(MeATP)}$ value was the x-intercept of the resulting line, as determined by linear regression.

The inactivation of APH(3′)-IIIa by CrATP and RhATP was performed at a concentration of 1.5 μg/μL enzyme in a total volume of 300 μL at 37 °C. The incubation reaction mixture also contained 0.5 mM kanamycin A in 50 mM MES (pH 6.5) and CrATP concentrations such as 0.075, 0.100, 0.150, 0.250, 0.500, and 3.00 mM or RhATP concentrations such as 0.031, 0.047, 0.093, 0.467, and 1.16 mM. At different time points between 0 and 235 min (CrATP) or 342 min (RhATP), 5 μL aliquots were removed from the incubation mixture and the remaining enzyme activity was measured. Enzyme activity was measured as described above and the concentration of ATP and $MgCl_2$ in the reaction mixture was 10 and 20 mM, respectively. All of the inactivation data were fitted to a first-order decay by P-Fit software (Biosoft) using the equation $y = Ae^{-kt} + C$ (constant). A pseudo first-order rate constant (k_{obs}) was calculated at each concentration of CrATP/RhATP. A double reciprocal plot ($1/k_{obs}$ vs. 1/[MeATP]) was used to calculate the rates of inactivation (k_{inact}; 1/y-intercept) and $K_{i(MeATP)}$ values (1/x-intercept).

5. Magnetic Resonance Studies of Binary Complexes

All low-field (pulsed) NMR experiments were carried out at 24.3 MHz with a Seimco pulsed NMR instrument using the 180°-τ-90° pulse sequence of Carr and Purcell (Carr & Purcell, 1954) with a delay of $5T_1$ to allow for complete relaxation. Relaxation rates were calculated from the null point ($1/T_1 = \ln 2/\tau_{null}$) where τ_{null} is the delay between the 180° and 90° pulses that yields a null signal (no FID) on the oscilloscope.

The enhancement factor describing the paramagnetic contribution to the longitudinal relaxation rate of water protons is defined in Equation III-2. The observed enhancement of the relaxation rate of water is the weighted average of the enhancements of all complexes of the paramagnetic species ($\varepsilon^* = \Sigma\chi_i\varepsilon_i$), where χ_i is the fraction of the *i*th complex of a paramagnetic species and ε_i is its enhancement.

When one considers a binary complex of CrATP and APH(3′)-IIIa, the observed enhancement (Equation III-3, Figure III-1) depends on the concentration of the free and bound CrATP species and the enhancement of the relaxation rate of water protons due to binary complex formation. In this and subsequent equations, f, b, and T refer to free, bound, and total, respectively. The term ε_f is the enhancement of the relaxation of water protons when water is bound to Cr^{3+} in free CrATP and ε_b is the enhancement of the relaxation of water protons when water is bound to Cr^{3+} in the APH(3′)-IIIa•CrATP binary complex. By definition, ε_f is 1 and $[CrATP]_b = [CrATP]_T - [CrATP]_f$. Based on these substitutions, a mathematical expression for $[CrATP]_f$, and subsequently $[CrATP]_b$, can be derived (Equation III-4,

Figure III-1). If the value of ε_b is measured for the APH(3′)-IIIa•CrATP complex, the values for $[CrATP]_f$ and $[CrATP]_b$ can be derived from Equation III-4, because ε^* can be measured and $[CrATP]_T$ is known. This information can be used to construct a Scatchard plot and determine the K_D for the binary complex and the number of CrATP binding sites on APH(3′)-IIIa. The value of ε_b for the APH(3′)-IIIa•CrATP complex can be determined by titrating CrATP with APH(3′)-IIIa and extrapolating to infinite enzyme concentration (y-intercept) in a plot of $1/\varepsilon^*$ vs. 1/[APH(3′)-IIIa]. In the Scatchard analysis, APH(3′)-IIIa is titrated with CrATP. $[CrATP]_f$ and $[CrATP]_b$ can be calculated using Equation III-4 and knowing $[CrATP]_b = [CrATP]_T - [CrATP]_f$.

In the determination of ε_b, a 83.3 μM CrATP solution in 50 mM MES (pH 6.5) was titrated with APH(3′)-IIIa to give concentrations of 100, 150, 200, 250, and 317 μM enzyme. At each concentration of APH(3′)-IIIa, the enhancement factor (ε^*) was determined and used to construct the double reciprocal plot. In the Scatchard analysis, a 200 μM solution of APH(3′)-IIIa in 50 mM MES (pH 6.5) was titrated with CrATP to give concentrations of 33.3, 50.0, 83.3, 200, 333, 500, and 833 μM. The enhancement factor (ε^*) was determined at each concentration of CrATP and used to derive the necessary information for the Scatchard plot. This is a plot of $[CrATP]_b/([CrATP]_f[APH(3′)\text{-}IIIa]_T)$ vs. $[CrATP]_b/[APH(3′)\text{-}IIIa]_T$ which yields the binding stoichiometry (n, x-intercept) and the dissociation constant (K_D, n/y-intercept).

Information about the binary complex between CrATP and the antibiotic

molecules can also be derived from water relaxation studies. Equation III-5 is analogous to Equation III-4 and can be used to describe this system where ε_a, the enhancement in the CrATP•Antibiotic binary complex, replaces ε_b. In these experiments, CrATP (50 and 100 μM) was titrated with amikacin or butirosin A to give concentrations of 5, 10, 15, and 30 mM antibiotic. The value of ε^* obtained at these concentrations of antibiotic were used to generate a double reciprocal plot ($1/\varepsilon^*$ vs. 1/[Antibiotic]). Extrapolation to infinite antibiotic concentration yields the ε_a values (1/*y*-intercept) for the antibiotics in the binary complex with CrATP. The dissociation constant (K_1) for complex formation was calculated using equation III-6, where $[\text{Antibiotic}]_f = [\text{Antibiotic}]_T - [\text{CrATP}]_b$ and $[\text{CrATP•Antibiotic}] = [\text{CrATP}]_b$. A dissociation constant was calculated at each concentration of antibiotic in the titration experiments at both of the CrATP concentrations. These values were averaged to yield the K_1 values for amikacin and butirosin A.

6. Magnetic Resonance Studies of the Ternary Complexes

The ternary APH(3′)-IIIa•CrATP•Antibiotic complexes involving amikacin and butirosin A can also be studied using low-field NMR methods. Once again, ε^* is the weighted average of the enhancements due to all complexes of CrATP (Equation III-7, Figure III-2). The terms ε_a and ε_b have been described above and ε_T is the enhancement of water protons when bound to Cr^{3+} in the APH(3′)-IIIa•CrATP•Antibiotic ternary complex. The value of ε_T and three of the six equilibrium binding constants that describe ternary and binary complex formation

(Mildvan & Cohn, 1966; Serpersu *et al.*, 1986; Serpersu *et al.*, 1987) can be obtained by titrating the antibiotics into their respective ternary complexes and measuring ε^*. The six binding constants can be incorporated into Equation III-7 to yield Equation III-8 (Figure III-2). The binding constants (Equations III-9 to III-14) are described in Figure III-3 and are related to each other by the following relationship:

$$K_1K_2 = K_3K_D = K_A{}'K_S \qquad \text{Eq. III-15}$$

Low-field NMR was used to study ternary complex formation for butirosin A and amikacin. In these experiments, an initial solution that contained 50 mM MES (pH 6.5), 100 μM CrATP, and 200 μM APH(3′)-IIIa was titrated with an antibiotic mixture that contained 2 or 10 mM antibiotic, 50 mM MES (pH 6.5), 100 μM CrATP, and 200 μM APH(3′)-IIIa. The titrant solution was constructed such that after each addition, only the concentration of antibiotic was increased while the other components remained the same concentration. Antibiotic concentrations in the low-field solutions used to measure ε^* ranged from 0 to 3.5 mM. A plot of ε^* vs. [Antibiotic] was constructed and the data iteratively fit to Equations III-8 and III-15 using the computer program EPS7A (Mildvan & Engle, 1972; Serpersu *et al.*, 1986). This involves providing the program with the previously determined binary enhancement values (ε_b and ε_a), K_1, K_D (from Scatchard analysis), and $K_A{}'$ (K_I from competitive inhibition and inactivation studies). Based on the provided values, the computer program determines the remaining binding constants and ε_T by varying

the value of K_S and computing what values give the smallest error.

C. Results and Discussion

1. Kinetic Studies with CrATP and RhATP

To use CrATP and RhATP as active site probes with APH(3′)-IIIa, it was first necessary to demonstrate that these metal-ATP analogs bind to the active site of the enzyme. Kinetic analysis of the inhibition of APH(3′)-IIIa by CrATP/RhATP (Figure III-4) showed that CrATP and RhATP are linear competitive inhibitors with respect to MgATP. Secondary plots of the slope vs. [MeATP] yielded a $K_{I(CrATP)}$ of 124 ± 16 μM and a $K_{I(RhATP)}$ of 130 ± 20 μM. Incubation of APH(3′)-IIIa with various concentrations of CrATP/RhATP showed a time-dependent pseudo first-order loss of enzyme activity. The rate of inactivation was dependent on the concentration of MeATP and showed saturation behavior (Figure III-5). This type of kinetic behavior is consistent with a binding equilibrium followed by a first-order chemical process leading to inactivation. After the inactivation chemistry, there is formation of a long-lived APH(3′)-IIIa•MeATP complex (EI*) as denoted below:

$$E + I \rightleftarrows EI \rightleftarrows EI^*$$

Since Cr^{3+} and Rh^{3+} exchange their ligands very slowly, it is likely that this complex may be formed by donation of a ligand from the enzyme to the coordination sphere of the Me^{3+} ion involved in the MeATP complex. The pseudo first-order rate constants (k_{obs}) for each concentration of MeATP were determined

and plotted in double reciprocal form ($1/k_{obs}$ vs. 1/[MeATP]). This is a linear plot which yielded an inactivation rate of 0.024 ± 0.005 min^{-1} for CrATP and 0.014 ± 0.004 min^{-1} for RhATP. These plots also yielded a $K_{I(CrATP)}$ for CrATP of 88 ± 26 μM and a $K_{I(RhATP)}$ of 90 ± 17 μM for RhATP. The results from the kinetic studies suggest that CrATP and RhATP bind stoichiometrically to the active site of APH(3′)-IIIa and can be used as active site probes.

2. Binding Studies Using Pulsed NMR Spectroscopy

The binding of CrATP to the enzyme was studied by pulsed NMR spectroscopy at 24.3 MHz. APH(3′)-IIIa•CrATP complex formation was indicated by an increase in the enhancement (ε^*) of the paramagnetic effect of CrATP on the longitudinal relaxation rates ($1/T_{1p}$) of water protons when the enzyme was titrated with CrATP. A double reciprocal plot of the data ($1/\varepsilon^*$ vs. 1/[APH(3′)-IIIa]) yielded a straight line which describes the enhancement of $1/T_{1p}$ of water protons (ε_b) resulting from the binding of CrATP to the enzyme (Figure III-6). The value of ε_b in this case was 1.88, which is similar to the values found with other CrATP•Enzyme complexes (Gregory & Serpersu, 1993; Gupta *et al.*, 1976). The relaxation data was used to determine the stoichiometry of binding and the dissociation constant for the CrATP•Enzyme complex through a Scatchard plot (Figure III-7). A K_D of 238 ± 32 μM with a 1:1 binding stoichiometry was determined for the CrATP•APH(3′)-IIIa complex from the Scatchard analysis. For subsequent studies to be interpretable, it is important that only one paramagnetic probe is bound per active site of the

enzyme. The approximate (3-fold) agreement between $K_{i(CrATP)}$ of CrATP, determined by reversible and irreversible methods, and K_D, determined by direct binding studies, is reasonable.

Binary CrATP•Antibiotic complexes were also studied in a similar manner as described above for the CrATP•APH(3′)-IIIa complex using amikacin and butirosin A. Dissociation constants of 11.8 mM and 14.1 mM and the enhancement values (ε_a) of 1.43 and 1.59 were determined for amikacin and butirosin A, respectively.

The thermodynamic properties of ternary and binary complexes of enzyme, CrATP, and antibiotic can be described by six equilibrium binding constants as described in Figure III-3. To determine ε_T, and various binding constants, solutions of APH(3′)-IIIa and CrATP were titrated with antibiotics and the enhancement of $1/T_{1p}$ of water protons was measured. Representative titrations, with amikacin and butirosin A, are shown in Figure III-8 with the computer fitted curves. All of the relevant dissociation constants and ε_T values determined in this study are given in Table III-1. As shown in Figure III-8, conversion of the binary APH(3′)-IIIa•CrATP complex to the ternary APH(3′)-IIIa•CrATP•Antibiotic complex increases the observed enhancement of $1/T_{1p}$ of water protons by the bound CrATP ($\varepsilon_T > \varepsilon_b$). This suggests that the immediate environment of Cr^{3+} is altered as the antibiotic binds to APH(3′)-IIIa to form the ternary complex. The observed differences in ε_T for amikacin and butirosin A reflect structural differences in the coordination sphere of Cr^{3+} in the respective ternary complexes. Also, K_3 for amikacin is higher than K_3 for butirosin A by an order of magnitude. These findings are in agreement with the

kinetic studies which yielded K_m values of 245 μM and 34 μM for amikacin and butirosin A, respectively (McKay *et al.*, 1994). The observed differences between the antibiotics may reflect the orientation of substituents of the 2-DOS ring since amikacin is 4,6-disubstituted and butirosin A is 4,5-disubstituted. However, examination of the kinetic data (McKay *et al.*, 1994) shows that K_m values for other antibiotics with 4,6- or 4,5-disubstitutions are different only by a factor of 2 or 3. Amikacin and butirosin A are substituted with a AHB chain at N-1 of the 2-DOS ring. Substitution of the 2-DOS ring with the AHB chain may interfere with some antibiotic-enzyme interactions.

Comparison of K_S and K_3 values for amikacin and butirosin A reveal that CrATP increases the affinity of both antibiotics to the enzyme by a factor of two (Table III-1). This suggests that when the nucleotide is bound to the enzyme, the geometry of the active site is altered to create more favorable interactions between the side chains of APH(3′)-IIIa and the antibiotics. This is consistent with the Theorell-Chance kinetic mechanism observed for APH(3′)-IIIa.

Chapter IV

The Arrangement of APH(3′)-IIIa-Bound Aminoglycosides

A. Introduction

One of the most important questions in biology and chemistry is "what is the structure of this molecule?". With powerful instrumentation becoming available in the last few decades, this question is answered on a regular basis by many laboratories throughout the world. This question applies not only to large macromolecules but to smaller molecules that are involved in signal transduction, biosynthetic pathways, or have potential therapeutic value. Structural information on proteins can provide insight on its folding pathway or its catalytic mechanism, if it is an enzyme. Information on the bound state of a small biomolecule can be very valuable in the design of novel drugs.

X-ray diffraction has proven to be the most powerful method to determine the structure of large macromolecules such as proteins. Not only does X-ray data give a tremendous amount of structural information but has proven to be very valuable in the elucidation of enzymatic mechanisms. NMR spectroscopy is by far the most powerful method to study the structure of smaller molecules. Only a few years ago, multidimensional NMR techniques were only able to solve the structure of proteins smaller than 20 kDa (Bax & Grzesiek, 1993). However, the more recent literature has examples of the use of NMR combined with isotopic labeling (^{15}N, ^{13}C)

strategies to solve the structure of proteins larger than 20 kDa (Wu *et al.*, 1997; Riek *et al.*, 1996).

In order to study enzyme-substrate interactions, a combination of X-ray and NMR methods may have to be employed. X-ray crystallography can be used to determine the structure of the enzyme, possibly with one or more bound substrates. However, it is sometimes difficult to crystallize an enzyme with bound substrates, especially if one of the substrates has some mobility when bound to the active site. Additionally, as in the case with APH(3′)-IIIa, an enzyme can have many substrates that have diverse structures. Obtaining an X-ray structure with a variety of substrates would be difficult and probably not worthwhile. Fortunately, NMR methods are available that can provide information about enzyme-bound substrates without having detailed structural information about the enzyme.

The variety of NMR methods available to study protein-ligand interactions makes NMR a popular and powerful means of studying a variety of biomolecules (Otting, 1993). The utility of NMR methods relies on the fact that each atom of a molecule, that has a nuclear spin, yields an individual resonance in an NMR spectrum. The chemical shift and relaxation rate of the magnetic nuclei depends on the local chemical environment of the molecule. Therefore, magnetic nuclei can act as structural reporters when a molecule is free in solution or bound to its biological target. The most useful information derived from NMR experiments comes the measurement of relaxation rates ($1/T_1$) and the observation of nuclear Overhauser effects (NOEs) between magnetic nuclei.

The knowledge of the molecular basis of enzymatic catalysis is dependent upon the collection of dependable structural information on enzyme-bound substrate complexes. Measurement of the paramagnetic relaxation rates ($1/T_{1p}$) of substrate magnetic nuclei (protons), in the presence of a paramagnetic probe, allows for the calculation of distances from the ^1H nuclei of an enzyme-bound molecule to a paramagnetic center (Mildvan & Gupta, 1978; Mildvan & Cohn, 1970). Information about the conformation and arrangement of enzyme-bound substrates can be derived from these distances.

The magnitude of the relaxation of a substrate nucleus by a paramagnetic species exhibits a $1/r^6$ dependence on the distance between the nucleus and the paramagnet. As the substrate molecule exchanges into and out of the paramagnetic ternary complex, $1/T_{1p}$ for the magnetic nuclei (such as ^1H) of the substrate molecule depends mainly on five parameters (Mildvan & Gupta, 1978): the lifetime of the complex (τ_M), the relative stoichiometry of the paramagnet and substrate in the complex (q), the correlation time for electron-nuclear dipolar interaction (τ_c), the outer sphere contribution to the relaxation rate due to ligand molecules beyond the inner coordination sphere (usually small), and the distance (r) from the magnetic nucleus to the unpaired electron(s). The value of τ_c is a measure of the efficiency of magnetic energy transfer between the paramagnetic species and the nucleus and can be calculated by evaluating the frequency dependence on the $1/T_{1p}$ of ligand nuclei. It is not necessary to calculate a value of τ_M, it only needs to be demonstrated that ligand exchange rates are much faster than relaxation rates ($1/\tau_M$

» $1/T_{1p}$) of ligand nuclei. Since $1/T_{1p}$ is inversely proportional to the sixth power of r, errors in the measurement of $1/T_{1p}$ and in the evaluation of τ_c are minimized and as a result the errors in the determination of distances may only be 10% (Mildvan, 1977).

β,γ-bidentate CrATP is a stable exchange-inert metal-ATP analog, which has been successfully used as a paramagnetic probe for intersubstrate distance measurements (Gupta *et al.*, 1976; Fry *et al.*, 1985; Wolkers *et al.*, 1991; Gregory & Serpersu, 1993). In this study, CrATP was used to explore the conformation and arrangement of amikacin and butirosin A at the active site of APH(3′)-IIIa in order to better understand the molecular details of the inactivation chemistry that renders the aminoglycosides inoffensive. As in many biochemical reactions, the reaction catalyzed by APH(3′)-IIIa involves the interaction of two substrates with an enzyme to yield a ternary complex. It is experimentally advantageous to have a substrate analog that is a paramagnetic species so that intersubstrate distances can be calculated. Therefore, the use of CrATP will allow structural information to be obtained that cannot be derived from the current X-ray structure of APH(3′)-IIIa (Hon *et al.*, 1997).

The structural information gained about APH(3′)-IIIa-bound aminoglycosides in this project will complement the recently determined crystal structure of APH(3′)-IIIa. A discussion about the domain organization of APHs and the 3D structure of APH(3′)-IIIa will demonstrate the need for additional structural information about bound substrates that was the thrust of this project.

There are six other classes of APH(3′)s that have been identified and their sequences show homology in the carboxy-terminal region (Shaw *et al.*, 1993). Three conserved motifs for the APH(3′)s have been identified and their function putatively identified by homology searches of protein databases (Figure IV-1). Motif 1 is believed to be involved in the catalytic mechanism, motif 2 in nucleotide binding, and motif 3 in aminoglycoside binding. It was postulated that His-188 was a phosphate-accepting residue because it is conserved among all APH(3′)s (Martin *et al.*, 1988). However, kinetic studies with a H188A mutant of APH(3′)-IIIa and positional isotope-exchange experiments has shown that His-188 is not a phosphate-accepting residue and a direct attack of the reactive hydroxyl group of the aminoglycoside on the γ-phosphate of ATP is the mechanism of phosphoryl transfer (Thompson *et al.*, 1996b).

The motif 1 sequence of HXAXXXXN has been identified in many different protein kinases (Martin *et al.*, 1988; Heinzel *et al.*, 1988). The crystal structures of the tyrosine kinase domain of the human insulin receptor (IRK)(Hubbard *et al.*, 1994), the Ser/Thr cyclin-dependent kinase 2 (Cdk2)(De Bondt *et al.*, 1993), and the Ser/Thr MAP kinase Erk2 (Zhang *et al.*, 1994) have recently been determined. These structures serve to explain the role of this conserved sequence in protein kinases. It is believed that the conserved His residues in the protein kinases do not play a direct role in catalysis (Figure IV-2). However, based on the structure and proposed mechanism of cAMP-dependent protein kinase (cAPK), Asp-164 acts as a general base to deprotonate the hydroxyl group involved in phosphoryl transfer and

the conserved Asn residue is involved in a H-bond network used to coordinate Mg^{2+} (Zheng *et al.*, 1993). Additionally, mutation and X-ray studies of APH(3′)-IIIa suggest that Asp-190 is also a general base used to deprotonate the reactive hydroxyl group of the aminoglycosides at the active site of APH(3′)-IIIa (Hon *et al.*, 1997).

The sequence similarity between APH(3′)-IIIa and protein kinases suggest that the structure of APH(3′)-IIIa may resemble that of a protein kinase. In fact, the crystal structure of APH(3′)-IIIa shows that its structure is strikingly similar to the catalytic subunit of cAPK (Figure IV-3). Over 40% of the APH(3′)-IIIa enzyme is structurally identical to cAPK and other eukaryotic protein kinases (Hon *et al.*, 1997). The APH(3′)-IIIa monomer consists of two lobes, a smaller 94-residue N-terminal lobe and a larger 157-residue C-terminal lobe. These lobes are connected by a 12-residue stretch containing a short β-strand and an α-helix. The architecture of both the N-terminal and C-terminal lobes is very similar to that seen in the eukaryotic Ser/Thr and Tyr protein kinases. Therefore, it is believed that the APH(3′) enzymes and eukaryotic protein kinases evolved from a common ancestor (Hon *et al.*, 1997).

The X-ray structure of APH(3′)-IIIa was with bound ADP and may not represent a catalytically relevant conformation of the APH(3′)-IIIa•MgATP binary complex. In any event, the results presented in this chapter combined with the X-ray studies should provide a more complete description of ternary complex formation.

B. Experimental Procedures

1. Materials

Amikacin, butirosin A (sulfate salt), and ATP were from Sigma Chemical Co. Additional butirosin A was a gift from Dr. David Baker, Department of Chemistry, University of Tennessee. Deuterated Tris (Tris-d_{11}) was from Isotec, and ^2H_2O (99.9 and 99.96 atom %), deuterium chloride, and sodium deuteroxide were from MSD Isotopes. For this part of the project, APH(3′)-IIIa was provided by Dr. Gerard D. Wright of McMaster University. CrATP was prepared as described in the "Experimental Procedures" section of the Chapter III and diluted with ^2H_2O for the ^1H NMR experiments.

2. Magnetic Resonance Studies

The paramagnetic effect of CrATP on the relaxation rates of the protons of the aminoglycoside antibiotics amikacin and butirosin A, bound in ternary (APH(3′)-IIIa•CrATP• Antibiotic) and binary (CrATP•Antibiotic) complexes, were determined at 400 MHZ (Bruker AMX 400 widebore spectrometer). The inversion recovery method was used with 500 μL samples in ^2H_2O and 14 variable delays ranging from 20 ms to 7 s. Despite the multiplicity of resonances, the inversion recovery plots were not multiphasic within the time range used to determine T_1, indicating that the data could be used in the distance calculations.

APH(3′)-IIIa was first dialyzed against 2 mM deuterated Tris (Tris-d_{11}) buffer (pH 6.8) in order to avoid the interference of Tris protons. The enzyme was then

exchanged into ^2H_2O by three cycles of lyophilization and redissolving in ^2H_2O. The aminoglycosides were dissolved directly into ^2H_2O, underwent two cycles of lyophilization, and were redissolved in ^2H_2O. Samples contained 0.20-0.30 mM APH(3′)-IIIa, 7 mM amikacin or 6 mM butirosin A, 50 mM NaCl , and 20 mM Tris-d_{11} (pH 6.8). The solution was then titrated with CrATP and the increases in the longitudinal relaxation rates ($1/T_1$) of various protons of the antibiotics were measured. The data were analyzed by plotting the relaxation rates against the concentration of CrATP bound in the ternary CrATP•APH(3′)-IIIa•Antibiotic complexes . The slopes of these curves were then corrected by subtracting the contribution of the paramagnetic effects of CrATP in the binary CrATP•Antibiotic complex that was based on the known distribution of CrATP among the binary and ternary complexes, as calculated from the respective dissociation constants (Table III-1). The corrected slopes obtained in this fashion, when multiplied by the total antibiotic concentration, yielded the normalized relaxation rates ($1/fT_{1p}$), where f is defined as bound [CrATP]/[Antibiotic].

The temperature dependence of $1/T_1$ of the protons of amikacin and butirosin A in the ternary complex was examined at 12, 23, and 32 °C for amikacin and 22, 32, and 42 °C for butirosin A. Sample composition was as described above for the analysis of the paramagnetic effect of CrATP on the protons of amikacin and butirosin A in their ternary complexes.

The correlation time for the dipolar electron-nucleus interaction in the ternary APH(3′)-IIIa•CrATP•Antibiotic complexes was determined by studying the

frequency dependence of $1/T_{1p}$ of water protons at 90 MHZ on a FX 90Q Jeol spectrometer, 250 MHZ on a Bruker AC 250 spectrometer, and 400 MHZ on a Bruker AMX 400 widebore spectrometer by the inversion recovery method as described previously (Serpersu *et al.*, 1987; Mildvan & Engle, 1972). Samples contained 20 mM Tris-d_{11} (pH 6.8), 0.60 mM APH(3′)-IIIa, 8.0 μM CrATP, and 5.0 mM antibiotic. Corrections were made to account for the paramagnetic effect of free CrATP on the observed relaxation rates. The values of τ_c and $f(\tau_c)$ were calculated using a least squares fitting program (Penefsky, 1977) according to Equations IV-1 and IV-2 (Figure IV-4), respectively. In these equations, τ_c is the dipolar correlation time, τ_s is the longitudinal electron spin relaxation time, ω_I and ω_s are the nuclear and electron precession frequencies, respectively, B is the zero field splitting parameter, and τ_v is a time constant for ligand motion that modulates B.

Cr^{3+}-to-^1H distances were calculated according to Equation IV-3 presented in Figure IV-3 (Mildvan & Gupta, 1978). In this equation, r is the internuclear distance, C is a constant equal to 705 $Å/s^{1/6}$ for interactions between Cr^{3+} and protons (Mildvan *et al.*, 1980), q is the stoichiometry, and $f(\tau_c)$ is the correlation function which is described in Equation IV-2.

C. Results and Discussion

1. Evaluation of τ_c and the Temperature Dependence of $1/T_1$

The temperature dependence of $1/T_1$ of the protons of amikacin and butirosin A was examined to establish that these antibiotics are in fast exchange

from the APH(3′)-IIIa•CrATP•Antibiotic ternary complexes. This is a necessary condition in the evaluation of distances in the paramagnetic ternary complex. Relaxation rates and exchange rates have an opposite temperature dependence. Increasing relaxation rates with increasing temperature are indicative of exchange limitation since exchange rates ($1/\tau_M$) increase at higher temperatures. Therefore, fast exchange is indicated by a decrease in the relaxation rate with increasing temperature, which was observed for various protons of butirosin A (Figure IV-5) and amikacin. Therefore, the observed relaxation values were used in distance calculations.

Determination of metal-to-nucleus distances, from the measurement of relaxation rates, requires a measurement of τ_c, the correlation time for the dipolar Cr^{3+}-nucleus interaction. The value of τ_c was evaluated by measuring the $1/T_{1p}$ of solvent water protons of samples at three frequencies. The paramagnetic contributions to $1/T_{1p}$ were observed at 90, 250, and 400 MHZ for the ternary complexes of the two antibiotics. The measured relaxation rates were corrected to account for the contribution of free CrATP to the observed relaxation rates. The values of τ_c and other parameters that describe the interaction of CrATP and APH(3′)-IIIa in the ternary APH(3′)-IIIa•CrATP•Antibiotic complexes are presented in Table IV-1. These values are similar to those observed earlier for enzyme-bound CrATP complexes (Gupta *et al.*, 1976; Wolkers *et al.*, 1991; Gregory & Serpersu, 1993).

2. Paramagnetic Effects of CrATP on the Protons of Amikacin and Butirosin A

The paramagnetic effect of CrATP on the relaxation rates of antibiotic protons were measured to determine Cr^{3+}-to-^1H distances in the ternary APH(3′)-IIIa•CrATP•Antibiotic complexes. Titration of CrATP into samples containing butirosin A or amikacin and APH(3′)-IIIa resulted in an increase in the $1/T_{1p}$ values of antibiotic protons. Figures IV-6 and IV-7 show the observed paramagnetic effects of enzyme-bound CrATP on the longitudinal relaxation rates ($1/T_1$) of various protons of amikacin and butirosin A, respectively. To correct for the effects of free CrATP and the binary CrATP•Antibiotic complex, similar titrations were carried out in the absence of APH(3′)-IIIa. Comparison of the paramagnetic effects of CrATP on the $1/T_1$ values of the antibiotic protons in the binary CrATP•Antibiotic and ternary Enzyme•CrATP•Antibiotic complexes show that the presence of APH(3′)-IIIa causes an enhancement of the paramagnetic effects. The corrected and normalized relaxation rates ($1/fT_{1p}$) were then used to determine Cr^{3+}-to-^1H distances (Table IV-2) using Equation IV-3.

3. Arrangement of Substrates at the Active Site of APH(3′)-IIIa

From the distances presented in Table IV-2, models were built that represent possible arrangements for amikacin and butirosin A at the active site of APH(3′)-IIIa. The models presented in Figures IV-8 (amikacin) and IV-9 (butirosin A) were constructed and analyzed in Insight II (BIOSYM/Molecular Simulations) software on a Silicon Graphics Indigo^2 workstation and contain no van der Waals overlap

between the atoms.

Amikacin is 4,6-disubstituted at the 2-DOS ring and is regiospecifically phosphorylated at the 3′(3A)-OH by APH(3′)-IIIa (McKay *et al.*, 1994). The distances used to construct the enzyme-bound arrangement, presented in Figure IV-8, allowed the phosphorus atom of the γ-phosphoryl group of ATP to be placed approximately 4 Å away from the oxygen atom of the 3′(3A)-OH group. Studies have shown that direct transfer of the phosphoryl group from ATP to the aminoglycosides is the mechanism of phosphorylation (Thompson *et al.*, 1996b). The model presented in Figure IV-8 places the substrates so that only the 3′(3A)-oxygen is colinear with the P-O bond of the γ-phosphoryl group of ATP, which may explain the specific phosphorylation of the 3′(3A)-OH group in the presence of several other hydroxyl groups.

Butirosin A is 4,5-disubstituted at the 2-DOS ring and recent studies have shown that APH(3′)-IIIa catalyzed phosphorylation can result in three different phosphorylation products (Thompson *et al.*, 1996a). Butirosin A can be monophosphorylated at the 3′(3A)- or 5″(5C)- oxygen or a diphosphorylated product can result in which both the 3′(3A)- and 5″(5C)- oxygens are phosphorylated. An arrangement was constructed (Figure IV-9) that satisfies the distance constraints and may explain why different phosphorylation products can be produced. The distance constraints allow both the 3′(3A)-OH and 5″(5C)-OH to be placed into a position that is equidistant from the phosphorus atom of the γ-phosphoryl group. Even though neither of the two oxygen atoms in this

arrangement is colinear with the P-O bond of the γ-phosphoryl group, it takes very little movement of the antibiotic to bring the 3′(3A)- or 5″(5C)-oxygen into a reactive position. An arrangement was also constructed in which the P-O bond of the γ-phosphoryl group of ATP could be placed colinear and 4 Å away from the 3′(3A)-OH. However, when CrATP was left in a fixed position and butirosin A was rotated to bring the 5″(5C)-oxygen colinear with the P-O bond of the γ-phosphoryl group, the distance constraints could not be met. This suggests that butirosin A may only have one productive arrangement in which either the 3′(3A)-OH or 5″(5C)-OH can be brought into a reactive position with respect to ATP. Since butirosin A was found to be in fast exchange in the APH(3′)-IIIa•CrATP•Butirosin ternary complex, it seems likely that the monophosphorylated butirosin product has to bind APH(3′)-IIIa again to be doubly phosphorylated. This implies that the active site of APH(3′)-IIIa is flexible such that a singly phosphorylated butirosin A product can still bind to the enzyme. This is also consistent with the kinetic mechanism which has recently been determined to be Theorell-Chance with ATP binding first followed by aminoglycoside, immediate release of phosphorylated antibiotic, and slow release of ADP (McKay & Wright, 1995; McKay & Wright, 1996).

The conformation of butirosin A presented in Figure IV-9 has the 2,6-diamino-2,6-dideoxy-D-glucose and D-xylose rings in a stacking arrangement. The stacking arrangement of these rings was necessary to satisfy all distance constraints in any of the satisfactory enzyme-bound arrangements constructed for butirosin A. The enzyme-bound conformation of butirosin A described above is similar to the

previously described solution structure of butirosin A (Cox & Serpersu, 1995). Therefore, it seems that the enzyme does not force butirosin A to adopt a conformation much different to that found in solution.

Figure IV-10 has the metal-triphosphate complexes of Figures IV-8 and IV-9 superimposed and allows a direct comparison of the arrangement and conformation of the enzyme-bound aminoglycosides. Figure IV-10 reveals that amikacin and butirosin A adopt different geometries at the active site of APH(3′)-IIIa. Amikacin has a more extended structure, due to its 4,6-disubstitution at the 2-DOS ring, which allows Cr^{3+} and the triphosphate group of ATP to move in closer to the antibiotic. The compact shape of butirosin A prevents such an approach of the metal-nucleotide. This is reflected in the Cr^{3+}-to-^{1}H distances presented in Table IV-2, where the distances in the amikacin ternary complex are significantly shorter. The compactness of butirosin A may make it more mobile at the active site and allows both the 3′(3A)- and 5″(5C)-OH groups to be extended out toward the γ-phosphoryl group of ATP. However, the extended structure of amikacin may make it more rigid at the active site and allow only the 3′(3A)-oxygen to be in a reactive position. Any movement of amikacin to bring another hydroxyl group into a reactive position (such as the 2′(2A)-OH) would be prevented by steric hindrance with the triphosphate moiety of ATP.

The mobility of substrates at the active site of an aminoglycoside-modifying enzyme was demonstrated when the X-ray structure of kanamycin bound to a nucleotidyltransferase enzyme was determined (Pederson et al., 1995). The electron

density of kanamycin was too blurred to yield a definitive structure.

The difference in binding of amikacin and butirosin A to the ATP•APH(3′)-IIIa binary complex, observed here by NMR, may hold the answer to a vexing problem. The K_m values for 7 of 8 aminoglycosides tested vary only by a maximum of 3.7-fold (9.3 μM - 34.3 μM) and many show substrate inhibition (McKay *et al.*, 1994). These include both 4,6- and 4,5-disubstituted aminoglycoside antibiotics. One aminoglycoside which does not fit this pattern is amikacin with a K_m some 7 - 26-fold higher than the others and does not show substrate inhibition. These differences may reflect a fundamental structural difference between the interactions of these aminoglycosides with APH(3′)-IIIa. The extended conformation, roughly parallel to the Cr^{3+}-$\beta\gamma$ phosphate complex, exhibited by amikacin, does not result in efficient phosphorylation. It may be that it is difficult for amikacin to have a productive collision in the ternary complex. The net result is that amikacin is poorly phosphorylated *in vivo* and is still a useful clinical drug, even in environments where APH(3′)s exist, while the other aminoglycosides are not.

Various questions arise while looking at Figure IV-10 such as "how can two substrates that adopt different arrangements bind to the same active site and how do the arrangements account for the observed regiochemistry?". The answer to these questions may be found in Figure IV-11. In this figure, the arrangements of the two aminoglycosides are shown with only certain atoms highlighted. The reactive hydroxyl groups are represented by red balls (3A-$OH_{(but)}$, 5C-$OH_{(but)}$, and 3A-$OH_{(amik)}$) and extend out from the structures. These hydroxyl groups extend out

from the structures and it is reasonable to suggest that they are in the best position to attack the γ-phosphorus of ATP. The amino (ammonium) group nitrogens in the molecules are represented as blue balls. As shown in Figure IV-11, the nitrogens that correspond to each other in the two molecules (ie, 6A-$NH_{2(but)}$/6A-$NH_{2(amik)}$, 3B-$NH_{2(but)}$/3B-$NH_{2(amik)}$) do not occupy the same space at the active site. However, 6A-$NH_{2(amik)}$ and 3B-$NH_{2(but)}$ are near each other and the amino or ammonium groups at these positions could make similar contacts with the enzyme such as an electrostatic interaction or hydrogen bond. Similarly, 3B-$NH_{2(amik)}$ is near 4D-$NH_{2(but)}$ and 6B-$OH_{(but)}$. Therefore, if the amino group at 3B-$NH_{2(amik)}$ is involved in a noncovalent interaction with the enzyme, the functional groups at 4D-$NH_{2(but)}$ and 6B-$OH_{(but)}$ might also be able to make a similar contact with the enzyme. The models presented in Figure IV-11 are static and the effect of antibiotic motion cannot be ignored. Subtle motions of the antibiotics may allow for proper recognition of the antibiotics by the enzyme.

The binding and relaxation data presented above show that amikacin and butirosin A adopt different arrangements and conformations at the active site of APH(3′)-IIIa. The geometric information derived from these studies provides insight into how APH(3′)-IIIa modifies both 4,5- and 4,6-disubstituted aminoglycoside antibiotics and the regioselectivity unique to both types of antibiotics. It is also an important step in understanding the inactivation of aminoglycoside antibiotics by APH(3′)-IIIa.

Chapter V

Biologically Important Conformations of APH(3′)-IIIa-Bound Aminoglycosides

A. Introduction

An understanding of the specificity and selectivity inherent in enzymatic catalysis requires a detailed characterization of the structure and dynamics of enzyme-bound ligands. The most powerful method in which to obtain structural and dynamical information on protein-bound ligands is transferred nuclear Overhauser effect spectroscopy (TRNOESY)(Clore & Gronenborn, 1982; Ni & Scheraga, 1994; Campbell & Sykes, 1993). Distance constraints derived from TRNOE experiments can be combined with modern computational/molecular modeling techniques to yield biologically relevant structures. The information derived from TRNOE studies complement the paramagnetic relaxation studies presented in Chapter IV. These two independent NMR methods can be used to characterize the geometry of enzyme-bound aminoglycosides. The geometry of the antibiotic includes its arrangement with respect to ATP and the relative positions of the antibiotic rings with respect to each other. The latter can be determined by TRNOESY and modeling studies and is the focus of this chapter.

A review of the recent literature reveals that TRNOE experiments are used extensively to derive information on protein- and lipid-bound molecules (Xiang & Markham, 1996; Gounarides *et al.*, 1993; Okada *et al.*, 1994; Blommers *et al.*,

1997; Barsukov *et al.*, 1996). Additionally, TRNOE methodology has been extremely useful in obtaining structural information on protein-bound carbohydrates (Casset *et al.*, 1996; Scheffler *et al.*, 1995; Espinosa *et al.*, 1996). Therefore, this method was a logical choice to study the structure of aminoglycosides (pseudosaccharides) bound to APH(3′)-IIIa.

A theoretical discussion of the nuclear Overhauser effect (NOE) will not be presented; however, an introduction to this important phenomenon will be given to demonstrate its importance in modern structural biology. In general, a NOE can be detected between two magnetic nuclei (i.e. two protons) when they are closer than 5 Å from each other. The cross-peaks (NOEs) that appear in a NOESY spectrum are the result of a magnetic interaction between two nuclei related by spatial proximity and not through scalar coupling, as is the case for other two-dimensional NMR experiments. In essence, the NOE is an aspect of nuclear relaxation where the change in intensity of one resonance is observed upon the perturbation of the transitions of another resonance. The magnitude of the NOE observed between two protons exhibits a $1/r^6$ dependence on the distance separating the protons. This is analogous to the distance dependence used to calculate Cr^{3+}-to-^1H distances in Chapter IV.

The interaction between the two protons is mediated through the coupling of the magnetic fields of the two protons (dipolar coupling), which behave as magnetic dipoles due to the nuclear spin of the nuclei. Dipolar-coupled nuclei can exchange magnetic energy, a process which is termed cross-relaxation. Cross-relaxation

involves a change in intensity of the resonance of spin x (from one proton) when spin y (from another proton) is perturbed, which is the basis of the nuclear Overhauser effect.

One complication that arises in interpreting the data from a NOESY spectrum is spin diffusion. This arises when two nuclei exchange spin states through cross-relaxation (primary NOE) and then the magnetization is transferred to a neighboring nuclei. These higher-order NOEs do not carry any distance or structural information. To avoid these ambiguities, several NOESY experiments are performed at different mixing times and a buildup curve (NOE intensity vs. mixing time) is constructed to derive the appropriate mixing time in which to minimize spin diffusion. The mixing time is implemented into the pulse program that governs the time period allowed for the formation of the NOE, which is the duration that dipolar interaction is allowed to occur between the nuclei.

TRNOE experiments can provide information about the structure of a protein-bound ligand due to binding-induced NMR relaxation enhancements. During these experiments, geometric information about the bound ligand is transferred to the free ligand by the ligand association with, and dissociation from, the binding protein. Detailed structural information about protein-bound ligands can be derived from approximate distances obtained from transferred NOEs between ligand protons adjacent and distant in the sequential chemical structure.

This method allows observation of a bound ligand as it transfers cross-relaxation to the free state, if the rate of chemical exchange is reasonably rapid

relative to the spin-lattice relaxation (T_1) of the free ligand. The cross-relaxation rates of a ligand in the free and bound state are of opposite sign, such that the NOEs in the free state are positive while those in the bound state are negative. These can be clearly identified in the two-dimensional TRNOESY spectrum (acquired in the phase-sensitive (TPPI) mode) since the NOEs will be on opposite sides of the spectrum.

The fact that the NOEs for the aminoglycosides will be of opposite sign when bound to APH(3′)-IIIa and free in solution can be explained by a consideration of correlation time (τ_c). Molecular tumbling in solution is commonly described by τ_c, which embodies the complex influences on molecular motion into a single parameter, and is a function of molecular weight, solution viscosity and temperature. Typically, molecules with high molecular weight tend to move more slowly in solution than small molecules, and hence will have a longer τ_c. Specifically, ligands in the unbound form are generally characterized by short correlation times ($\tau_c \sim 10^{-10}$ s) with $\omega\tau_c \ll 1$, where NOEs are small and negative, if the data is collected in the TPPI mode. When bound to a protein, the ligand is characterized by the long correlation time of the protein ($\tau_c > 10^{-8}$ s) with $\omega\tau_c \gg 1$, where NOEs are large and positive, again if the data is collected in the TPPI mode. The value of ω above is the angular precession frequency of a ^1H in a magnetic field.

Since an observed NOE between a pair of protons denotes a spatial proximity between these protons, structural information on a molecule can be

derived from NOESY (solution studies) and TRNOESY (bound structure) studies. A variety of methods are available to convert information derived from observed NOEs to distances. The calculation of the distances between proton pairs can serve as restraints in molecular modeling protocols.

Among the methods used for the interpretation of NOE-derived distance data in terms of biopolymer structure, the isolated spin pair approximation (ISPA) and the spin relaxation matrix method are the most common (Bush, 1994). The latter involves a description of homonuclear dipolar relaxation in a multiple spin system and requires solving the complete set of coupled differential equations describing the evolution of longitudinal magnetizations of the individual spins. The differential equations are given by the Bloch equations (Bloch, 1957) and will not be described in this chapter. The set of coupled linear differential equations is cast into a relaxation matrix form. The relaxation matrix represents the mutual cross-relaxation pathways of all the protons in the biomolecule. The advantage of using a relaxation matrix is that one is not restricted to short mixing times where the signal-to-noise ratio may be low.

A low signal-to-noise ratio can be a problem in the ISPA method where short mixing times are used to avoid spin diffusion. Since only two particular spins are considered, spin diffusion has to be avoided because if a higher-order NOE is observed between protons that are not in spatial proximity, the resulting structure(s) may be in error. The assumption in the ISPA method is that the NOE cross-peak volume is proportional to the sixth power of the distance between the protons:

$$(r_{std}/r_{xy})^6 = (v_{xy}/v_{std}) \qquad \text{Eq. V-2}$$

where r_{std} is the calibration distance (known distance between a proton pair), v_{std} is the volume of the cross-peak for the calibration proton pair, r_{xy} and v_{xy} is the distance between another proton pair and the volume of their cross-peak, respectively. To assure that spin diffusion is not a problem, a buildup curve (mentioned above) is constructed so that an appropriate mixing time can be selected for data analysis. This appropriate mixing time is in the linear part of the buildup curve.

Fortunately, smaller mixing times and the ISPA has been used successfully in many cases to study protein-bound carbohydrates (Casset *et al.*, 1996; Scheffler *et al.*, 1995; Geyer *et al.*, 1996). After the distance between various protons are calculated, models of the ligand which fit the distance constraints can be constructed. Typically, this is done through simulated annealing employing energy minimization and molecular dynamics routines.

Computational chemistry/biology has become one of the most powerful tools available to scientists over the past decade. For example, researchers in protein folding, X-ray crystallography, NMR spectroscopy, and molecular biology have all seen computational techniques enrich their field. The analysis of the data produced in these and other areas of research sometimes require advanced computational techniques that result in structure determination and refinement. Molecular modeling is usually the ultimate goal in computational approaches that yield structures of molecules that fit experimentally derived distances or other physical

parameters. Any structure that is reported in the literature is in fact a model. Modern computational methods allows one to make better models.

Computational methods can be carried out in a variety of computers and modeling packages. Typically, computational methods are performed in an unix, PC, or MacIntosh environment. For example, Silicon Graphics Indigo^2 or Octane computers are used for the unix-based modeling programs such as DISCOVER/Insight II (BIOSYM/Molecular Simulations), SYBYL (Tripos), or Spartan (Wavefunction). One of the ultimate goals of these modeling packages and protocols is to produce a model that embodies the simultaneous agreement of all experimental data (i.e. distance restraints). They do this by the non-linear optimization of a target function, which is the potential energy function (E_{pot}) function chosen for the molecule of interest.

Before energy minimization and molecular dynamics are employed, a suitable forcefield is chosen to model the molecule of interest. A forcefield is essentially the functional form of the E_{pot} function and the parameters needed to fit the function. The choice of the E_{pot} function, and hence the forcefield, is important because the calculation of the potential energy of an ensemble of atoms, along with the first and second derivative with respect to the atomic coordinates, produces the information necessary for minimization and dynamics simulations. A variety of forcefields are available such as AMBER, CVFF, MM2, MM3, CFF91, ESFF, and Tripos. AMBER was utilized in this work and a discussion of this forcefield will be presented to describe the features of a forcefield.

AMBER (Assisted Model Building and Energy Refinement) originated from the lab of Peter Kollman at the University of California at San Francisco (Weiner & Kollman, 1981; Weiner *et al.*, 1984; Weiner *et al.*, 1986). AMBER was originally designed for the modeling of proteins and nucleic acids. However, it was parameterized for carbohydrates by Homans (Homans, 1990; Rutherford *et al.*, 1993), and a recent independent investigation has shown that the AMBER/Homans forcefield was appropriate for the modeling of carbohydrates (Martín-Pastor *et al.*, 1997).

The E_{pot} used in the AMBER forcefield is presented in Figure V-1. The first three terms handle the internal coordinates of bonds, angles, and dihedrals, respectively. These parts of the equation reflect the energy needed to stretch bonds (b), bend angles (θ), and rotate torsion angles (ϕ). For example, the first term accounts for every covalent bond and is treated as a simple Hooke's law spring with a force constant K_b and equilibrium bond length b_o. The second term monitors the deformation energy of valence angles of the covalent bonds from an atom, and term 3 characterizes the deformation energy for twisting a bond. Term 4 is a Lennard-Jones 6-12 potential used to describe the nonbonded (van der Waals) interactions of the atoms. In this term, r is the distance between two atoms, r* is an approximation to the sum of the average radii of the two atoms, and ε is the minimum in the potential. Term 5 is the Coulombic representation of electrostatic interactions. The dielectric constant, ε_{ij}, in this term can be made distance-dependent (a function of r_{ij}). Term 6 is a H-bond term that is used to augment the

electrostatic description of the H-bond. It is a weak 10-12 term because some repulsive term is required to prevent the occupancy of unrealistically short H-bonds. The coefficients C and D are constants that depend on the nature of the H-bond donor and H-bond acceptor.

The calculations associated with molecular modeling can be characterized as molecular dynamics and molecular mechanics. Molecular mechanics is the hallmark of energy minimization and focuses on the energetic aspect of particular geometries of the molecule of interest. On the other hand, molecular dynamics considers the energy of the system as a function of time to give a trajectory.

Before energy minimization can be performed, a target function is chosen and evaluated for given conformations of a molecule. The target function is the E_{pot} function and the particular one depends on the forcefield that is selected. The conformation of a molecule is altered to lower the value of the E_{pot} function. The process is repeated in an iterative process to find the "minimum" energy structure according to the E_{pot} being used. Many structural adjustments (iterations) may be necessary to converge on a minimum. Several algorithms exist which can direct the minimization process. The two most common are the method of steepest descents and the conjugate gradient method (McCammon & Harvey, 1987). Steepest descents is the algorithm that is most likely to generate a lower-energy structure independent of what E_{pot} function is being used or from what initial structure the calculation begins. However, the steepest descents method is inefficient because it converges slowly near the minimum structure. However, the method of conjugate

gradients is more efficient because each successive iteration moves the conformation toward the minimum. Energy minimization by itself cannot explore all of the conformational possibilities of even a small molecule. Therefore, it usually combined with molecular dynamics in a process known as simulated annealing.

Equilibrium motions of biological molecules are important in solution as well as bound to their biological target. Molecular dynamics (MD) is a simulation method that is used to study the equilibrium motions of molecules. The goal in MD is not to converge to one "minimized" structure, rather it allows a sampling of conformations of a molecule at a given temperature. Dynamics simulations are performed by classical mechanics and involves the integration of Newton's equation of motion:

$$-(\delta E_{pot}/\delta r_i) = m_i(\delta^2 r_i/\delta t^2) \qquad \text{Eq. V-3}$$

where the force on an atom i can be computed directly from the derivative of the E_{pot} with respect to the coordinates r (left side of the equation). Classical equations of motion are deterministic, that is, once initial coordinates are known, the coordinates at a later time can be computed. Therefore, it is necessary to integrate simultaneously the differential equation for each atom in the system. From the solution of these equations the atomic positions and velocities, as a function of time, are obtained. Knowledge of the time history (trajectory) of the atoms allows the computation of such things as structure and thermodynamics.

A combination of energy minimization and molecular dynamics is the best way to explore a variety of conformational space and then converge to a particular

structure after starting with a random structure. One way to accomplish this is to start with a random structure and then apply molecular dynamics at a few temperatures (from high to low) combined with energy minimization. Each random structure can generate a final structure after the modeling protocol. A comparison of the final structures can yield information about the geometry and dynamics of the molecule of interest. The type of analysis described above is referred to as simulated annealing, although this term is used loosely and can apply to a variety of methods (Brünger *et al.*, 1997).

B. Experimental Procedures

1. Materials

Amikacin, butirosin A (sulfate salt), ribostamycin, and ATP, NADPH, the dicyclohexylammonium salt of phosphoenolpyruvate (PEP), Tris, NaCl, ampicillin, kanamycin A, and 2-(morpholino)ethanesulfonic acid (MES) were from Sigma Chemical Co. Additional butirosin A was a gift from Dr. David Baker, Department of Chemistry, University of Tennessee. $CaCl_2$ was from Aldrich Chemical Co. ^2H_2O, deuterated Tris (Tris-d_{11}), deuterium chloride, and sodium deuteroxide (both 99.9 atom %) were from MSD Isotopes. Pyruvate kinase (PK) and lactate dehydrogenase (LDH) were obtained from Boehringer Mannheim. Bacto tryptone and Bacto yeast extract were from Difco. Isopropyl 1-thio-β-D-galactopyranoside (IPTG) was from Gibco. Macro Prep Q anion-exchange resin was from BioRad.

2. Purification of APH(3')-IIIa

APH(3')-IIIa was available from an overexpression system in which *E. coli.* BL21 was transformed with the plasmid pPCRG6, which has the aph(3')-IIIa gene under control of a bacteriophage T7 promoter and the lac operon (McKay *et al.*, 1994). The overexpressing *E. coli.* strain was a gift from Dr. Gerry Wright, McMaster University. The cells (1 L) were grown from an overnight inocula at 37 °C (25 rpm) in Lauria broth containing 100 μg/mL ampicillin. When the absorbance (600 nm) of the cell culture reached 0.3 - 0.4, IPTG was added to a concentration of 1 mM. The cells were grown for an additional 5 h and harvested at 5000*g* for 15 min at 4 °C. The cells were resuspended in 10 mL of a 0.85% NaCl solution and were harvested again by the same procedure. The cells were resuspended in 10 mL of lysis buffer which consisted of 50 mM Tris (pH 7.5), 5 mM EDTA, 200 mM NaCl, 0.1 mM DTT, and 1 mM PMSF. The cells were lysed with a French press by two passes through at 20,000 psi, and the debris was pelleted at 10,000*g* for 15 min at 4 °C. The supernatant was collected and diluted 4-fold with deionized H_2O. This sample was loaded onto a Macro Prep Q anion-exchange column (2 x 10 cm) that was equilibrated with buffer A (50 mM Tris pH 8.0, 1 mM EDTA). The column was then washed with 30 mL of buffer A. The buffer was then changed to 30% buffer B (50 mM Tris pH 8.0, 1 mM EDTA, 1 M NaCl)[30% B/70% A] for a total of 15 mL. APH(3')-IIIa was then eluted with a linear gradient of 30% B to 50 % B over a 60 mL volume. The column was rinsed with 50% B over 30 mL followed by 100% B for 45 mL. The column was then regenerated with 60 mL of

buffer A.

The fractions from the gradient elution that contained APH(3′)-IIIa were identified by enzymatic assay (as described previously) and SDS-PAGE. The fractions containing the enzyme were pooled and dialyzed against 4 L of buffer A. The sample was then treated with DNAse (15 μg/mL) at room temperature for 1 h to digest DNA. Following this incubation, the sample was loaded back on the MacroPrep Q column and eluted with the same buffer profile. The fractions were analyzed as before and the fractions that contained APH(3′)-IIIa were pooled. The concentration of the enzyme was calculated spectrophotometrically at A_{280} (ε = 4.8 x 10^4 M^{-1} cm^{-1}).

3. TRNOESY experiments

APH(3′)-IIIa was first dialyzed against 2 mM Tris-d_{11} buffer (pH 6.8) in order to avoid the interference of Tris protons. The enzyme was then exchanged into ^2H_2O by three cycles of lyophilization and redissolving in ^2H_2O. The aminoglycosides and ATP were dissolved directly into ^2H_2O, underwent two cycles of lyophilization, and redissolved in D_2O. Samples contained 0.20 mM APH(3′)-IIIa, 5 mM antibiotic (amikacin, butirosin A, or ribostamycin), 5 mM ATP, 5 mM $CaCl_2$, and 20 mM d_{11}-Tris buffer (pH 6.8). The TRNOESY spectra were collected in the TPPI mode with the transmitter offset placed on the $^1H^2HO$ resonance, which was irradiated with low power during a relaxation delay of 1.8 s to suppress the H_2O signal. A total of 256 FIDs of 2k data were collected. Mixing times of 40, 80, 120,

and 160 ms were employed in the amikacin and butirosin A experiments while mixing times of 30, 60, 90, and 120 ms were used in the ribostamycin experiments. The data were zero-filled to 1k points in t_1 and were multiplied by a shifted sine^2 window function before Fourier transformation.

4. ^1H-^1H Distance Calculations

The volume of the TRNOE cross-peaks in the TRNOESY experiments was calculated in the FELIX 95 software package (BIOSYM/Molecular Simulations) operating on a Silicon Graphics Indigo^2 workstation. The 80 and 90 ms experiments were used in distance calculations for butirosin A and ribostamycin, respectively. The volume of the cross-peak between H-1′ and H-2′ was taken to represent a calibration distance of 2.38 Å for each antibiotic. The remaining TRNOE volumes were converted into distance constraints by using measured cross-peak volumes, which are proportional to the sixth power of the distance between proton pairs (Gronenborn & Clore, 1985; Scheffler *et al.*, 1995; Casset *et al.*, 1996). A generous error of ±40% was employed for the TRNOE cross-peak volumes used to calculate the distance constraints (Scheffler *et al.*, 1995). %NOE values were calculated by dividing the volume of a cross-peak by the volume of the H3‴-H3‴ cross-peak at each mixing time and multiplying by 100 for amikacin and butirosin A. The H2a-H2e proton pair was used in the %NOE calculations for ribostamycin instead of the H3‴-H3‴ pair, which is not present in ribostamycin.

5. *Energy Minimization and Molecular Dynamics*

Butirosin A and ribostamycin were created in Insight II (BIOSYM/Molecular Simulations) operating on a Silicon Graphics Indigo^2 workstation. All calculations were accomplished with the AMBER forcefield (Weiner *et al.*, 1986) interfaced with the molecular mechanics package DISCOVER (BIOSYM/Molecular Simulations) on the same workstation. All potential types and charges of the aminoglycosides were set according to Homans' potential types for carbohydrates in the AMBER forcefield (Homans, 1990; Ha *et al.*, 1988). In butirosin A, the amino groups of the antibiotics were protonated and the nitrogens of these groups were given a formal charge of +1.00. In ribostamycin, the amino group nitrogens were given a formal charge of +0.50, except for N-6′ which was given a formal charge of +1.00. All of the formal charges were assigned based on the determined pK_a values (Chapter II).

To generate random structures of the aminoglycosides, they were subjected to unrestrained molecular dynamics at 600 K for 1000 ps. Distance restraints, derived from the TRNOE studies, were applied to the random structures and they underwent restrained molecular dynamics (500 ps) followed by conjugate gradient minimization (100 iterations) at 400 K, 350 K, and finally 300 K. As the final step, the structures underwent steepest descents or conjugate gradients minimization until the rms derivative was less than 0.001 kcal/Å. All calculations were carried out *in vacuo* with a dielectric constant of 4.00 and all force constants for the distance restraints were 50 kcal/mole•Å. In butirosin A, the *pro*-R and *pro*-S protons of C-5″ have the same chemical shift at the pH in which the TRNOESY experiments were

carried out. The distance restraints reported that involved H-5″ were assigned to the pro-S hydrogen. Similar structures were obtained when the restraints were applied to the pro-R hydrogen.

C. Results and Discussion

1. APH(3′)-IIIa-Bound Butirosin A

Complete NOE buildup curves were obtained for butirosin A by recording the TRNOESY spectra at different mixing times (Figure V-2). The intensities of the NOEs and the shape of the buildup curves suggest that spin diffusion is not significant at shorter mixing times. Therefore, a mixing time of 80 ms was chosen for data analysis because all of the NOEs were well developed, and this mixing time is in the linear part of the buildup curve for all of the observed NOEs.

A total of 32 TRNOEs was observed for butirosin A in the APH(3′)-IIIa•ATP•Butirosin A ternary complex. There were 17 intra-ring TRNOEs that serve to define the conformation of the three rings. A total of 5 intra-chain NOEs were observed among the protons of the AHB chain. The remaining 10 TRNOEs are inter-ring/chain and serve to define the conformational nature of enzyme-bound butirosin A. These NOEs are listed in Table V-1, with the distance restraints derived from the data obtained in the 80 ms TRNOE experiment. A portion of this spectrum is presented in Figure V-3, which shows interglycosidic and long range TRNOEs.

Eight of the final structures generated from the dynamics and minimization routines were superimposed at the 2-DOS ring and appear in Figure V-4. The

glycosidic dihedral angles of butirosin A can be defined as Φ_1 (H1′-C1′-O_α-C4), Ψ_1 (H4-C4-O_α-C1′), Φ_2 (H1″-C1″-O_β-C5), and Ψ_2 (H5-C5-O_β-C1″). The average values of these dihedral angles for the eight butirosin A structures are as follows: $\Phi_1 = 11° \pm 6°$, $\Psi_1 = 49° \pm 3°$, $\Phi_2 = 13° \pm 18°$, and $\Psi_2 = 48° \pm 3°$. In Figure V-5A and V-5B, the eight butirosin A structures are again superimposed; however, only the ring atoms, 3′(3A)-oxygens, and 5″(5C)-oxygens are shown. The structures of butirosin A presented in Figures V-4 and V-5 do not violate the distance restraints (within the error limits) derived from the TRNOE studies.

Previous paramagnetic NMR relaxation studies suggested that enzyme-bound butirosin A has the 2,6-diamino-2,6-dideoxy-D-glucose (ring A) and D-xylose (ring C) rings in a stacking arrangement (Chapter IV). This allows both the 3′(3A)- and 5″(5C)-OH groups to be extended out toward the γ-phosphoryl group of ATP in the ternary complex. The fact that there were four TRNOEs between H-5″ and ring A suggests that rings A and C are close to each other. In fact, the superimposed structures of butirosin A in Figure V-5B also show that these two rings are in a stacking arrangement in enzyme-bound butirosin A. Figure V-4 shows that the three rings of butirosin A have restricted motions when bound to the active-site of APH(3′)-IIIa. On the other hand, the AHB chain can adopt a variety of conformations.

The distance restraints, derived from the 17 intra-ring TRNOEs and molecular modeling studies, show that rings A and B adopt chair conformations as presented in Figure II-2, with the amino, hyroxyl, and hydroxymethyl groups

occupying equatorial positions. The pyranose ring (ring A) of butirosin A has a rigid conformation with a $^4C_1$ conformation.

Figures V-5A and V-5B focus on the relative positions of the 3′(3A)- and 5″(5C)-oxygens. In some structures, the 5″(5C)-oxygens are extended outward in the same plane as the 3′(3A)-oxygens. In the remaining structures, the 5″(5C)-oxygens are pointing in the opposite direction and not in an optimal position to be involved in a nucleophilic attack on the γ-phosphate of ATP. This may explain the observed preference for the initial phosphorylation event to occur at the 3′(3A)-OH of butirosin A. In fact, initial phosphorylation at this site occurs between 70-75% of the time, with the second phosphorylation reaction occuring at the 5″(5C)-OH (Thompson *et al.*, 1996a).

The initial phosphorylation of butirosin A is much faster than the second phosphorylation reaction. This is not observed with ribostamycin and neomycin B, other 4,5-disubstituted aminoglycosides with 3′(3A)- and 5″(5C)-OH groups, because both the phosphorylation reactions occur at approximately equal rates. The fact that ribostamycin and neomycin B do not have the AHB group at N-1, and they are easily diphosphorylated, point to an important role of the AHB group in the recognition of phosphorylated butirosin A by APH(3′)-IIIa.

It is intriguing that monophosphorylated butirosin A can bind to APH(3′)-IIIa and put the 3′(3A)- or 5″(5C)-OH into a reactive position. One plausible explanation is that the negatively charged phosphoryl group of monophosphorylated butirosin A is directed toward the positively charged Mg^{2+} ion

of MgATP. This would prevent the 3′(3A)- or 5″(5C)-phosphoryl group from directly approaching the γ-phosphoryl group of ATP and avoid steric and electronic repulsion. A model can be built where the 3′(3A)-phosphoryl group of butirosin A coordinates Mg^{2+} and the 5″(5C)-OH is colinear and approximately 4 Å from the γ-phosphate of ATP. This model conserves the stacking of rings A and C, which seems to persist in solution and at the active site of the enzyme, but overall requires a different arrangement of the antibiotic with respect to the triphosphate moiety of ATP. This is not unreasonable because APH(3′)-IIIa phosphorylates a broad range of substrates with different ring architectures. Additionally, the coordination of the phosphoryl group of 3-phospho-D-glycerate, to the metal ion of a MeATP complex, has been shown to occur in the phosphorylation reaction catalyzed by phosphoglycerate kinase (PGK), to produce 1,3-bisphosphoglycerate (Pappu *et al.*, 1994). Conformational studies with 3′-phosphorylated butirosin A, both in solution and bound to APH(3′)-IIIa, is a logical extension of the work presented in this chapter.

2. APH(3′)-IIIa-Bound Amikacin

There were a total of 23 TRNOEs observed for amikacin in the APH(3′)-IIIa•ATP•Amikacin ternary complex. However, spectral overlap of important NOEs prevented a quantitative analysis. A portion of the 80 ms mixing time experiment is presented in Figure V-6. In this spectrum, the H1″-H5 and H1″-H6 NOEs are under the same cross-peak (g). Also, the H1′-H5 and H1′-H3′ NOEs appear

under the same cross-peak (h) in the 80 ms experiment. The assignment of H-5, H-6, and H-3′ in these two cross-peaks comes from the one-dimensional ^{1}H assignments of amikacin (Anderson *et al.*, 1988; Thompson *et al.*, 1996a) and additional connectivities in the TRNOESY spectra.

In the TRNOESY spectrum presented in Figure V-6, there are three strong TRNOEs across the glycosidic linkage involving H-1′. The TRNOEs H1′-H5, H1′-H4, and H1′-H3 are visible even in the shortest mixing time experiment (40 ms). The observed intensity of the overlapping H1′-H5 and H1′-H3′ cross-peak (h) indicates that a strong H1′-H5 TRNOE must contribute to the volume of this cross-peak. The H1′-H3′ contribution to this cross-peak should be minor due to the distance between these two protons in the chair conformation of the primed ring (ring A). Therefore, the H1′-H5 cross-peak should be the major contributor to the intensity of cross-peak h in Figure V-6. The observation of strong H1′-H3 and H1′-H5 TRNOEs, along with modeling studies, suggest that different enzyme-bound conformations of amikacin are present in ternary complexes in which there are significant differences in the glycosidic torsional angles around O_α, which links ring A and ring B.

One could argue that the enzyme binds amikacin in which ring A can have a variety of Φ and Ψ values. This would create a population of APH(3′)-IIIa•ATP•Amikacin ternary complexes in which the 3′(3A)-OH of amikacin is in a reactive position and a population where the 3′(3A)-OH is not in the correct position to attack the γ-phosphate of ATP. Alternatively, ring A may be mobile

while amikacin is bound to the active site of the enzyme. If ring A adopts a conformation where the 3′(3A)-OH can attack the γ-phosphoryl group of ATP, phosphorylation can occur and the modified antibiotic will be released. In some cases, ring A may not place the 3′(3A)-OH into a reactive position and the antibiotic will be released unmodified. Support for the above hypotheses may come from the fact that the phosphorylation of amikacin, catalyzed by APH(3′)-IIIa, is inefficient compared to other aminoglycoside antibiotics, and its k_{cat}/K_m value is 6 to 27 times lower than the value for other aminoglycoside substrates (McKay *et al.*, 1994).

Intra-ring transfer NOEs observed between the protons of amikacin support the chair conformations of rings A, B, and C presented in Figure II-1. For example, the following strong transfer NOEs were observed in these rings: H3′-H5′, H3″-H5″, and H2ax-H6. This suggests that all of the amino, hydroxyl, and hydroxymethyl groups in amikacin occupy equatorial positions, with the pyranose rings adopting a $^4C_1$ conformation.

The results from the paramagnetic NMR relaxation and TRNOE studies of amikacin provide insight into the interaction of this antibiotic with APH(3′)-IIIa. Amikacin is structurally unique among other substrates of the enzyme. It is 4,6-disubstituted at the 2-DOS ring which is modified at N-1 with the AHB group. These unique structural features most likely dictate the geometry and dynamics of enzyme-bound amikacin.

3. APH(3′)-IIIa-Bound Ribostamycin

In the TRNOE experiments with ribostamycin, mixing times of 30, 60, 90, and 120 ms were used and %NOE buildup curves suggests that spin diffusion was not significant at 90 ms, the mixing time used for the distance calculations.

A portion of the 90 ms TRNOESY spectrum of ribostamycin is shown in Figure V-7 with a few important long-range TRNOEs labeled. The inter-ring TRNOEs observed with the anomeric protons (H-1′ and H-1″) were the most important in determining the conformation of enzyme-bound ribostamycin. A total of 34 TRNOEs was observed for ribostamycin in the APH(3′)-IIIa•ATP•Ribostamycin ternary complex. There were 25 intra-ring transfer NOEs that served to define the conformation of the three rings. The remaining 9 TRNOEs were inter-ring and serve to define the conformational nature of enzyme-bound ribostamycin. These TRNOEs are listed in Table V-2, with the distance restraints derived from the data obtained in the 90 ms TRNOE experiment.

The modeling studies yielded two conformers of ribostamycin that fit the distance restraints derived from the TRNOESY experiments. A representative structure of each conformer (1 and 2) appear in Figure V-8. Conformer 1 and 2 are each a representative structure of six similar conformations.

Important H-bonds may play a role in stabilizing the two conformers. The hydrogen of the 6(6B)-OH is in a position to form a H-bond with the oxygen of 2″(2C)-OH in both conformers. In conformer 1, a hydrogen of the 2′(2A)-NH_2 is in a position to form a H-bond with O_β of the β-glycosidic bond between rings B

and C. In conformer 2, a hydrogen of the 2′(2A)-NH_2 is in a position to form a H-bond with the oxygen of the ribose ring. These two structures can be classified according to the spatial relationship between ring A and ring C. Conformer 1 has rings A and C in a stacking arrangement and in conformer 2 the rings are bisecting. The glycosidic dihedral angles of the structures that are represented by conformer 1 can be defined as Φ_3 (H1′-C1′-O_α-C4), Ψ_3 (H4-C4-O_α-C1′), Φ_4 (H1″-C1″-O_β-C5), and Ψ_4 (H5-C5-O_β-C1″). The glycosidic dihedral angles of the structures that are represented by conformer 2 are defined as the same atoms but are denoted with a 5 (α-glycosidic) and 6 (β-glycosidic). The average values are as follows: $\Phi_3 = -35 \pm 5°$, $\Psi_3 = -30 \pm 10°$, $\Phi_4 = -4 \pm 3°$, $\Psi_4 = 45 \pm 2°$, $\Phi_5 = -21 \pm 11°$, $\Psi_5 = 39 \pm 18°$, $\Phi_6 = -14 \pm 6°$, and $\Psi_6 = 50 \pm 9°$. Φ vs. Ψ plots for the two glycosidic bonds of enzyme-bound ribostamycin (Figures V-9 and V-10) show that there are two enzyme-bound conformers. These figures clearly show that the principle difference between the two classes of conformers is the conformation around the α-glycosidic bond between rings A and B.

An interesting feature of the superimposed structures (at ring B) of conformer 1 and conformer 2 is that both of them put the 3′(3A)- and 5″(5C)-OH groups in a similar position (Figure V-11). Therefore, both conformations allow the reactive hydroxyl groups to be extended out toward ATP at the active site of APH(3′)-IIIa.

The APH(3′)-IIIa-bound structures of butirosin A and ribostamycin (conformer 1) are very similar with rings A and C in a stacking arrangement. Additionally, three of the four dihedral angles described above for enzyme-bound

ribostamycin (Ψ_3, Φ_4, and Ψ_4) are the same (within error limits) for enzyme-bound butirosin A (Ψ_1, Φ_2, Ψ_2). APH(3′)-IIIa can catalyze the diphosphorylation of both butirosin A and ribostamycin but with different rates of the second phosphorylation reaction (Thompson *et al.*, 1996a). Since these antibiotics can adopt a similar conformation at the active site of APH(3′)-IIIa, the observed differences in the kinetics of phosphorylation must be due to a different arrangement with respect to ATP. This is most likely mediated by the AHB group of butirosin A.

The other conformer of ribostamycin (conformer 2) is similar to the recently reported structure of paromomycin complexed to a 27-nucleotide piece of rRNA (Figure V-12A) (Fourmy *et al.*, 1996). In Figure V-12B, a representative structure of each are superimposed at the 2-DOS ring (ring B). The fact that aminoglycosides can adopt similar conformations when bound to a modifying enzyme and to its natural RNA target can have significant implications in drug design. Efforts to design nonaminoglycoside phosphotransferase inhibitors, based on the structure of ribostamycin (conformer 2), might also yield molecules with antibacterial activity.

Recently, a great deal of attention has been focused on the structure of complexes formed by RNA aptamers, especially with the report of paromomycin (Fourmy *et al.*, 1996) and tobramycin (Jiang *et al.*, 1997) bound to RNA. Other studies have demonstrated that RNA is similar to proteins in that binding sites can be created that allows specificity in complex formation (Egli, 1997). This report is significant in that it demonstrates that a molecule can use a similar conformation to bind both protein- and RNA-based targets.

Chapter VI

General Discussion and Conclusions

This research has yielded the arrangement and conformation of APH(3′)-IIIa-bound aminoglycoside antibiotics. The results provide insight into the structural basis in which APH(3′)-IIIa catalyzes the phosphorylation of a broad range of aminoglycosides. This work has provided a foundation for the comparison of aminoglycoside structures when bound to different modifying enzymes and a rational drug design program to design inhibitors of aminoglycoside phosphotransferases. It has also provided insight into how a particular class of molecules can bind both protein and RNA.

The work presented in this dissertation shows the evolution of an NMR project. The first part of the project was based on the assignment of the one-dimensional ^{1}H NMR assignments of a few aminoglycosides. This work set the stage for more advanced two-dimensional NMR experiments to determine the structure of aminoglycosides bound to APH(3′)-IIIa. This project also demonstrated the synergy between NMR-derived distance restraints and computational chemistry. In the literature today, there are many reports of the use of NMR spectroscopy to solve the structure of important biological molecules. Without exception, an initial study had to be performed to determine the one-dimensional assignments (^{1}H,^{13}C,^{15}N) of the molecule. The data derived from NMR does not directly yield structural information. NMR techniques yield distance restraints between two atoms of a

molecule, which have to be translated into a structure. There are a variety of computer programs and modeling packages available for structure determination. Overall, all of the computational approaches involve the use of classical molecular mechanics/dynamics. The advances and continuing challenges in this field have recently been reviewed by Dr. Peter Kollman, a leader in the field (Kollman, 1996).

The work presented in Chapter II demonstrates the large body of work that is needed to provide the foundation for structural studies. The importance of NMR studies on nuclei other than ^{1}H, which is the most utilized nucleus in biological NMR because of its natural abundance (99.98%), is also demonstrated. ^{15}N NMR spectroscopy was used to determine the pK_a values of the amino groups of various aminoglycosides. This was important because aminoglycosides have many amino groups, and studies have shown that electrostatic interactions are important in their complexation with proteins and RNA (Roestamadji *et al.*, 1995; Clouet-d'Orval *et al.*, 1995). The problem with ^{15}N NMR on aminoglycosides is that ^{15}N has a very low natural abundance (0.36%) and high concentrations of sample are necessary. ^{15}N-labeled aminoglycosides are not available. However, aminoglycosides are produced naturally by certain organisms. For example, *Bacillus circulans* produces butirosin and *Streptomyces kanamyceticus* produces kanamycin. These and other strains are commercially available in the American Type Culture Collection (ATCC) catalog. A future project could include producing ^{15}N-labeled aminoglycosides from these organisms if they are cultured in media that contains a ^{15}N-labeled salt (such as $^{15}NH_4Cl$).

Exchange-inert metal-ATP analogs have been extremely useful in studying ATP-utilizing enzymes (Pappu *et al.*, 1994; Gregory & Serpersu, 1993; Serpersu *et al.*, 1992; Wolkers *et al.*, 1991). The utility of CrATP relies on the fact that it is a paramagnetic species. Chapters III and IV describe how CrATP was used to determine the binding constants that describe ternary complex formation with antibiotics and APH(3′)-IIIa, along with Cr^{3+}(CrATP)-to-^{1}H (antibiotic) distances in these ternary complexes. Although preliminary studies with RhATP and APH(3′)-IIIa were performed, this metal-ATP analog can be used further to map out the metal-coordination region in APH(3′)-IIIa (Pappu *et al.*, 1997). This will complement the X-ray studies of APH(3′)-IIIa.

Solving the X-ray structure of APH(3′)-IIIa may be an important event in understanding antibiotic resistance. The fact that the 3D structure of APH(3′)-IIIa is similar to that of cAPK suggests that bacteria sculpted the phosphotransferase-modifying enzymes from cAPK or similar protein kinases. From an antibiotic resistance point of view, cAPK would be an excellent kinase to emulate. It is the prototypic model of a multisubstrate protein kinase (Walsh & van Patten, 1994). In fact, all of the APH(3′)s are also multisubstrate (Shaw *et al.*, 1993), which allows them to phosphorylate, and thus detoxify, a great number of existing aminoglycosides.

How can enzymes such as cAPK and APH(3′)-IIIa each bind and regiospecifically phosphorylate such structurally diverse substrates? In the case of cAPK, studies have shown that the sequence of amino acids around the

phosphorylation site in the substrate contain the structural elements for recognition by cAPK. After comparing the sequences of the substrates of cAPK, a consensus phosphorylation sequence of -LRRAS*LG-, where S* is the phosphorylated serine residue, along with a hydrophobic residue in the P-11 position (11 residues on the amino side of the serine) was suggested (Kemp *et al.*, 1994). When the crystal structure of the catalytic subunit of cAPK was solved with a tight binding inhibitor (PKI), the function of the consensus site residues became apparent (Knighton *et al.*, 1991). The arginine residues (P-2, P-3) make electrostatic contacts with glutamate residues on the enzyme, while the L (P+1) and F (P-11) residues of PKI fit into hydrophobic binding pockets on cAPK. The family of substrates for cAPK have all or some of the residues in the consensus sequence described above. The results clearly show that the number of contacts (electrostatic/hydrophobic) that are made by substrates (with cAPK) will determine how efficacious each is as a substrate (Walsh & van Patten, 1994).

The case does not seem that straightforward with APH(3′)-IIIa. The results presented in Chapter IV suggest that aminoglycosides can bind to APH(3′)-IIIa with different arrangements with respect to ATP. As discussed in Chapter IV, the same functional groups on the aminoglycosides do not necessarily have to make the important contacts with the enzyme. This may be how a variety of aminoglycosides, with different patterns of hydroxyl and amino groups and a variety of ring architectures, are accommodate in the active site. Generally, when a ligand interacts with a protein binding site, the specificity of the interaction can be

mediated by surface and/or electrostatic complementarity. The active site of APH(3′)-IIIa seems to be larger than the aminoglycosides it binds, as demonstrated by the binding of both neamine (2 rings) and lividomycin A (5 rings). Attractive r^{-6} dispersion forces can only dominate a binding event if there is surface complementarity. Therefore, with aminoglycosides, which are polar and charged, the major driving force for complexation to APH(3′)-IIIa is probably electrostatic. Different arrangements and conformations of enzyme-bound aminoglycosides may have to bind in their own unique way to find contacts with the enzyme necessary for complexation. An excellent example is amikacin, which is the worst substrate of APH(3′)-IIIa. Its catalytic efficiency (k_{cat}/K_m) is 6 to 27 times lower than the efficiency of other substrates. The results in Chapter V suggest that amikacin has different conformations that can bind the enzyme or that its enzyme-bound structure is flexible about the glycosidic bond between rings A and B. Amikacin also has the AHB group at N-1, which may disrupt its interaction with the enzyme. Taken together, these facts suggest that amikacin is inefficient at orienting itself correctly to make necessary contacts with the enzyme and/or placing the 3′(3A)-OH in the proper orientation with respect to the γ-phosphate of ATP.

This project was initiated approximately four years ago, long before the relationship between APH(3′)-IIIa and cAPK was understood or the X-ray structure of APH(3′)-IIIa was known. There was a possibility that the X-ray structure may not be solved or that a ternary complex may not be crystallized. Even if a ternary complex was crystallized and the structure solved, it is extremely doubtful that

several structures would be solved to represent the variety of aminoglycosides that are substrates of the enzyme. However, NMR techniques were available to determine the structure of APH(3′)-IIIa-bound aminoglycosides that required no knowledge of the target enzyme. Now that the X-ray structure of APH(3′)-IIIa has been solved, the results presented in Chapters IV and V may be able to complement this structure and allow for a more complete description of ternary complex formation. This is an excellent example of how X-ray and NMR techniques can be used together to study enzyme-substrate interactions.

The APH(3′)-IIIa-bound structures can also be used as a template for the design of inhibitors of APH(3′)-IIIa. Electrostatics play a large role in a variety of biological process. Recently, it has been suggested that determining the similarity in the electrostatic environment of molecules may be a useful tool in drug design (Apaya *et al.*, 1995). One way of determining molecular electrostatic similarity is to examine the overlay of the maxima and minima in the electrostatic potential outside the molecules (Náray-Szabo & Ferenczy, 1995). This approach has been validated in a study of phosphodiesterase III inhibitors (Apaya *et al.*, 1995). Accurate calculations of the electrostatic potential can be derived from a calculation of the Poisson-Boltzmann equation (PBE) (Honig and Nicholls, 1995). A matching of the electrostatic extrema should be a good method to determine if molecules can bind to the same site. Alternatively, the transition state structure of the kinase reaction can be used to design inhibitors of the enzymatic reaction (Bagdassarian *et al.*, 1996). The electrostatic potential of the 3D structure of APH(3′)-IIIa can also be

calculated. It would be interesting to see if regions of positive charge on the aminoglycosides match regions of negative charge in the active site of the enzyme.

CAVEAT (Lauri and Bartlett, 1994) is designed to aid the structure-based design of enzyme inhibitors and related bioactive molecules. CAVEAT uses the relative orientation of bond vectors in a 3D target structure in order to identify rigid structural templates for molecular design. CAVEAT focuses on the orientation of bonds and not the precise location of atoms in the target molecule (which can be a NMR-derived structure). In essence, CAVEAT is designed to search and receive, from a database of 3D structures, molecules with specific bonds that match a vector relationship specified by the target structure. In CAVEAT, the geometrical attributes of the bonds in the target molecule rather than their chemical or electronic character is the important factor. This program is not designed to generate complete molecules but to provide structural ideas. In CAVEAT, important structural elements can be given greater weight in the search algorithm. Therefore, molecular recognition studies that identify important residues or groups on a ligand can be combined with CAVEAT to carry out efficient searches based only on the important attributes of the ligand. CAVEAT is compatible with several large 3D databases such as the Cambridge Structural Database (Allen *et al.*, 1983) and the Protein Data Bank. The usefulness of CAVEAT has been demonstrated in the design of α-amylase inhibitors (Kuntz *et al.*, 1994) and peptidomimetics (Tian & Bartlett, 1996).

The NMR-derived structures of butirosin A and ribostamycin, or a transition state structure (using the enzyme-bound structures) can be used with CAVEAT to try

to identify non-aminoglycosides that have similar geometric characteristics. If some molecules are identified, they can be tested as inhibitors of APH(3′)-IIIa. However, in many cases CAVEAT does not identify complete molecules but provides structural ideas in the form of rigid structural templates. These templates may provide the framework for a potential inhibitor, but additional synthetic work may be required to produce an inhibitor.

In conclusion, this project demonstrated the close relationship that can exist between NMR spectroscopy and X-ray crystallography and the relationship that always exists between NMR spectroscopy and computational chemistry in structure determination. Overall, the results presented in this dissertation help corroborate and explain both mechanistic and kinetic information previously obtained on APH(3′)-IIIa. Additionally, this work has allowed the comparison of protein- and RNA-bound aminoglycosides and has provided a foundation for a drug design program that can be used to design nonaminoglycoside phosphotransferase inhibitors to help combat antibiotic resistance.

LIST OF REFERENCES

List of References

Abraham, E. P., & Chain, E. (1940) *Nature* **146**, 827.

Allen, F. H., Kennard, O., & Taylor, R. (1983) *Acc. Chem. Res.* **16**, 146-153.

Anderson, N. H., Eaton, H. L., Nguyen, K. T., Hartzell, C., Nelson, R. J., & Priest, J. H. (1988) *Biochemistry*, **27**, 2782-2790.

Apaya, R. P., Lucchese, B., Price, S. L., & Vinter, J. G. (1995) *J. Comput.-Aided Mol. Design* **9**, 33-43.

Bagdassarian, C. K., Schramm, V. L., & Schwartz, S. D. (1996) *J. Am. Chem. Soc.* **118**, 8825-8836.

Barsukov, I. L., Lian, L. -Y., Ellis, J., Sze, K. -H., Shaw, W. V., & Roberts, G. C. K. (1996) *J. Mol. Biol.* **262**, 543-558.

Bax, A. (1983) *J. Magn. Reson.* **53**, 517-520.

Bax, A. & Davis, D. G. (1985) *J. Magn. Reson.* **65**, 355-360.

Bax, A. & Grzesiek, S. (1993) *Acc. Chem. Res.* **26**, 131-138.

Berkelman, R. L. & Hughes, J. M. (1993) *Ann. Intern. Med.* **119**, 426-428.

Bloch, F. (1957) *Phys. Rev.* **105**, 1206-1222.

Blomberg, F. & Rüterjans, H. (1983) in *Biological Magnetic Resonance* (Berliner, L. J. & Reuben, J., Eds.) Ch. 2, Plenum Press, New York.

Blommers, M. J. J., Fendrich, G., García-Echeverría, C., & Chêne, P. (1997) *J. Am. Chem. Soc.* **119**, 3425-3426.

Botto, R. E. & Coxon, B. (1983) *J. Am. Chem. Soc.* **105**, 1021-1028.

Bryan, L. E. (1989) in *Microbial Resistance to Drugs* (Bryan, L. E., Ed.) Ch. 2, Springer-Verlag, Berlin.

Braunschweiler, L. & Ernst, R. R. (1983) *J. Magn. Reson.* **53**, 521-528.

Brünger, A. T., Adams, P. D., & Rice, L. M. (1997) *Current Biology* **5**, 325-336.

Bryan, L. E. & Godfrey, A. J. (1991) in *Antibiotics in Laboratory Medicine, 3rd ed.* (V. Lorian, Ed.) Ch. 16, Williams and Wilkins, Baltimore.

Bush, C. A. (1992) *Curr. Opin. Struc. Biol.* **2**, 655-660.

Bush, C. A. (1994) *Methods Enzymol.* **240 (20)**, 446-459.

Campbell, A. P. & Sykes, B. D. (1993) *Annu. Rev. Biophys. Biomol. Struct.* **22**, 99-122.

Carr, H. Y. & Purcell, E. M. (1954) *Phys. Rev.* **94**, 630-638.

Casset, F., Peters, T., Etzler, M., Korchagina, E., Nifant'ev, N., Pérez, S., & Imberty, A. (1996) *Eur. J. Biochem.* **239**, 710-719.

Chu, D. T. W., Plattner, J. J., & Katz, L. (1996) *J. Med. Chem.* **39**, 3853-3874.

Cleland, W. W. & Mildvan, A. (1979) *Adv. Inorg. Biochem.* **1**, 163-169.

Clore, G. M. & Gronenborn, A. M. (1982) *J. Magn. Reson.* **48**, 402-417.

Clouet-d'Orval, B., Stage, T. K., & Uhlenbeck, O. C. (1995) *Biochemistry* **34**, 11186-11190.

Cotton, F. A., Wilkinson, G., & Gaus, P. L. (1987) *Basic Inorganic Chemistry*, Ch. 24, Wiley, New York.

Davies, J., Gorini, L., & Davis, B. D. (1965) *Mol. Pharmacol.* **1**, 93-106.

Davies, J. (1991) in *Antibiotics in Laboratory Medicine, 3rd ed.* (V. Lorian, Ed.) Ch. 18, Williams and Wilkins, Baltimore.

Davies, J. (1994) Science **264**, 375-381.

Davis, D. G. & Bax, A. (1985) *J. Am. Chem. Soc.* **107**, 2820-2821.

DeBondt, H., Rosenblatt, J., Jancarik, J., Jones, H. D., Morgan, D. O. & Kim, S.- H. (1993) *Nature* **363**, 595-602.

DePamphilis, M. L. & Cleland, W. W. (1973) *Biochemistry* **12**, 3714-3723.

Dorman, D. E., Paschal, J. W., & Merkel, K. E. (1976) *J. Am. Chem. Soc.* **98**, 6885-6888.

Douglas, E. B. (1983) *Concepts and Methods of Inorganic Chemistry*, 2nd ed., Ch. 9, Wiley, New York.

Dunaway-Mariano, D. & Cleland, W. W. (1980a) *Biochemistry* **19**, 1506-1515

Dunaway-Mariano, D. & Cleland, W. W. (1980b) *Biochemistry* **19**, 1496-1505.

Egli, M. (1997) *Angew. Chem. Int. Ed. Engl.* **36**, 480-482.

Eneva, G. I. & Spassov, S. L. (1991) *Spectrochim. Acta* **47A**, 875-880.

Espinosa, J. -F., Cañada, F. J., Asensio, J. L., Dietrich, H., Martin-Lomas, M., Schmidt, R. R., & Jiménez-Barbero, J. (1996) *Angew. Chem. Int. Ed. Engl.* **35**, 303-306.

Fersht, A. (1985) *Enzyme Structure and Mechanism*, 2nd ed., Ch. 8, W. H. Freeman, New York.

Foster, D. M. & Mildvan, A. S. (1972) *Bioinorg. Chem.* **1**, 133-139.

Fourmy, D., Recht, M. I., Blanchard, S. C., & Puglisi, J. D. (1996) *Science* **274**, 1367-1371.

Fry, D. C., Kuby, S. A., & Mildvan, A. S. (1985) *Biochemistry* **24**, 4680-4694.

Geyer, A., Hummel, G., Eisele, T., Reinhardt, S., & Schmidt, R. R. (1996) *Chem. Eur. J.* **2**, 981-988.

Gronenborn, A. M. & Clore, G. M. (1985) *Prog. Nucl. Magn. Reson. Spectrosc.* **17**, 1-32.

Gliemann, G. & Schläfer, H. L. (1969) *Basic Principles of Ligand Field Theory*, Ch. 5, Wiley, New York.

Gounarides, J. S., Broido, M. S., Becker, J. M., & Naider, F. R. (1993) *Biochemistry* **32**, 908-917.

Gregory, J. D. & Serpersu, E. H. (1993) *J. Biol. Chem.* **268**, 3880-3888.

Gupta, R. K., Fung, C. H., & Mildvan, A. S. (1976) *J. Biol. Chem.* 251, 2421-2430.

Ha, S. N., Giammona, A., Field, M., & Brady, J. W. (1988) *Carbohydr. Res.* **180**, 207-221.

Heinzel, P., Werbitsky, O., Distlen, J., & Piepersberg, W. (1988) *Arch. Microbiol.* **150**, 184-192.

Hicks, R. P., Young, J. K., & Moskau, D. (1994) *Concepts Magn. Reson.* **6**, 115-130.

Homans, S. W. (1990) *Biochemistry* **29**, 9110-9118.

Hon, W.- C., McKay, G. A., Thompson, P. R., Sweet, R. M., Yang, D. S. C., Wright, G. D., & Berghuis, A. M. (1997) *Cell* **89**, 887-895.

Honig, B. & Nicholls, A. (1995) *Science* **268**, 1144-1149.

Hooper, I. R. (1982) in *Aminoglycoside Antibiotics* (Umezawa, H. & Hooper, I. R., Eds.) Ch. 1, Springer-Verlag, Berlin.

Hubbard, S. R., Wei, L., Ellis, L. & Hendrickson, W. A. (1994) *Nature* **372**, 746-754.

Jiang, L., Suri, A. K., Fiala, R., & Patel, D. J. (1997) *Chemistry & Biology* **4**, 35-50.

Jørgensen, K. (1956) *Acta Chem. Scand.* **10**, 500-517.

Kawaguchi, H. T., Naito, T., Nakagawa, S., & Fujisawa, K. (1972) *J. Antibiot.* **25**, 358-363.

Kemp, B. E., Parker, M. W., Hu, S., Tiganis, T., & House, C. (1994) *Trends Biochem. Sci.* **19**, 440-444.

Knighton, D. R., Zheng, J., Ten Eyck, L. F., Xuong, N. -H., Taylor, S. S., & Sowadski, J. M. (1991) *Science* **253**, 401-413.

Kocabiyik, S., & Perlin, M. H. (1992) *FEMS Microbiol. Lett.* **93**, 199-202.

Kollman, P. A. (1996) *Acc. Chem. Res.* **29**, 461-469.

Kunin, C. M. (1993) *Ann. Intern. Med.* **118**, 557-561.

Kuntz, I. D., Meng, E. C., & Schoichet, B. K. (1994) *Acc. Chem. Res.* **27**, 117-123.

Lauri, G. & Bartlett, P. A. (1994) *J. Comp.-Aided Mol. Design* **8**, 51-66.

Lemieux, R. U. & Lown, J. W. (1963) *Can. J. Chem.* **41**, 889-896.

Lemieux, R. U. & Koto, S. (1973) Abstracts, 165th National Meeting of the American Chemical Society, Dallas, Texas, 1973.

Lemieux, R. U., Nagabhushan, T. L., Clemetson, K. J., & Tucker, C. N. (1973) *Can. J. Chem.* **51**, 53-66.

Lemieux, R. U. & Bock, K. (1979) *Japan. J. Antibiot.* **32 (Suppl.)**, 163-177.

Lin, I., Knight, W. B., Ting, S. J., & Dunaway-Mariano, D. (1984) *Inorg. Chem.* **23**, 988-991.

Lu, Z., Shorter, A. L., & Dunaway-Mariano, D. (1993) *Biochemistry* **32**, 2378-2385.

Lu, Z., Shorter, A. L., Lin, I., & Dunaway-Mariano, D. (1988) *Inorg. Chem.* **27**, 4135-4139.

Marion, D. & Wütrich, K. (1983) *Biochem. Biophys. Res. Commun.* **113**, 967-974.

Markley, J. L. (1975) *Acc. Chem. Res.* **8**, 70-80.

Martin, N. L. & Beveridge, T. J. (1986) *Antimicrob. Agents Chemother.* **29**, 1079-1087.

Martin, P., Jullien, E., & Corvalin, P. (1988) *Mol. Microbiol.* **2**, 615-625.

Martín-Pastor, M.; Espinosa, J. F.; Asensio, J. L.; Jiménez-Barbero, J. (1997) *Carbohydr. Res.* **298**, 15-49.

Mason, J. (1996) in *Encyclopedia of Nuclear Magnetic Resonance*, pp 3222-3251, John Wiley & Sons, New York.

McCammon, J. A. & Harvey, S. C. (1987) in *Dynamics of proteins and nucleic acids*, Ch. 4, Cambridge University Press, New York.

McKay, G. A., Thompson, P. R., & Wright, G. D. (1994) *Biochemistry* **33**, 6936-6944.

McKay, G. A. & Wright, G. D. (1995) *J. Biol. Chem.* **270**, 24686-24692.

McKay, G. A. & Wright, G. D. (1996) *Biochemistry* **35**, 8680-8685.

McKay, G. A., Roestamadji, J, Mobashery, S., & Wright, G. D. (1996) *Antimicrob. Agents Chemother.* **40**, 2648-2650.

Mildvan, A. S. (1977) *Acc. Chem. Res.* **10**, 246-252.

Mildvan, A. S. (1979) *Adv. in Enzymol.* **49**, 103-126.

Mildvan, A. S. & Cohn, M. (1963) *Biochemistry* **2**, 910-919.

Mildvan, A. S. & Cohn, M. (1966) *J. Biol. Chem.* **241**, 1178-1193.

Mildvan, A. S. & Cohn, M. (1970) *Adv. Enzymol.* **33**, 1-70.

Mildvan, A. S. & Engle, J. L. (1972) *Methods Enzymol.* **26C**, 654-683.

Mildvan, A. S. & Gupta, R. K. (1978) *Methods Enzymol.* **49**, 322-359.

Mildvan, A. S., Granot, J., Smith, G. M., & Liebman, M. N. (1980) *Adv. Inorg. Biochem.* **2**, 211-236.

Mingeot-Leclercq, M.-P., Brasseur, R., & Schanck, A. (1995) *J. Toxicol. Environ. Health* **44**, 263-300.

Moellering, R. C. (1991) *J. Antimicrob. Chemother.* **28**, 1-12.

Mønsted, L. & Mønsted, O. (1989) *Coord. Chem. Rev.* **94**, 109-150.

Náray-Szabo, G. & Ferenczy, G. G. (1995) *Chem. Rev.* **95**, 829-847.

Neu, H. C. (1992) *Science* **257**, 1064-1073.

Ni, F. & Scheraga, H. A. (1994) *Acc. Chem. Res.* **27**, 257-264.

Noller, H. F. (1991) *Ann. Rev. Biochem.* **60**, 191-227.

Okada, A., Wakamatsu, K., Miyazawa, T., & Higashijima, T. (1994) *Biochemistry* **33**, 9438-9446.

Otting, G. (1993) *Curr. Opin. Struc. Biol.* **3**, 760-768.

Pappu, K. M., Gregory, J. D., & Serpersu, E. H. (1994) *Arch. Biochem. Biophys.* **311**, 503-508.

Pappu, K. M., Kunnumal, B., & Serpersu, E. H. (1997) *Biophys. J.* **72**, 928-935.

Pecoraro, V. L., Hermes, J. D., & Cleland, W. W. (1984) *Biochemistry* **23**, 5262-5271.

Pederson, L. C., Benning, M. M., & Holden, H. M. (1995) *Biochemistry* **34**, 13305-13311.

Penefsky, H. S. (1977) *J. Biol. Chem.* **252**, 2891-2899.

Purohit, P. & Stern, S. (1994) *Nature* **370**, 659-662.

Recht, M. I., Fourmy, D., Blanchard, S. C., Dahlquist, K. D., & Puglisi, J. D. (1996) *J. Mol. Biol.* **262**, 421-436.

Reid, D. G., & Gajjar, K. (1987) *J. Biol. Chem.* **262,** 7967-7972.

Reuben, J. & Cohn, M. (1970) *J. Biol. Chem.* **245**, 6539-6546.

Rhinehart, K. L. & Shield, L. S. (1980) in *Aminocyclitol Antibiotics* (Rhinehart, K. L. & Suami, T., Eds.) Ch. 1, American Chemical Society, Washington, D. C.

Riek, R., Hornemann, S., Wider, G., Billeter, M., Glockshuber, R., Wüthrich, K. (1996) *Nature* **382**, 180-182.

Roestamadji, J., Grapsas, I., & Mobashery, S. (1995) *J. Am. Chem. Soc.* **117**, 11060-11069.

Rutherford, T. J., Partridge, J., Weller, C. T., & Homans, S. W. (1993) *Biochemistry* **32**, 12715-12724.

Schaberg, D. R., Culver, D. H., & Gaynes, R. P. (1991) Am. J. Med. 91, 72S-75S.

Schanck, A., Brasseur, R., Mingeot-Leclercq, M.-P., & Tulkens, P. M. (1992) *Magn. Reson. Chem.* **30**, 11-15.

Schatz, A., Bugie, E., & Waksman, S. A. (1944) *Proc. Soc. Exp. Biol. Med.* **55**, 66-69.

Scheffler, K., Ernst, B., Katopodis, A., Magnami, J. L., Wang, W. T., Weisemann, R., & Peters, T. (1995) *Angew. Chem. Int. Ed. Engl.* **34**, 1841-1844.

Serpersu, E. H., Summitt, L. L., & Gregory, J. D. (1992) *J. Inorg. Biochem.* **48**, 203-215.

Serpersu, E. H., Shortle, D., & Mildvan, A. S. (1986) *Biochemistry* **25**, 68-77.

Serpersu, E. H., Shortle, D., & Mildvan, A. S. (1987) *Biochemistry* **26**, 1289-1300.

Shaka, A. J., Keeler, J., & Freeman, R. (1983) *J. Magn. Res.* **53**, 313-340.

Shlaes, D. M., Binczewski, B., & Rice, L. B. (1993) *Clin. Infect. Dis.* **17 (Suppl 2)**, S527-S536.

Shaw, K. J.; Rather, P. N.; Hare, R. S.; Miller, G. H. (1993) *Microbiol. Rev.*, **57**, 138-163.

Silverstein, R. M., Bassler, G. C., & Morrill, T. C. *Spectrometric Identification of Organic Compounds*, 5th ed.; John Wiley and Sons: New York, 1991, pp 174-175.

Szilágy, L. (1987) *Carbohydr. Res.* **170,** 1-17

Szilágyi, L. & Pusztahelyi, Z. S. (1992) *Magn. Reson. Chem.* **30,** 107-117.

Tanaka, N. (1982) in *Aminoglycoside Antibiotics* (Umezawa, H. & Hooper, I. R., Eds.) pp 221-266, Springer-Verlag, Berlin.

Taube, H. (1952) *Chem. Rev.* **50**, 69-126.

Taylor, S. S., Knighton, D. R., Zheng, J., Sowadski, J. M., Gibbs, C. S. & Zoller, M. J. (1993) *Trends Biochem. Sci.* **18**, 84-89.

Thompson, P. R., Hughes, D. W., & Wright, G. D. (1996a) *Biochemistry* **35**, 8686-8695.

Thompson, P. R., Hughes, D. W., & Wright, G. D. (1996b) *Chemistry & Biology* **3**, 747-755.

Tian, Z. -Q. & Bartlett, P. A. (1996) *J. Am. Chem. Soc.* **118**, 943-949.

Tolmasky, M. E., Chamorro, R. M., Crosa, J. J., & Marini, P. M. (1988) *Antimicrob. Agents Chemother.* **32**, 1500-1505.

Umezawa, H., Okanishi, M., Kondo, S., Hamana, K., Utahara, R., Maea, K., & Mitsuhashi, S. (1967) *Science* **157**, 1559-1561.

Umezawa, H. & Kondo, S. (1982) in *Aminoglycoside Antibiotics* (Umezawa, H. & Hooper, I. R., Eds.) Ch. 6, Springer-Verlag, Berlin.

van Halbeek, H. (1994) *Curr. Opin. Struc. Biol.* **4**, 697-709.

von Itzstein, M., Wu, W. Y., Kok, G. B., Pegg, M. S., Dyason, J. C., Jin, B., Phan, T. V., Smythe, M. L., White, H. F., Oliver, S. W., Colman, P. M., Varghese, J. N., Ryan, D. M., Woods, J. M., Bethell, R. C., Hotham, V. J., Cameron, J. M., & Penn, C. R. (1993) *Nature* **363**, 418-423.

Walsh, D. A. & van Patten, S. M. (1994) *FASEB J.* **8**, 1227-1236.

Weiner, P. R. & Kollman, P. A. (1981) *J. Comput. Chem.* **2**, 287-303.

Weiner, S. J., Kollman, P. A., Case, D. A., Singh, U. C., Ghio, C., Alagona, G., Profeta, S., & Weiner, P. (1984) *J. Am. Chem. Soc.* **106**, 765-784.

Weiner, S. J., Kollman, P. A., Nguyen, D. T., & Case, D. A. (1986) *J. Comp. Chem.* **7**, 230-252.

Weinstein, M. J., Luedmann, G. M., Oden, E. M., Wagman, G. H., Rosselet, J. P., Marquez, J. A., Coniglio, C. T., Charney, W., Herzog, H. L., & Black, J. (1963) *J. Med. Chem.* **6**, 463-464.

Wilde, J. A. & Bolton, P. H. (1984) *J. Magn. Reson.* **59**, 343-346.

Wolkers, W. F., Gregory, J. D., Churchich, J. E., & Serpersu, E. H. (1991) *J. Biol. Chem.* **266**, 20761-20766.

Wu, Z. R., Ebrahimian, S., Zawrotny, M. E., Thornburg, L. D., Perez-Alvarado, G. C., Brothers, P., Pollack, R. M., & Summers, M. F. (1997) *Science* **276**, 415-418.

Xiang, B. & Markham, G. D. (1996) *J. Biol. Chem.* **271**, 27531-27535.

Zhang, F., Strand, A., Robbins, D., Cobb, M. H. & Goldsmith, E. J. (1994) *Nature* **367**, 704-711.

Zheng, J., Knighton, D. R., Ten Eyck, L. F., Karlsson, R., Xuong, N -H., Taylor, S. S., & Sowadski, J. M. (1993) *Biochemistry* **32**, 2154-2161.

Appendices

Appendix A

Figures

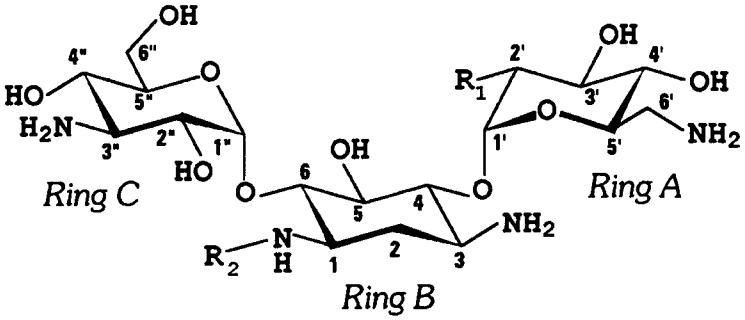

	R_1	R_2
Kanamycin A	OH	H
Kanamycin B	NH_2	H
Amikacin	OH	Y

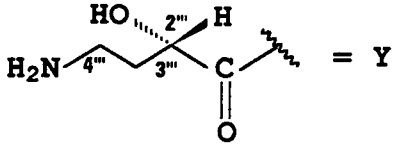

Figure II-1. Structures of 4,6-disubstituted aminoglycosides.

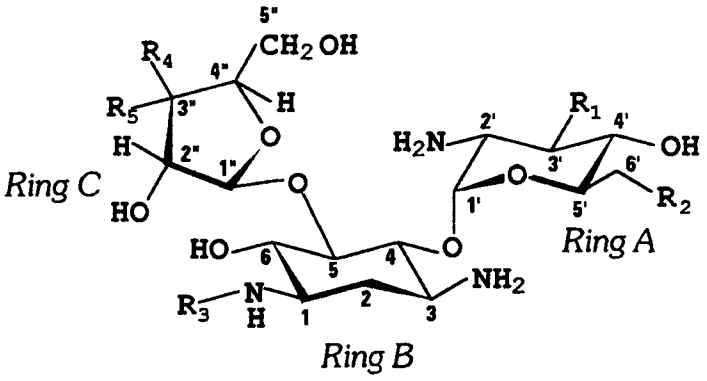

	R_1	R_2	R_3	R_4	R_5	R_6
Butirosin A	OH	NH_2	Y	OH	H	----
Ribostamycin	OH	NH_2	H	H	OH	----
Neomycin B	OH	NH_2	H	H	X	H
Paromomycin	OH	OH	H	H	X	H
Lividomycin A	H	OH	H	H	X	mannose

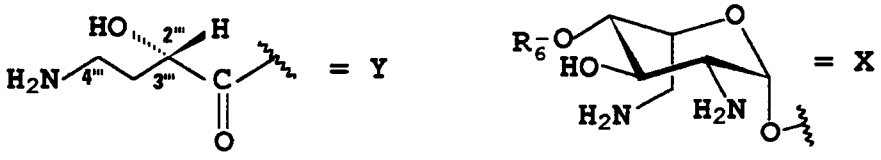

Figure II-2. Structures of 4,5-disubstituted aminoglycosides.

A.

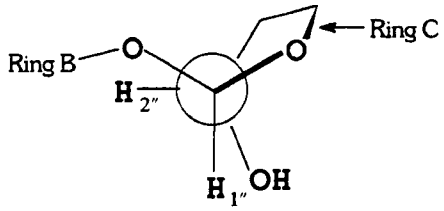

B.

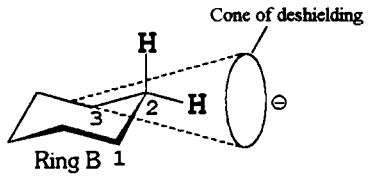

C.

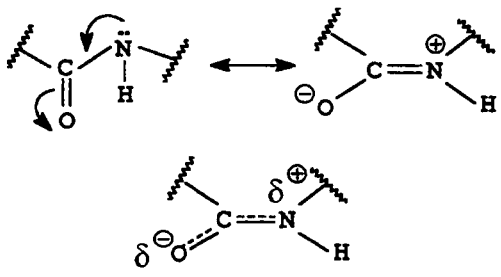

Figure II-3. Structures describing the conformation (Newmann projection) of the xylose ring in butirosin A (A), the cone of deshielding in a rigid six-membered ring (B), and the resonance forms of an amide bond (C).

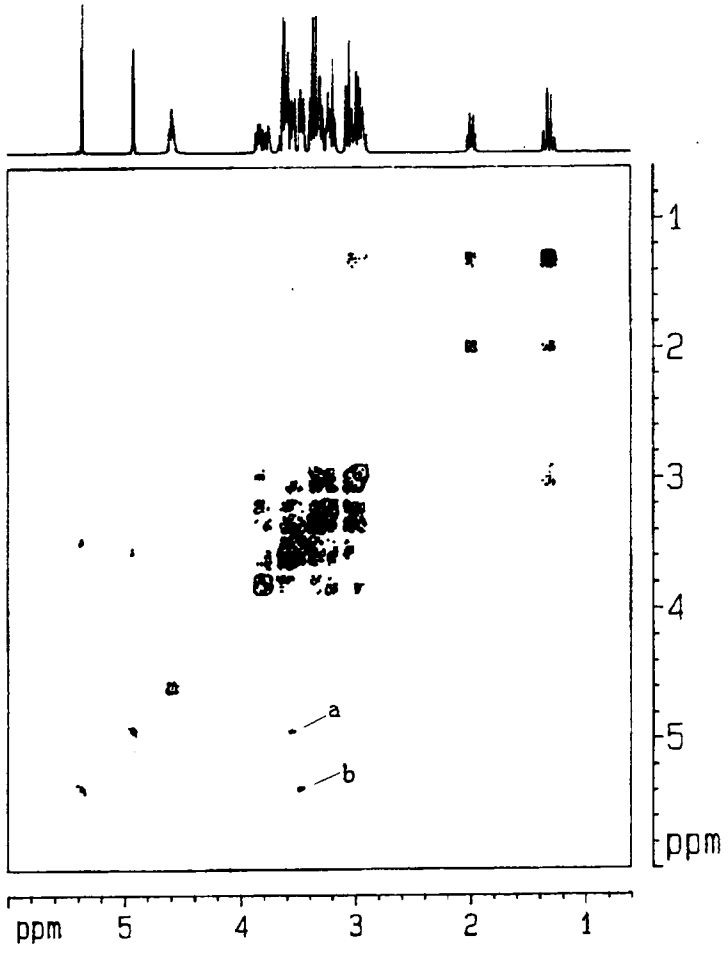

Figure II-4. Two-dimensional ^{1}H-^{1}H COSY spectrum of kanamycin A. The sample consisted of 100 mM kanamycin A in 99.9% $^{2}H_2O$ at pH 6.5. The cross-peaks labeled are H1″-H2″ (a) and H1′-H2′ (b).

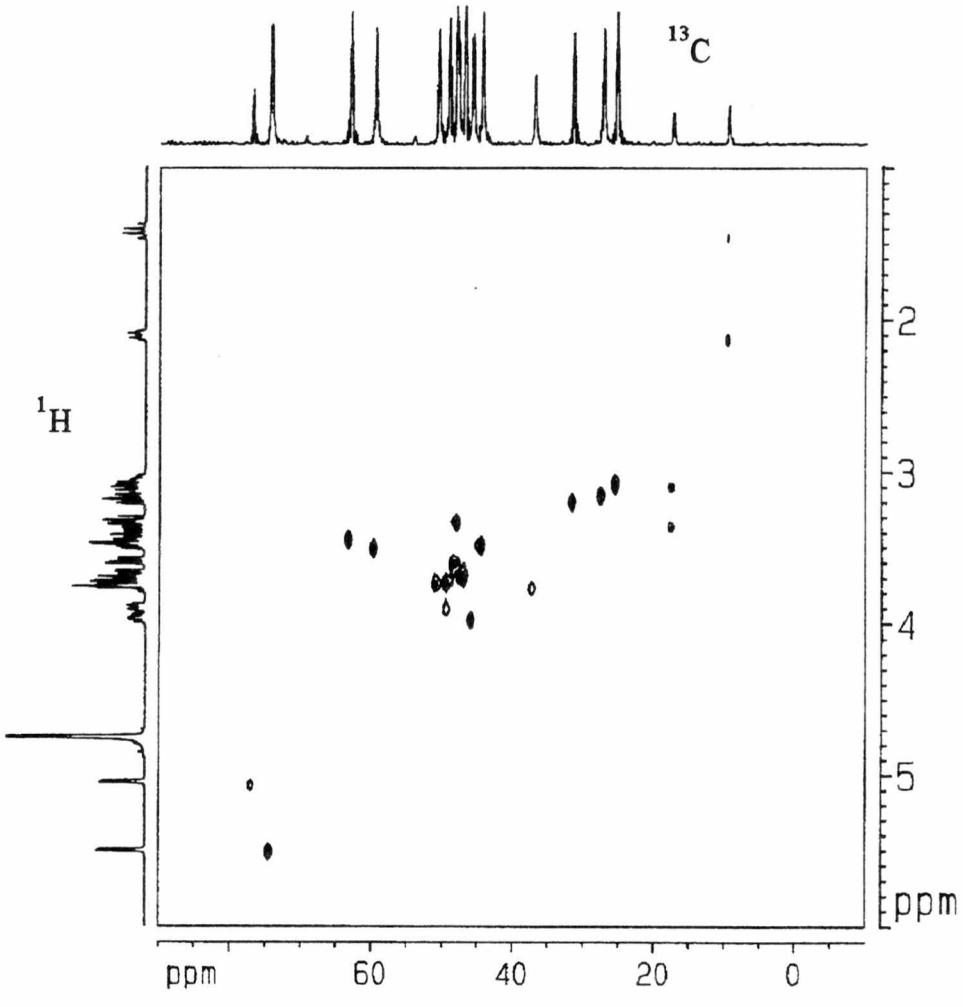

Figure II-5. Two-dimensional ^{1}H-^{13}C COSY spectrum of kanamycin A. The sample consisted of 100 mM kanamycin A in 99.9% $^{2}H_2O$ at pH 6.5.

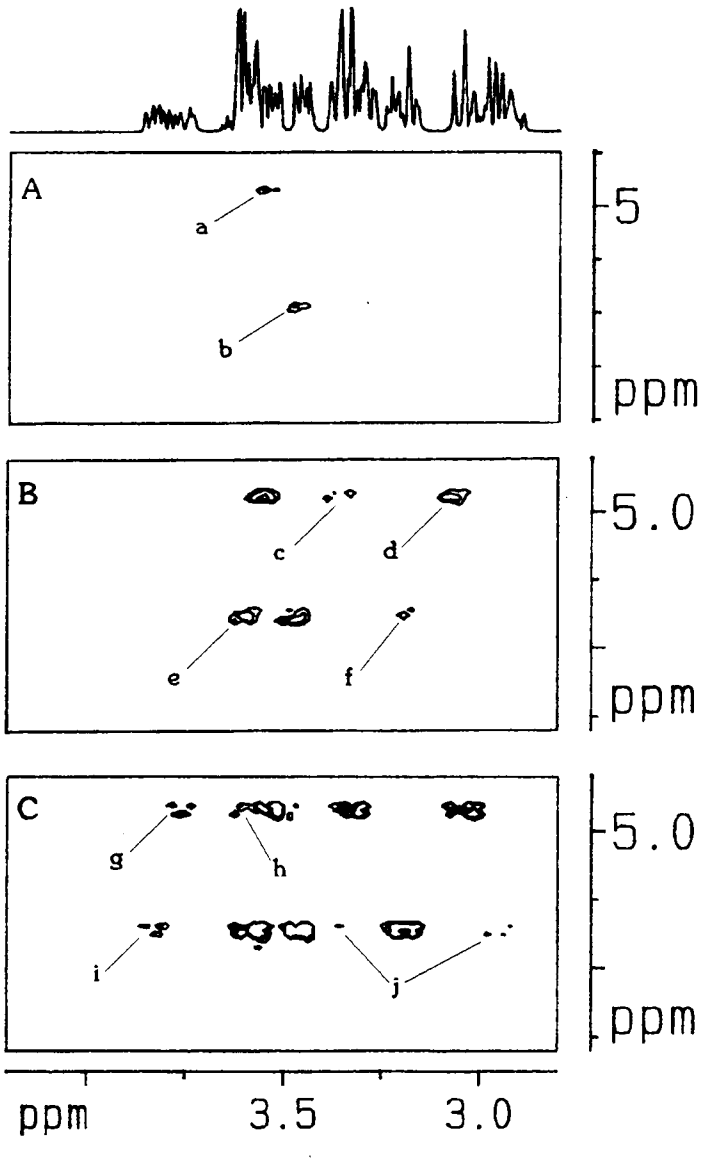

Figure II-6. Expanded regions of homonuclear NMR spectra of kanamycin A used to follow the appearance of cross-peaks. Panel A is from the ^{1}H-^{1}H COSY spectrum, while panels B and C are from HOHAHA spectra with mixing times of 45.4 ms and 61.6 ms, respectively. The sample was 100 mM kanamycin A in 99.9% $^{2}H_{2}O$ at pH 6.5. Labeled cross-peaks are in panel A: H1″-H2″ (a) and H1′-H2′ (b). Panel B: H1″-H4″ (c), H1″-H3″ (d), H1′-H3′ (e), and H1′-H4′ (f). Panel C: H1″-H5″ (g), H1″-H6″ (h), H1′-H5′ (i), and H1′-H6′ (j).

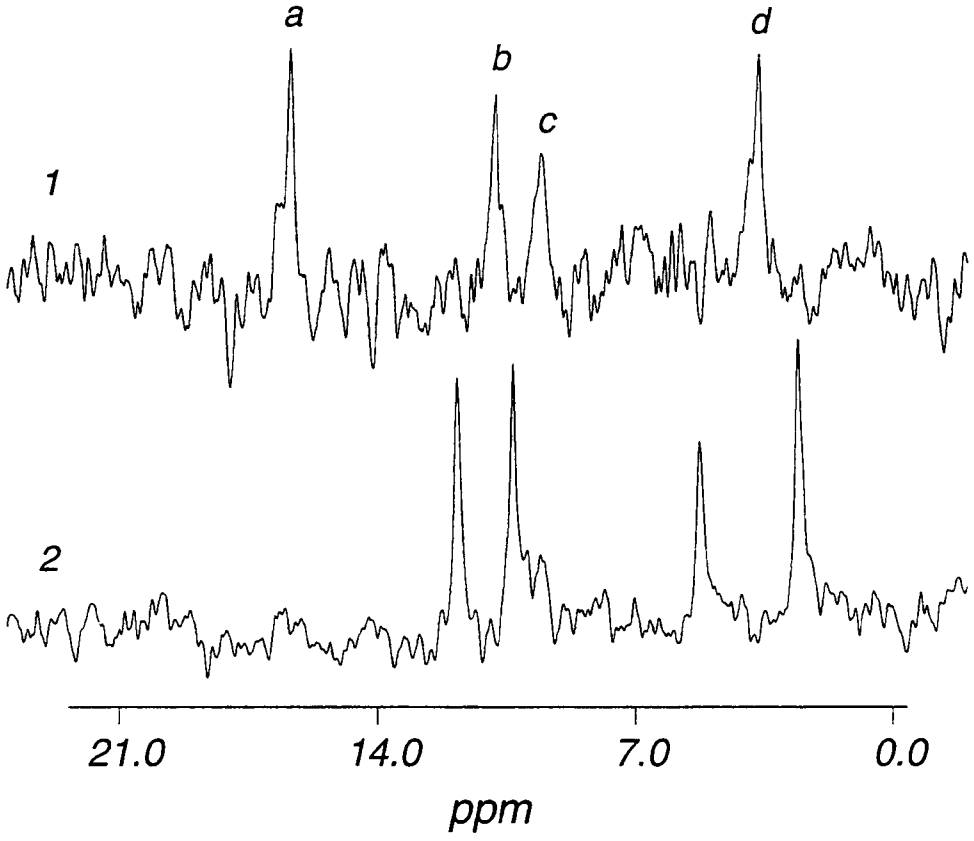

Figure II-7. ^{1}H-decoupled ^{15}N spectra of butirosin A. The sample consisted of 0.5 M butirosin A in 85:15 (v/v) H_2O:$^{2}H_2O$. Peak **a** (N-3), **b** (N-2′), **c** (N-4‴), and **d**(N-6′) are shown at two pH values in trace **1** (pH 5.94) and **2** (pH 8.20). There was no evidence for a crossover of any ^{15}N resonances during the titration. The peak for N-1 is not shown.

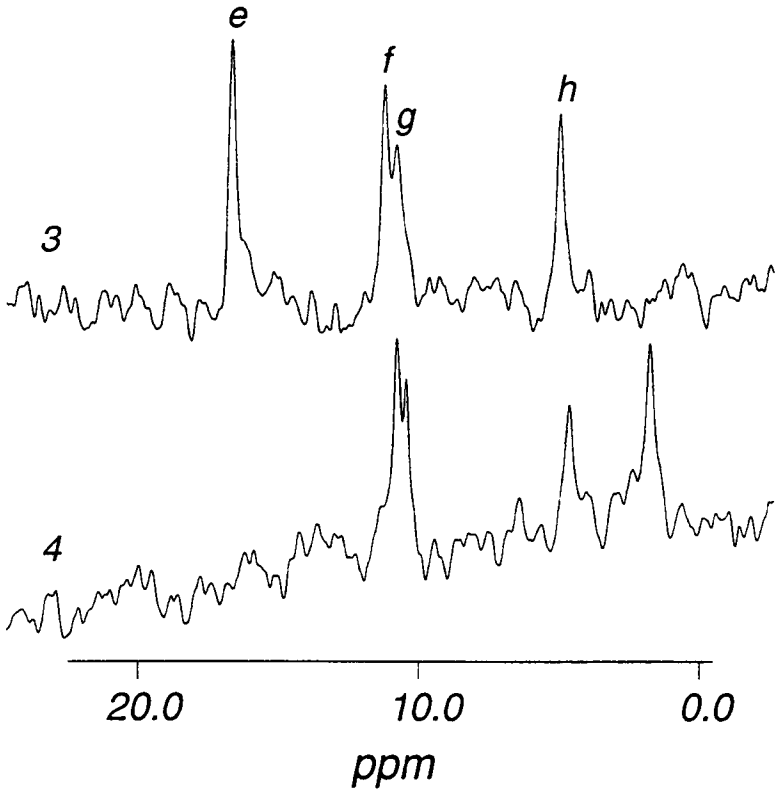

Figure II-8. ^{1}H-decoupled ^{15}N spectra of amikacin. The sample consisted of 0.8 M amikacin in 85:15 (v/v) H_2O:$^{2}H_2O$. Peak **e** (N-3), **f** (N-3″), **g** (N-4‴), and **d**(N-6′) are shown at two pH values in trace **3** (pH 5.71) and **4** (pH 8.50). There was no evidence for a crossover of any ^{15}N resonances during the titration. The peak for N-1 is not shown.

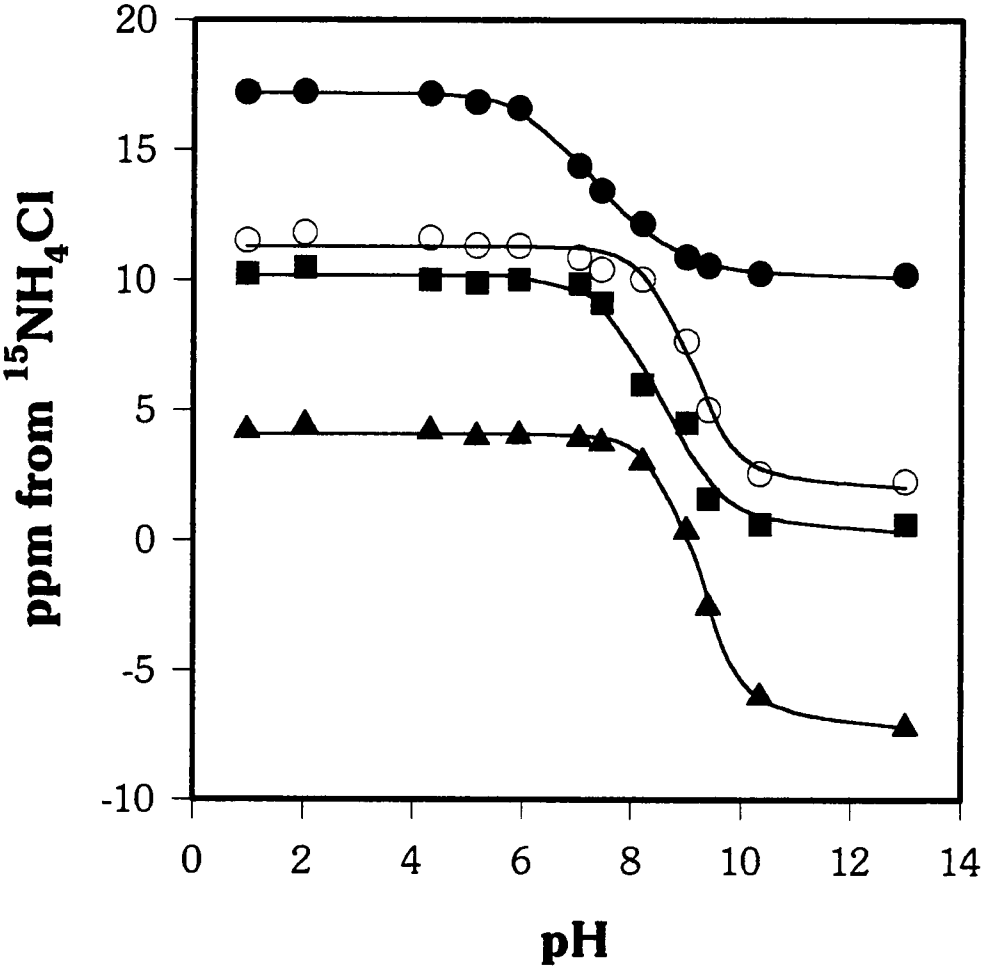

Figure II-9. The pH dependence of ^{15}N chemical shifts of butirosin A. The samples initially contained 0.5 M butirosin A in 85:15 (v/v) H_2O:^2H_2O. The titration curves for the amino groups at N-3 (●), N-2′ (○), N-4‴ (■), and N-6′(▲) are presented.

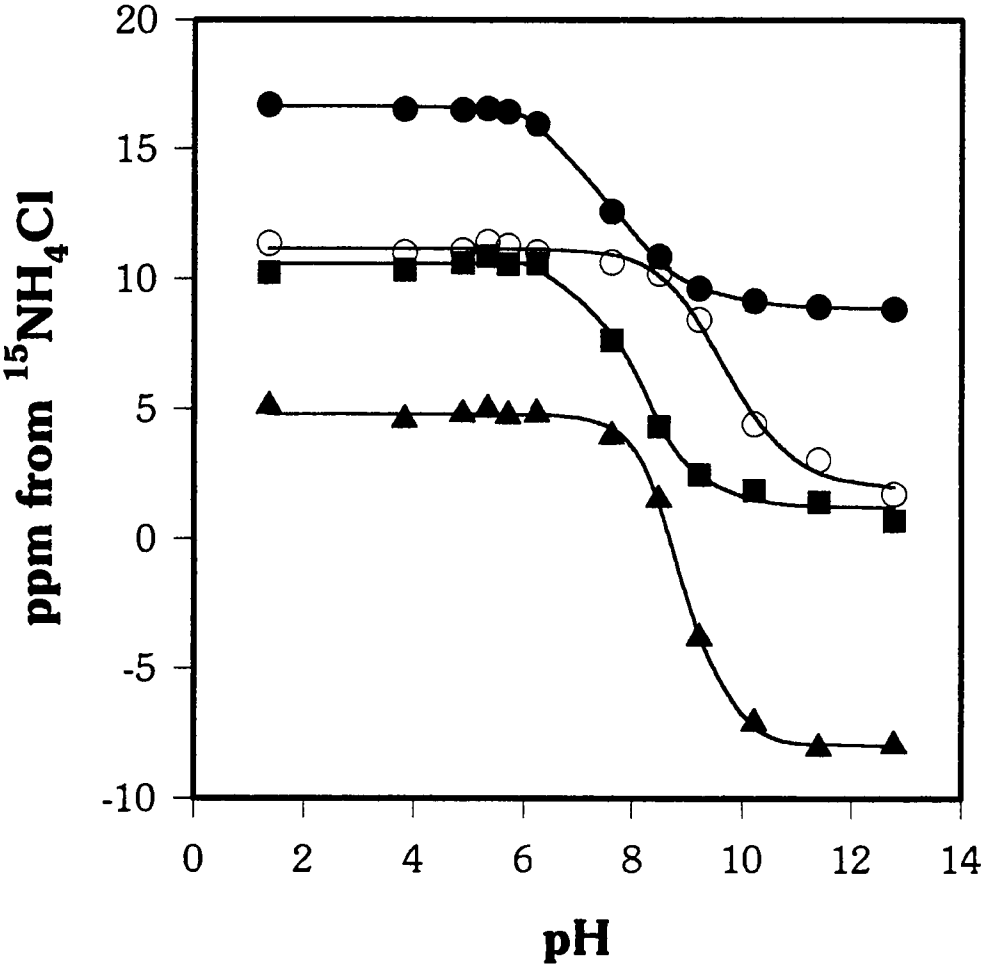

Figure II-10. The pH dependence of ^{15}N chemical shifts of amikacin. The samples initially contained 0.8 M amikacin in 85:15 (v/v) H_2O:^2H_2O. The titration curves for the amino groups at N-3 (●), N-3″ (○), N-4‴ (■), and N-6′(▲) are presented.

$$\frac{1}{T_{1p}} = \left(\frac{1}{T_1}\right) - \left(\frac{1}{T_1}\right)_o \qquad \text{Eq. III-1}$$

$$\varepsilon^* = \frac{1/T_{1p}^*}{1/T_{1p}} = \frac{1/T_1^* - (1/T_1^*)_o}{1/T_1 - (1/T_1)_o} \qquad \text{Eq. III-2}$$

$$\varepsilon^* = \frac{[CrATP]_f}{[CrATP]_T}\varepsilon_f + \frac{[CrATP]_b}{[CrATP]_T}\varepsilon_b \qquad \text{Eq. III-3}$$

$$[CrATP]_f = \left(\frac{\varepsilon_b - \varepsilon^*}{\varepsilon_b - 1}\right)[CrATP]_T \qquad \text{Eq. III-4}$$

$$[CrATP]_f = \left(\frac{\varepsilon_a - \varepsilon^*}{\varepsilon_a - 1}\right)[CrATP]_T \qquad \text{Eq. III-5}$$

$$K_1 = \frac{[CrATP]_f\,[Antibiotic]_f}{[CrATP \bullet Antibiotic]} \qquad \text{Eq. III-6}$$

Figure III-1. Various equations describing the relaxation rate ($1/T_{1p}$), the enhancement factor (ε^*), the binary complexes of CrATP and APH(3′)-IIIa, and binary complexes of CrATP and the antibiotics. Specific details about the equations are given in the text.

$$\varepsilon^* = \frac{[CrATP]_f}{[CrATP]_T} + \frac{[CrATP \bullet Antibiotic]}{[CrATP]_T}\varepsilon_a +$$

$$\frac{[APH(3')\text{-}IIIa \bullet CrATP]}{[CrATP]_T}\varepsilon_b + \frac{[APH(3')\text{-}IIIa \bullet CrATP \bullet Antibiotic]}{[CrATP]_T}\varepsilon_T \qquad \text{Eq. III-7}$$

$$\varepsilon^* = \frac{\dfrac{K_3K_D}{[APH(3')\text{-}IIIa][Antibiotic]} + \dfrac{K_2}{[APH(3')\text{-}IIIa]}\varepsilon_a + \dfrac{K_3}{[Antibiotic]}\varepsilon_b + \varepsilon_T}{\dfrac{K_3K_D}{[APH(3')\text{-}IIIa][Antibiotic]} + \dfrac{K_2}{[APH(3')\text{-}IIIa]} + \dfrac{K_3}{[Antibiotic]} + 1} \qquad \text{Eq. III-8}$$

Figure III-2. The enhancement factor (ε^*) describing the ternary complexes between APH(3')-IIIa, CrATP, and the antibiotics. The dissociation constants are defined in Figure III-3.

$$K_D = \frac{[CrATP]_f[APH(3')\text{-}IIIa]_f}{[APH(3')\text{-}IIIa\bullet CrATP]} \qquad \text{Eq. III-9}$$

$$K_S = \frac{[Antibiotic]_f[APH(3')\text{-}IIIa]_f}{[APH(3')\text{-}IIIa\bullet Antibiotic]} \qquad \text{Eq. III-10}$$

$$K_1 = \frac{[CrATP]_f[Antibiotic]_f}{[CrATP\bullet Antibiotic]} \qquad \text{Eq. III-11}$$

$$K_A' = \frac{[CrATP]_f[APH(3')\text{-}IIIa\bullet Antibiotic]}{[APH(3')\text{-}IIIa\bullet CrATP\bullet Antibiotic]} \qquad \text{Eq. III-12}$$

$$K_2 = \frac{[APH(3')\text{-}IIIa]_f[CrATP\bullet Antibiotic]}{[APH(3')\text{-}IIIa\bullet CrATP\bullet Antibiotic]} \qquad \text{Eq. III-13}$$

$$K_3 = \frac{[Antibiotic]_f[APH(3')\text{-}IIIa\bullet CrATP]}{[APH(3')\text{-}IIIa\bullet CrATP\bullet Antibiotic]} \qquad \text{Eq. III-14}$$

Figure III-3. The definition of the equilibrium binding constants that describe binary and ternary complex formation among the antibiotics, CrATP, and APH(3')-IIIa.

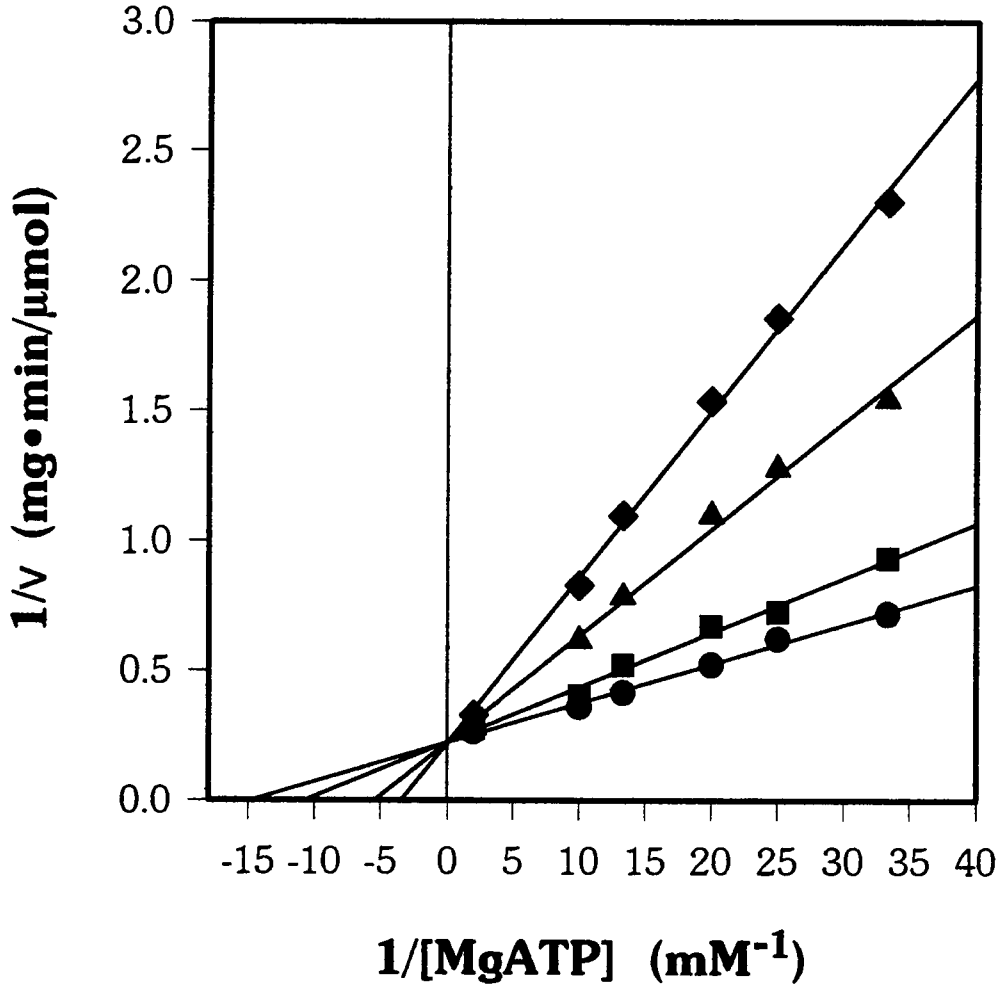

Figure III-4. Inhibition of APH(3′)-IIIa by CrATP. CrATP concentrations used were 0.00 mM (●), 0.05 mM (■), 0.20 mM (▲), and 0.40 mM (♦). Enzyme activity was measured as described in the "Experimental Procedures" section of Chapter III.

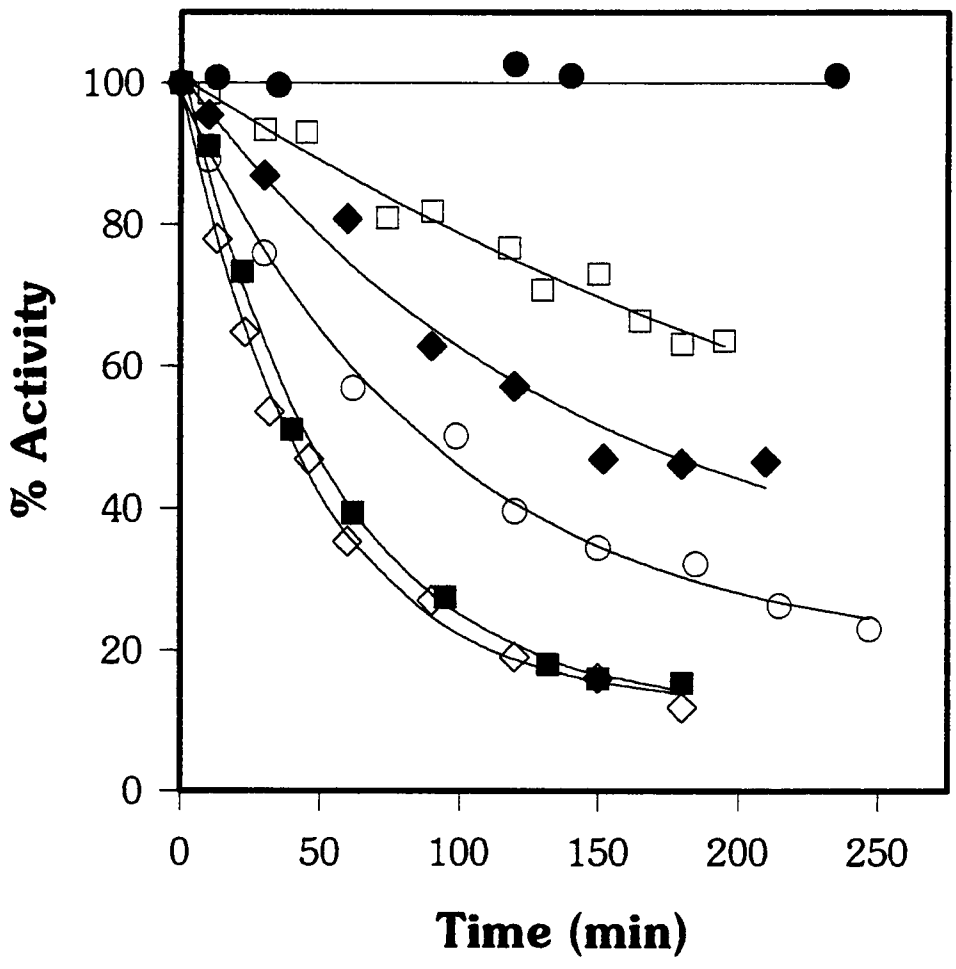

Figure III-5. Inactivation of APH(3′)-IIIa by CrATP. The enzyme was incubated at 37 °C in 50 mM MES (pH 6.5), 0.5 mM kanamycin A and CrATP. CrATP concentrations used were 0.00 mM (●), 0.025 mM (□), 0.040 mM (♦), 0.075 mM (○), 0.250 mM (■), 3.00 mM (◇). Residual enzyme activity was measured as described in the "Experimental Procedures" section of Chapter III.

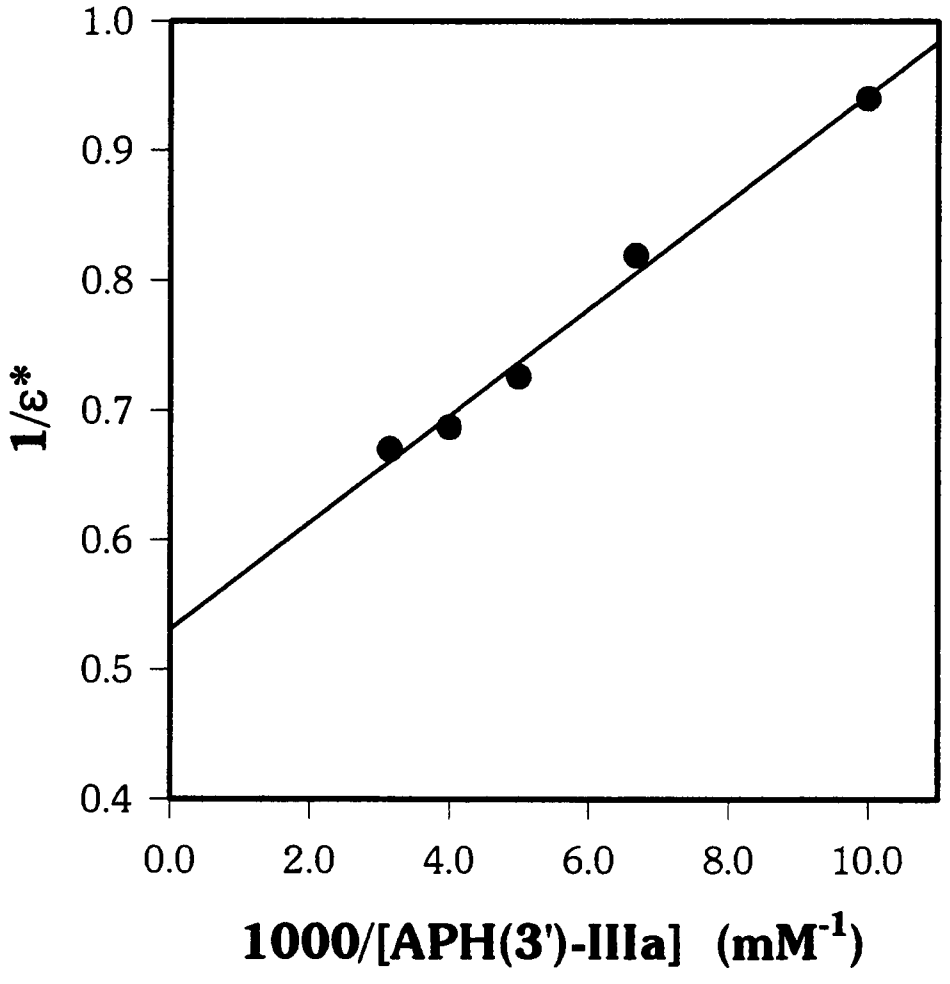

Figure III-6. The enhancement of the relaxation rates of water protons upon APH(3′)-IIIa•CrATP complex formation. This double-reciprocal plot was used to calculate ε_b (1/*y*-intercept). In this experiment, a 83.3 μM CrATP solution in 50 mM MES (pH 6.5) was titrated with APH(3′)-IIIa.

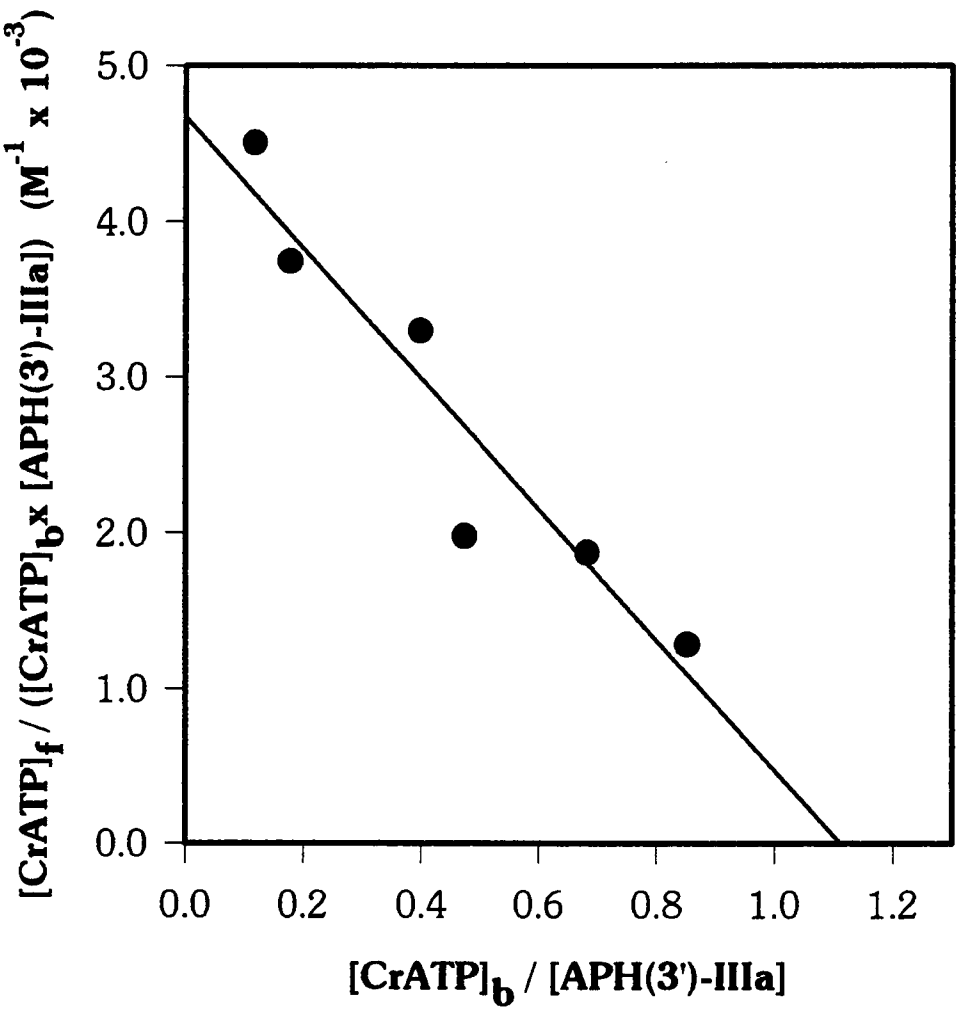

Figure III-7. Scatchard plot used to determine the stoichiometry of binding and dissociation constant for the APH(3′)-IIIa•CrATP complex. A 200 μM solution of APH(3′)-IIIa in 50 mM MES (pH 6.5) was titrated with CrATP to give concentrations of 33.3 to 833 μM.

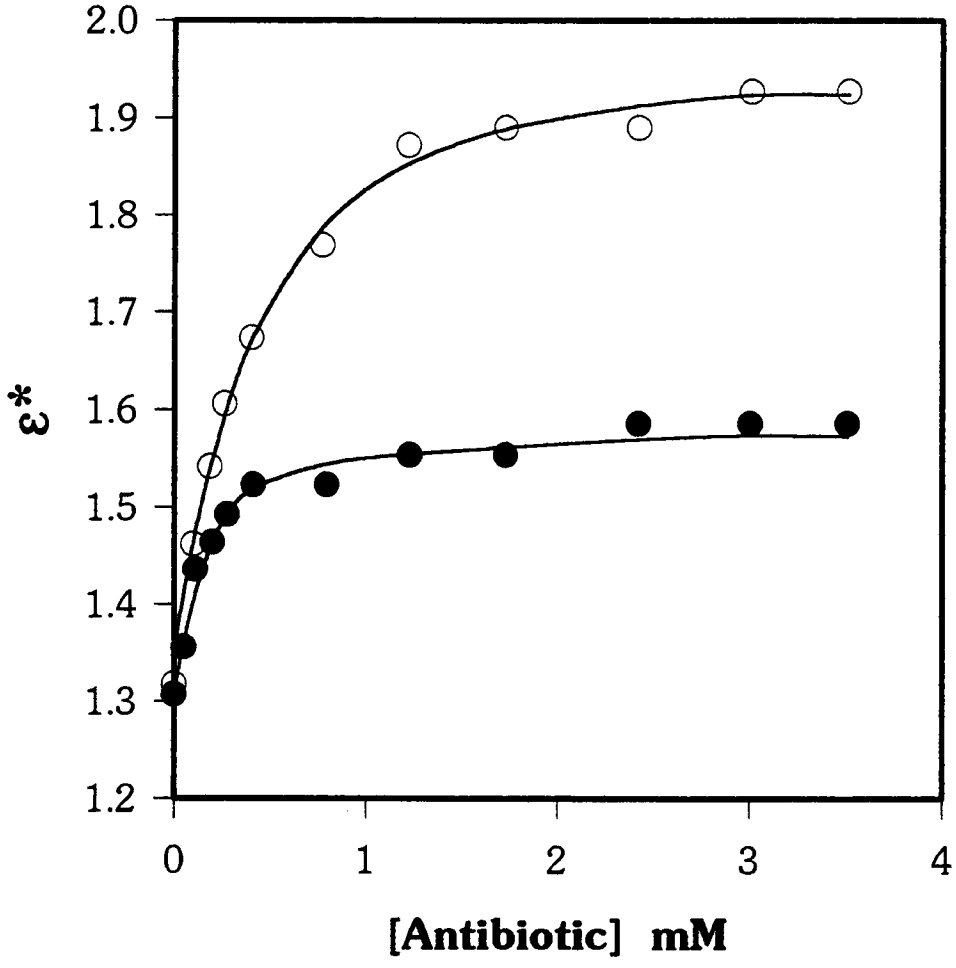

Figure III-8. The enhancement of the relaxation rates of water protons (ε^*) upon amikacin (○) and butirosin A (●) binding to the APH(3′)-IIIa•CrATP complex. In these experiments, an initial solution that contained 50 mM MES (pH 6.5), 100 μM CrATP, and 200 μM APH(3′)-IIIa was titrated with an antibiotic solution that contained 2 or 10 mM antibiotic, 50 mM MES (pH 6.5), 100 μM CrATP, and 200 μM APH(3′)-IIIa.

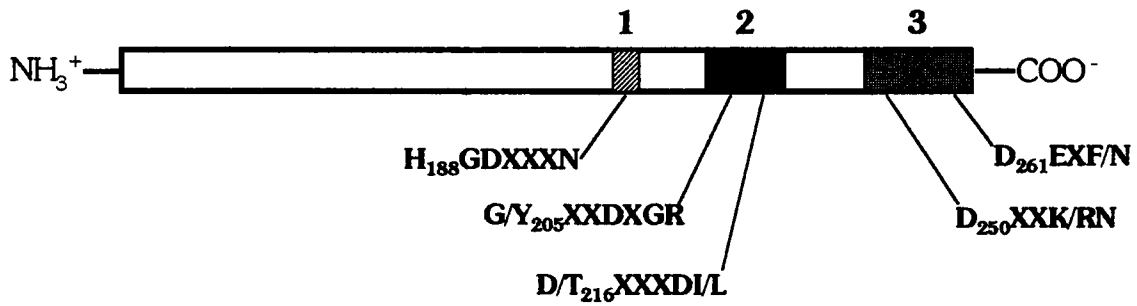

Figure IV-1. Conserved motifs in the APH(3′) enzymes. The amino acid sequences of APH(3′)s are used to indicate domain 1 (catalysis), domain 2 (nucleotide binding), and domain 3 (aminoglycoside binding).

APH(3′)-IIIa	H_{188}	**GDLGDSN**
cAPK	Y_{164}	**RDLKPEN**
CDK2	H_{125}	**RDLKPQN**
IRK	H_{1157}	**RDLAARN**
ERK2	H_{147}	**RDLKPSN**

Figure IV-2. Partial alignment of conserved kinase sequences. The sequences for APH(3′)-IIIa, human cAMP-dependent protein kinase (cAPK), human cyclin-dependent protein kinase 2 (CDK2), human insulin receptor precusor kinase (IRK), and human MAP kinase (ERK2) are shown.

Figure IV-3. The X-ray structures of APH(3′)-IIIa (Hon *et al.*, 1997) and cAMP-dependent protein kinase (cAPK) (Knighton *et al.*, 1991). This figure was provided by Dr. Gerard Wright.

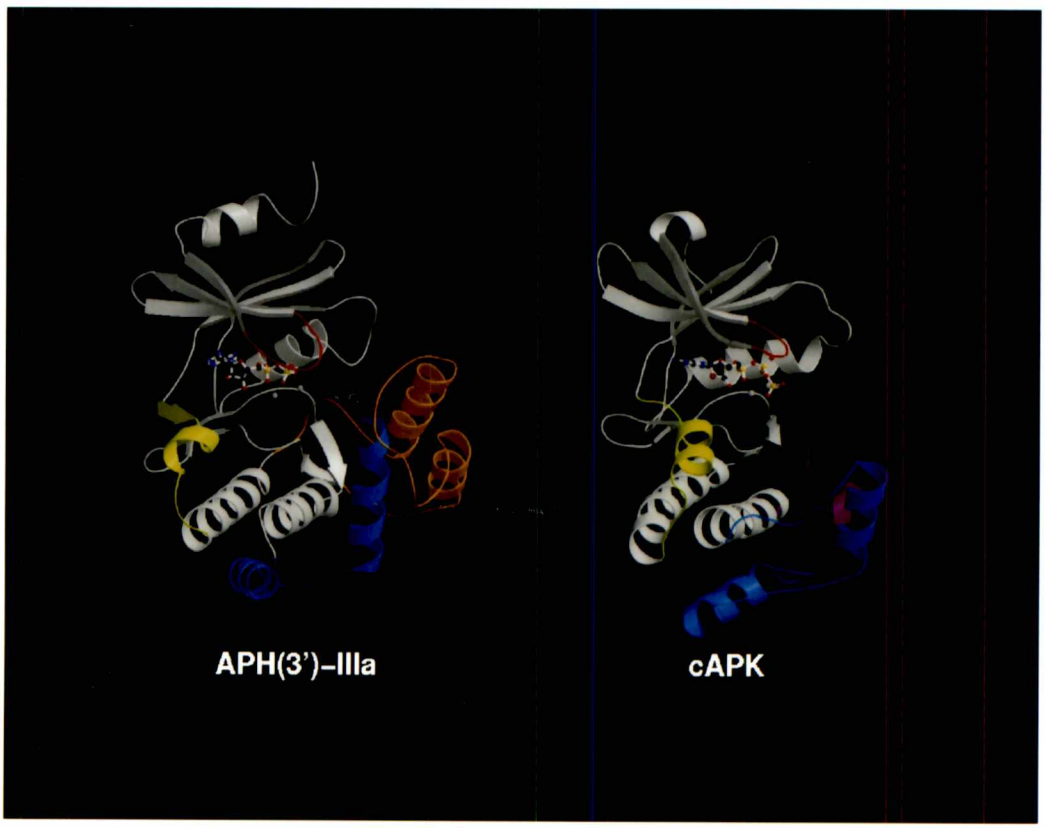
APH(3')-IIIa
cAPK

$$\frac{1}{\tau_c} \sim \frac{1}{\tau_s} = \frac{B\tau_v}{1+\omega_s^2\tau_v^2} + \frac{4B\tau_v}{1+4\omega_s^2\tau_v^2} \qquad \text{Eq. IV-1}$$

$$f(\tau_c) = \frac{3\tau_c}{1+\omega_I^2\tau_c^2} + \frac{7\tau_c}{1+\omega_s^2\tau_c^2} \qquad \text{Eq. IV-2}$$

$$r = C[(qfT_{1p})f(\tau_c)]^{1/6} \qquad \text{Eq. IV-3}$$

Figure IV-4. Equations used to calculate the Cr^{3+}-to-^1H distances (r), correlation time (τ_c), and correlation function ($f(\tau_c)$). τ_s is the longitudinal electron spin relaxation time, B is the zero-field splitting parameter, τ_v is a time constant for ligand motion that modulates B, and ω_s and ω_I are the electron and nuclear precession frequencies, respectively. C is a constant that describes the interaction of Cr^{3+} and ^1H, q is the stoichiometry, and fT_{1p} is the normalized relaxation time of the ^1H of interest.

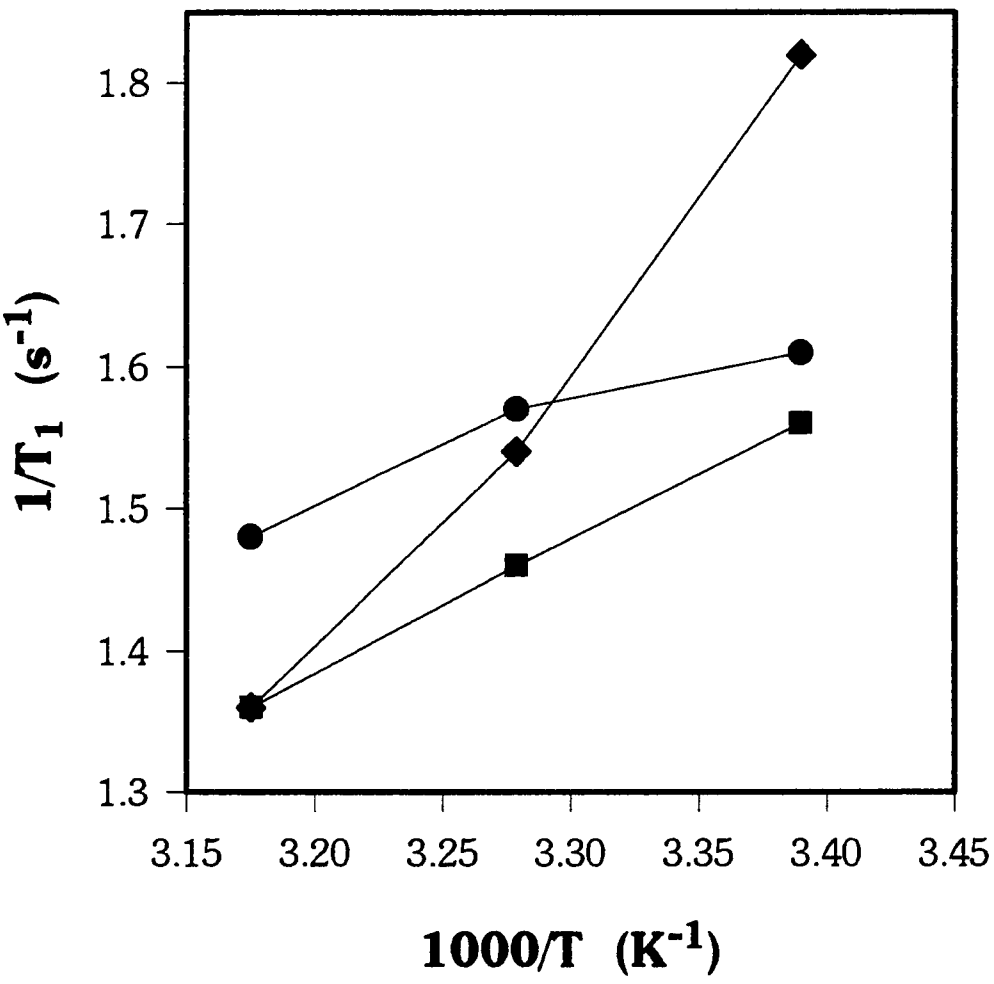

Figure IV-5. The effect of temperature on the relaxation rates ($1/T_1$) of H-1′ (●), H-4‴ (■), and H-6 (♦) of butirosin A. Sample contained 200 μM APH(3′)-IIIa, 6 mM butirosin A, 4 μM CrATP, and 20 mM Tris-d_{11} (pH 6.8).

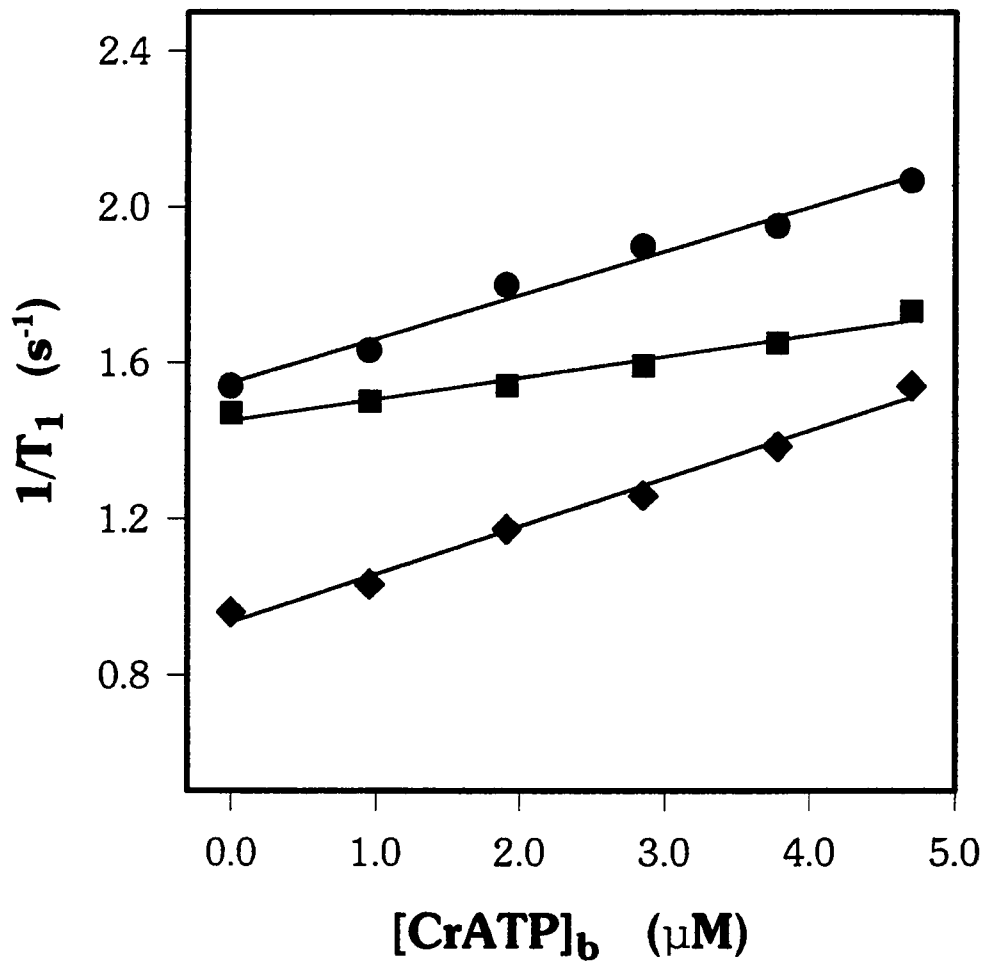

Figure IV-6. The paramagnetic effect of bound CrATP ([CrATP]$_b$]) on representative protons of amikacin. CrATP was titrated in samples that initially contained 0.30 mM APH(3′)-IIIa, 7 mM amikacin, 50 mM NaCl, and 20 mM Tris-d_{11} (pH 6.8). The above data had to be corrected to account for the paramagnetic effects of CrATP in the CrATP•Antibiotic complexes to obtain corrected $1/fT_{1p}$ values. The protons indicated for amikacin are H-1′ (●), H-1″ (■), and H-2‴ (♦).

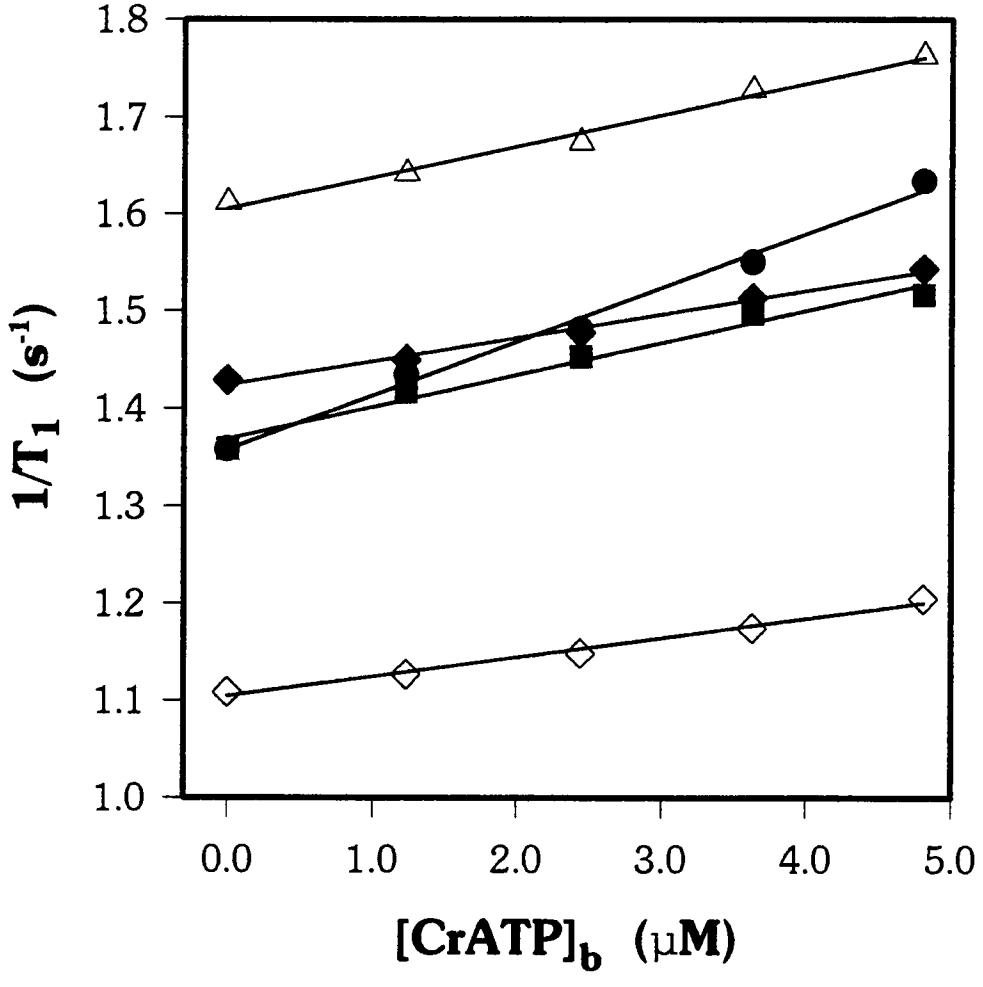

Figure IV-7. The paramagnetic effect of bound CrATP ($[CrATP]_b$]) on representative protons of butirosin A. CrATP was titrated in samples that initially contained 0.30 mM APH(3′)-IIIa, 6 mM butirosin A, 50 mM NaCl, and 20 mM Tris-d_{11} (pH 6.8). The above data had to be corrected to account for the paramagnetic effects of CrATP in the CrATP•Antibiotic complexes to obtain corrected $1/fT_{1p}$ values. The protons indicated for butirosin A are H-1′ (●), H-1″ (■), H-6 (♦), H3‴ (◇), and H4‴ (Δ).

Figure IV-8. A proposed arrangement of APH(3′)-IIIa-bound amikacin with respect to the MeATP. The model presented was constructed based on the distances presented in Table IV-2. Only the Me-triphosphate moiety of the MeATP is shown for clarity.

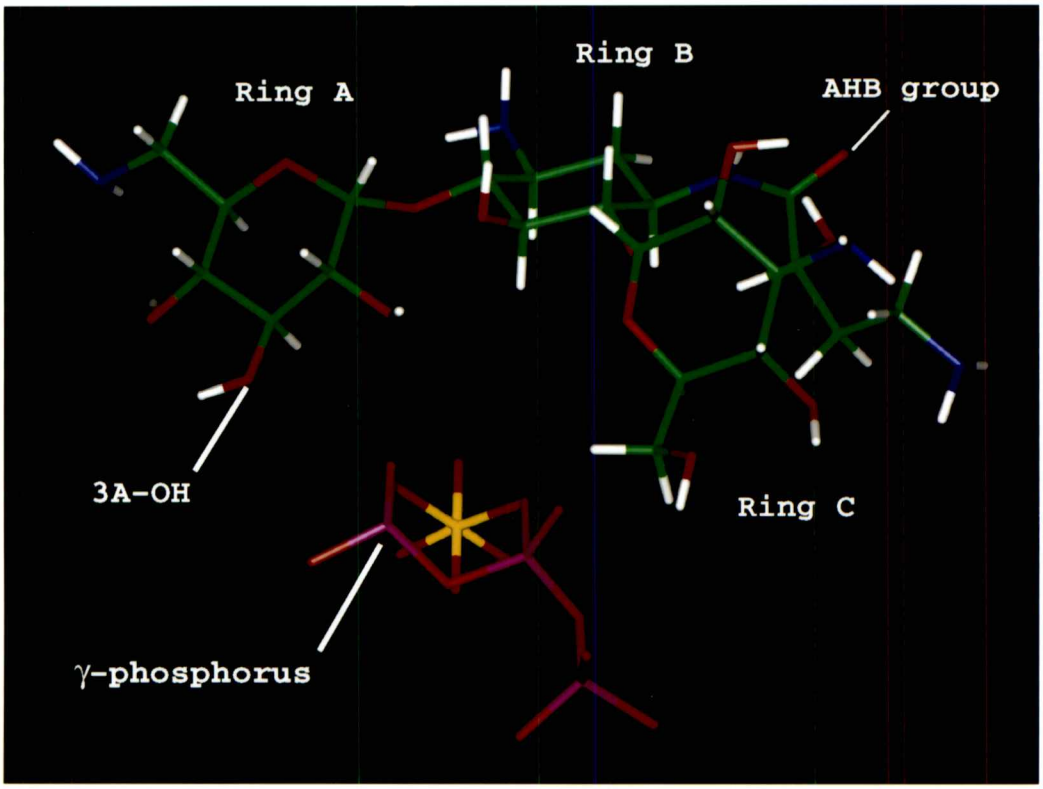
Ring A
Ring B
AHB group
3A-OH
Ring C
γ-phosphorus

Figure IV-9. A proposed arrangement of APH(3')-IIIa-bound butirosin A with respect to the MeATP. The model presented was constructed based on the distances presented in Table IV-2. Only the Me-triphosphate moiety of the MeATP is shown for clarity.

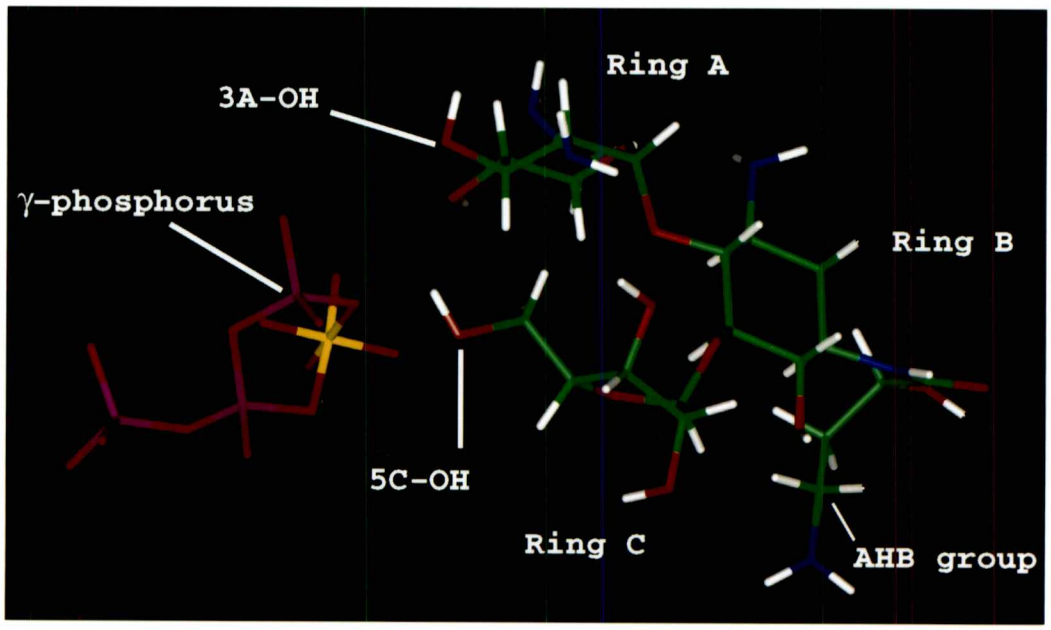
Ring A
3A-OH
γ-phosphorus
Ring B
5C-OH
Ring C
AHB group

Figure IV-10. A superposition of the arrangements of amikacin (white) and butirosin A (green) at the active site of APH(3′)-IIIa. The models presented in Figures IV-8 and IV-9 have been superimposed at the Me-triphosphate moieties. The solvent surfaces were generated by rolling a water molecule (1.4 Å in diameter) over the antibiotic molecules.

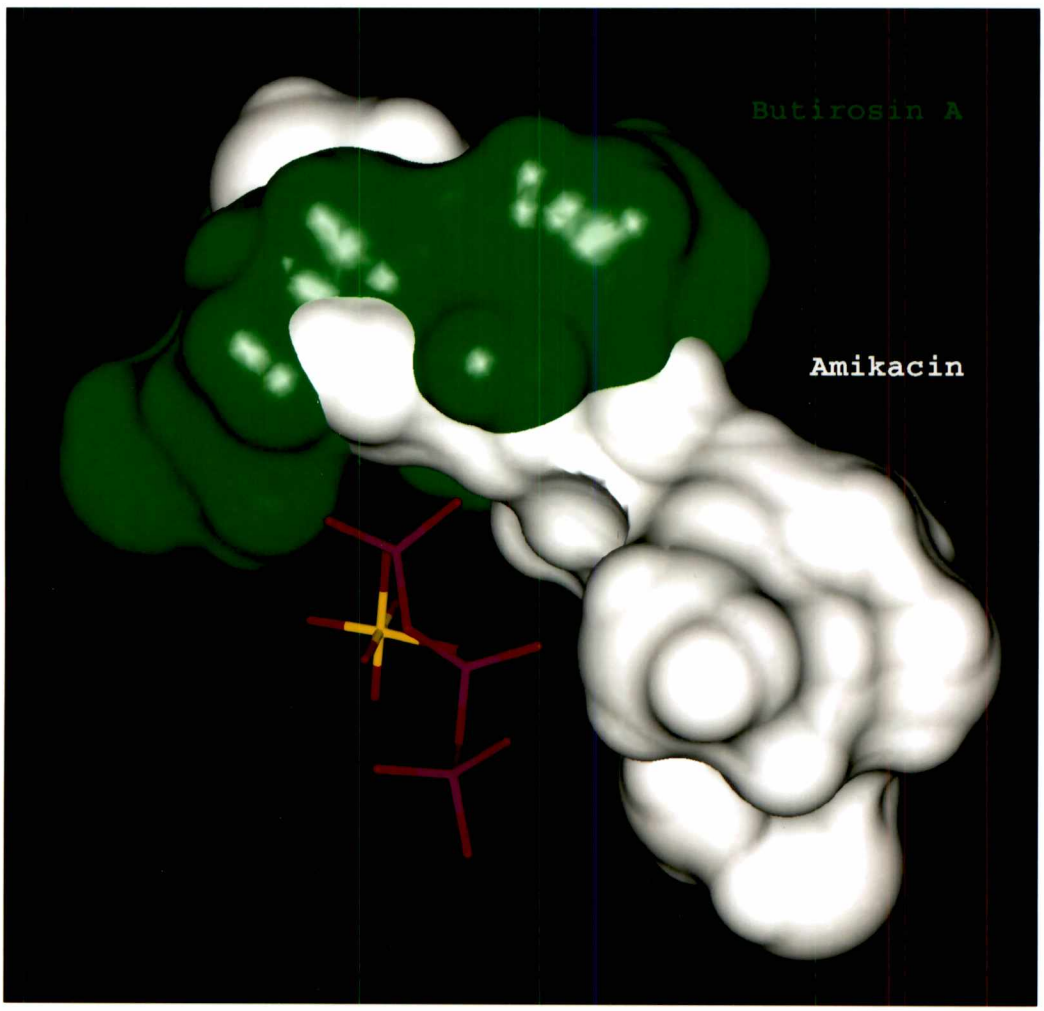
Butirosin A
Amikacin

Figure IV-11. The superimposed arrangements presented in Figure IV-10 without the solvent surfaces and only the nitrogens and oxygens of particular amino and hydroxyl groups presented as balls. The color of the label denotes whether an atom belongs to amikacin (white) or butirosin A (green).

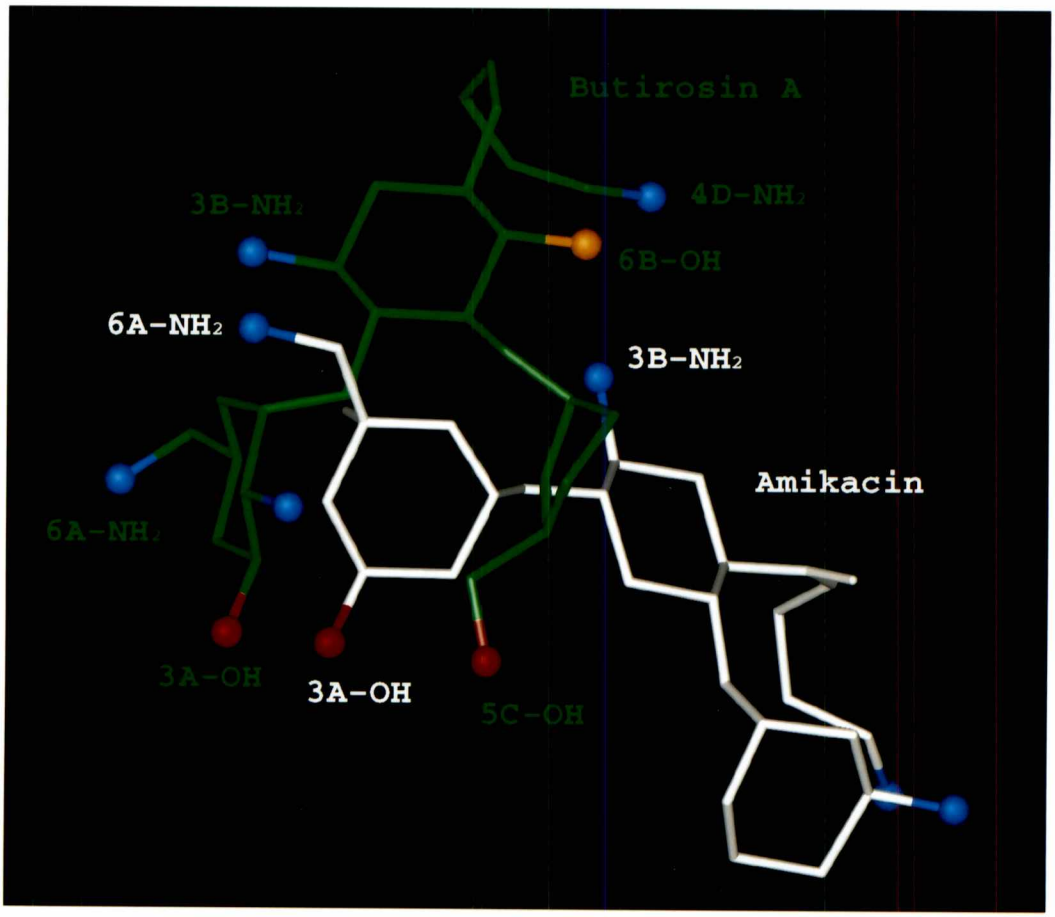
Butirosin A
3B-NH2
4D-NH2
6B-OH
6A-NH2
3B-NH2
Amikacin
6A-NH2
3A-OH
3A-OH
5C-OH

$$E_{pot} = \sum_{b} K_b(b-b_o)^2 + \sum_{\theta} H_\theta(\theta-\theta_o)^2 + \sum_{\phi} \frac{V_n}{2}[1 + \cos(n\phi-\phi_o)^2$$

$$+ \sum \varepsilon[(r^*/r)^{12}-2(r^*/r)^6] + \sum \frac{q_i q_j}{\varepsilon_{ij} r_{ij}} + \sum \left[\frac{C_{ij}}{r_{ij}^{12}} - \frac{D_{ij}}{r_{ij}^{10}}\right] \qquad \text{Eq. V-1}$$

Figure V-1. The potential energy function (E_{pot}) utilized in the AMBER forcefield. The various terms are described in the "Introduction" section of Chapter V.

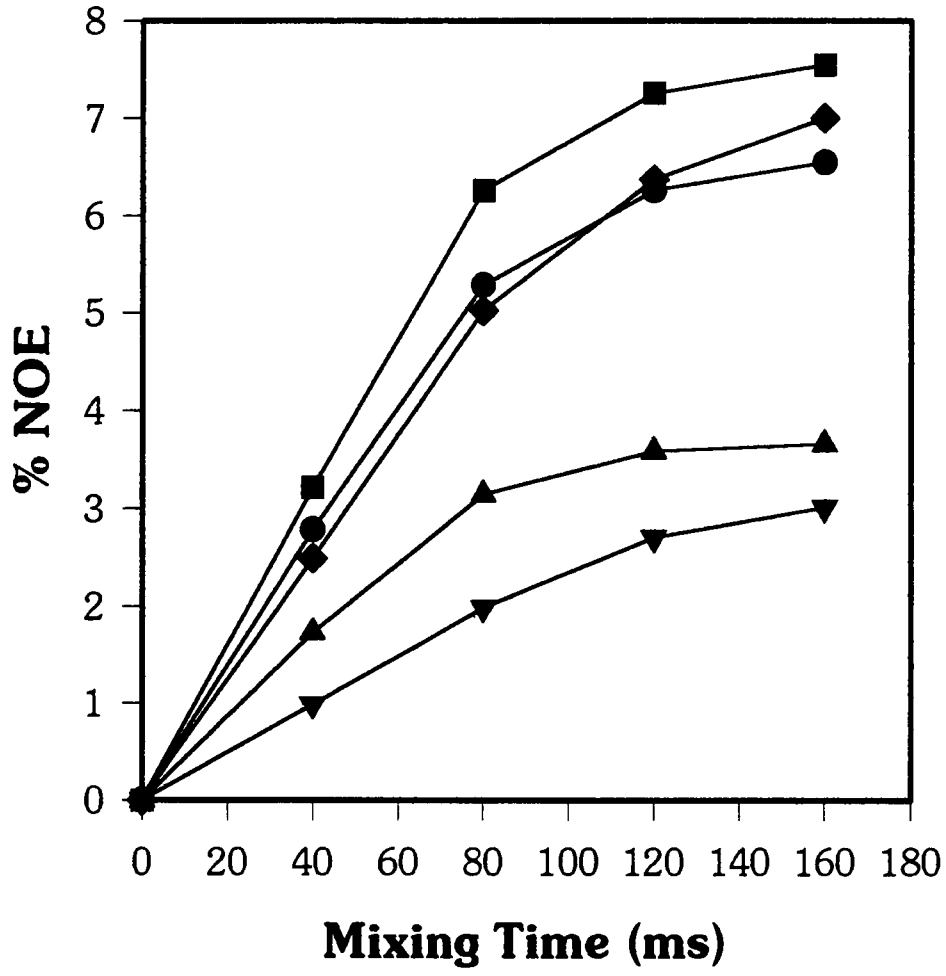

Figure V-2. %NOE buildup curves for various proton pairs of butirosin A. The following pairs are shown: H3′-H5″ (■), H2e-H1(♦), H1′-H4 (●), H1″-H2″ (▲), and H1′-H3 (▼). %NOE values were calculated by taking the ratio of the cross-peak volume of the NOE of interest to the volume of the H3‴-H3‴ cross-peak, at each mixing time, and multiplying by a 100.

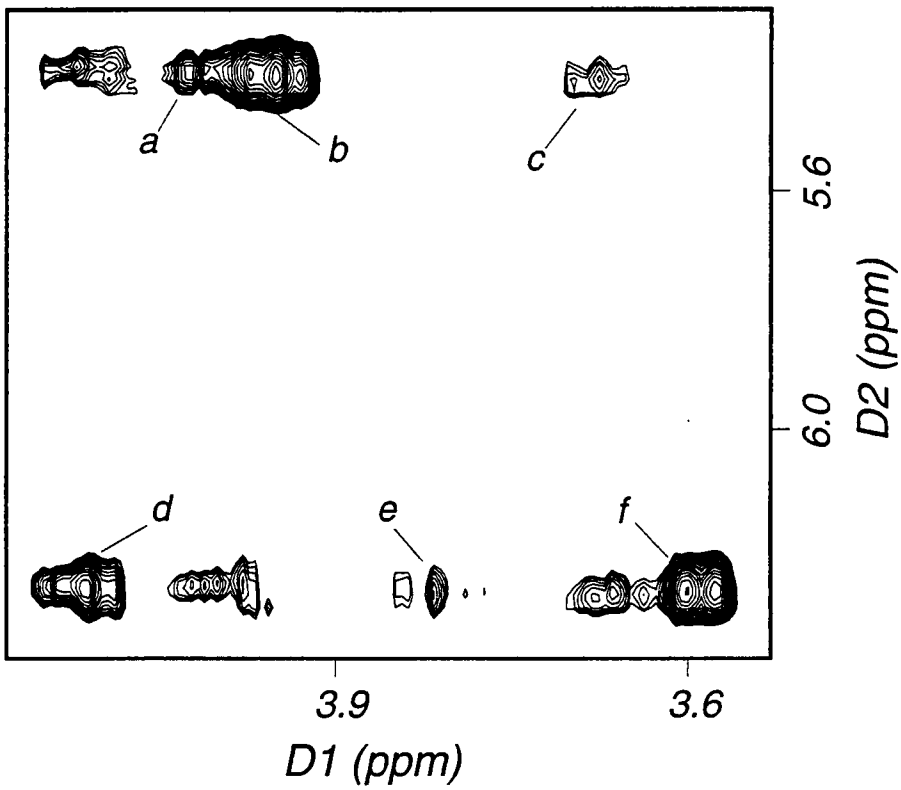

Figure V-3. Portion of the TRNOE spectrum (80 ms) of butirosin A. The cross-peaks labeled are H1″-H1 (a), H1″-H5 (b), H1″-H6 (c), H1′-H4 (d), H1′-H5″ (e), and H1′-H3 (f). The samples for the TRNOE spectroscopy contained 0.20 mM APH(3′)-IIIa, 5 mM butirosin A, 5 mM ATP, 5 mM $CaCl_2$, and 20 mM Tris-d_{11} buffer (pH 6.8).

Figure V-4. Representation of the APH(3′)-IIIa-bound conformations of butirosin A. These structures were obtained from restrained energy minimization and molecular dynamics as described in the "Experimental Section" of Chapter V. The structures have been superimposed at ring B.

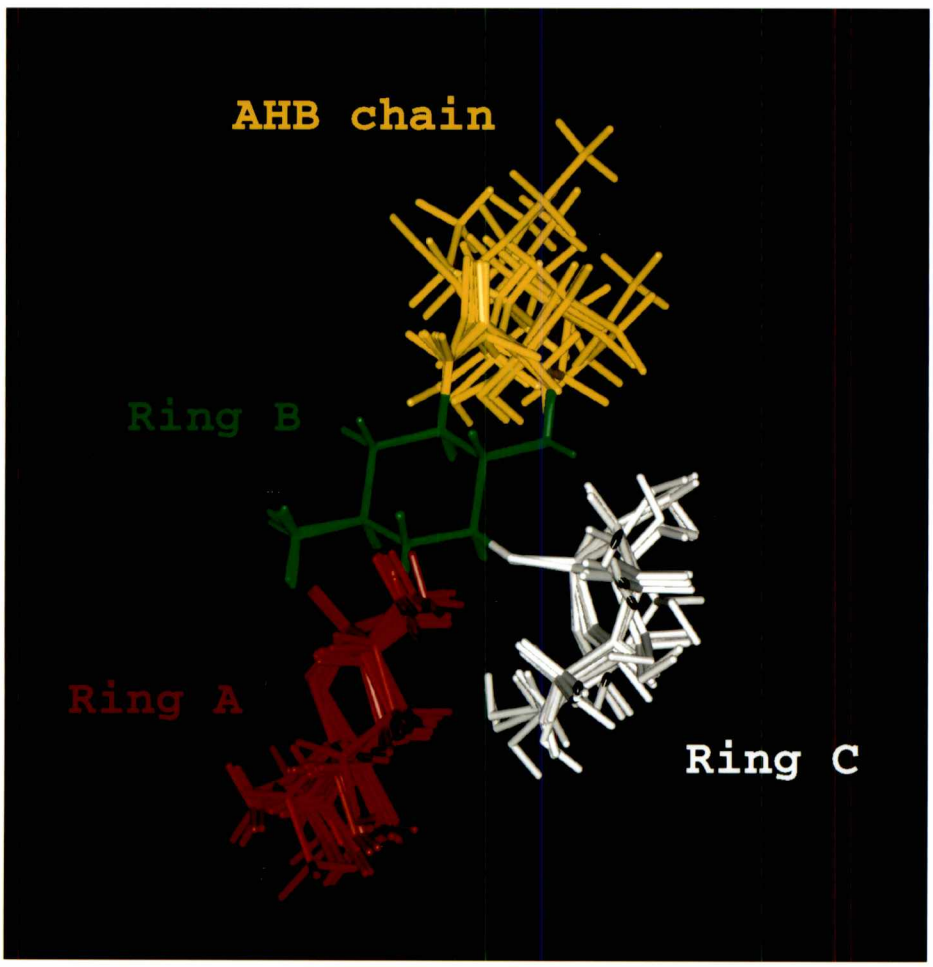
AHB chain
Ring B
Ring A
Ring C

Figure V-5. Superimposed structures (at ring B) of APH(3′)-IIIa-bound butirosin A with only the ring atoms and the 3′(3A)- and 5″(5C)-oxygens (balled) shown. Part A shows the front view of the structures, while part B shows a side view to demonstrate ring stacking.

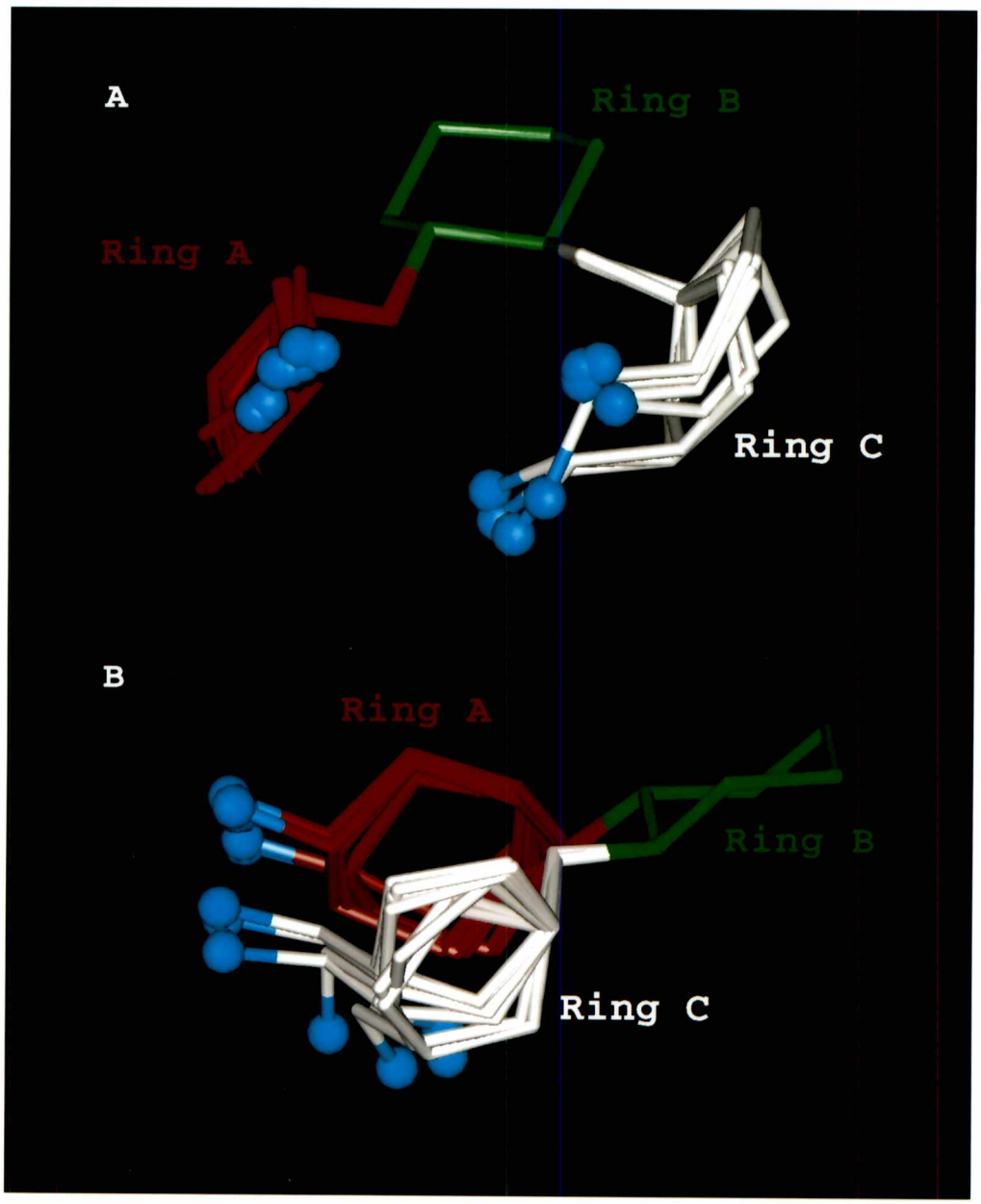
A
Ring B
Ring A
Ring C
B
Ring A
Ring B
Ring C

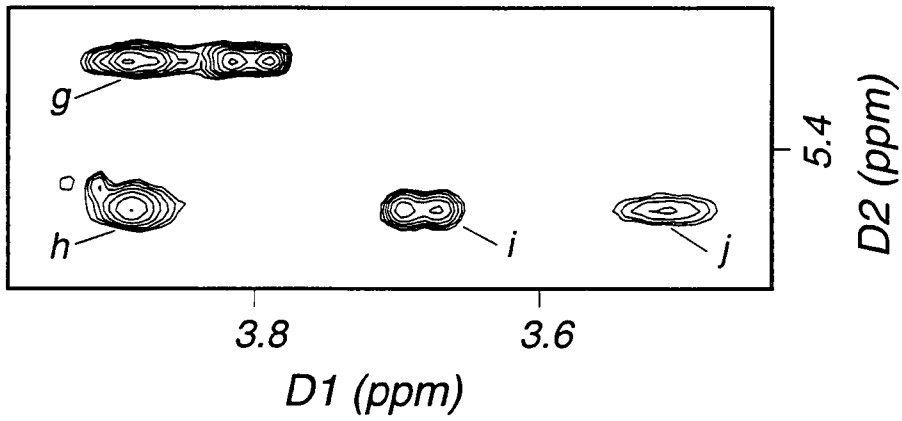

Figure V-6. Portion of the TRNOE spectrum (80 ms) of amikacin. The cross-peaks labelled in the amikacin spectrum are H1″-H5/H1″-H6 (g), H1′-H5/H1′-H3′ (h), H1′-H4 (i), H1′-H3 (j). The samples for the TRNOE spectroscopy contained 0.20 mM APH(3′)-IIIa, 5 mM amikacin, 5 mM ATP, 5 mM $CaCl_2$, and 20 mM Tris-d_{11} buffer (pH 6.8).

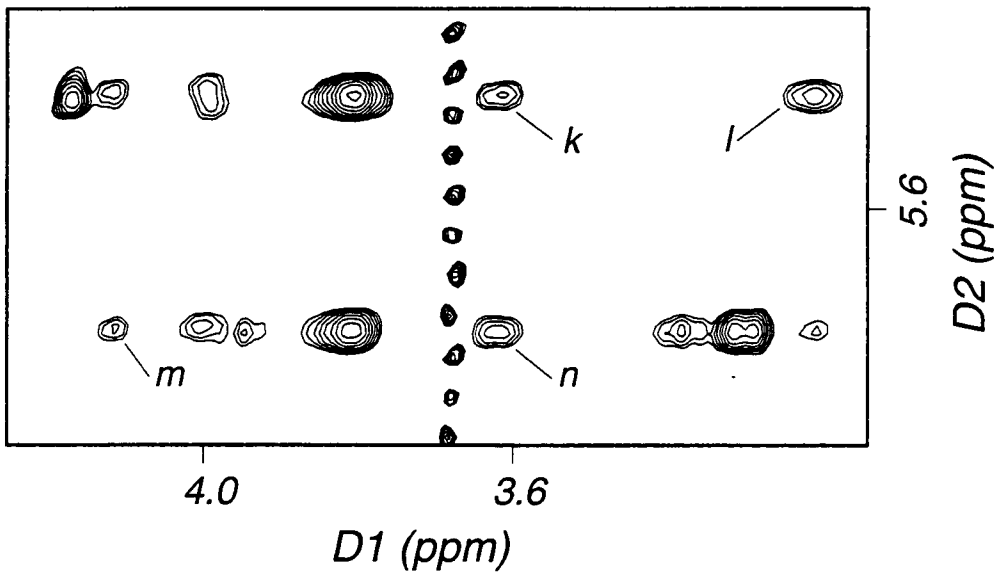

Figure V-7. Portion of the TRNOE spectrum (90 ms) of ribostamycin. The cross-peaks labeled are: H1″-H6 (k), H1″-H1 (l), H1′-H3″ (m), and H1′-H5″ (n). The samples for the TRNOE spectroscopy contained 0.20 mM APH(3′)-IIIa, 5 mM ribostamycin, 5 mM ATP, 5 mM $CaCl_2$, and 20 mM Tris-d_{11} buffer (pH 6.8).

Figure V-8. Representative structures of the two major conformers (1 and 2) of APH(3′)-IIIa-bound ribostamycin. These conformers are each a representative structure of six conformations that were derived from the modeling studies. The yellow dashed lines represent potential H-bonds.

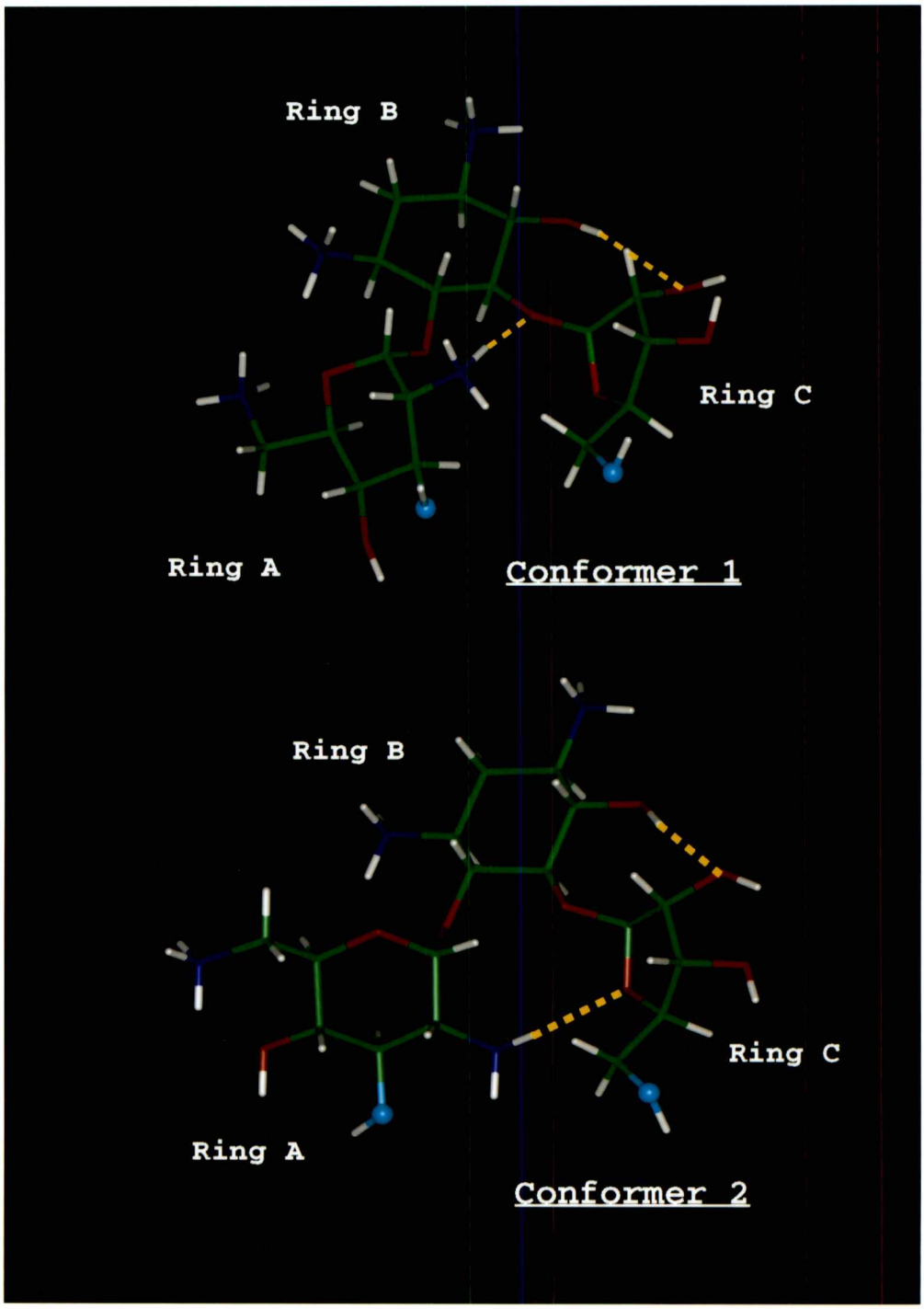
Ring B
Ring C
Ring A
Conformer 1
Ring B
Ring C
Ring A
Conformer 2

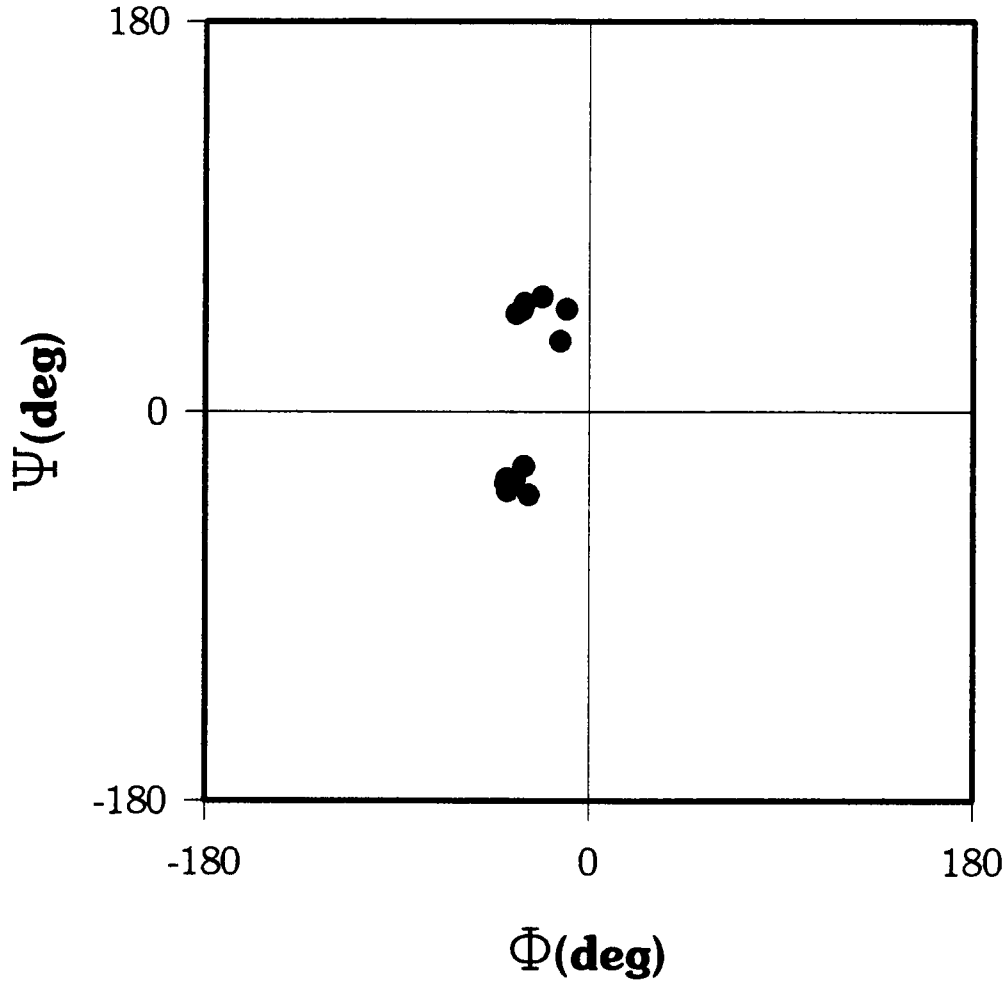

Figure V-9. A Φ vs. Ψ plot describing the nature of the α-glycosidic bond between the primed (ring A) and unprimed ring (ring B) in the APH(3′)-IIIa-bound ribostamycin structures. The Φ dihedral angle is defined by H1′-C1′-O_α-C4 and the Ψ dihedral angle is defined by H4-C4-O_α-C1′. The set of data points in the top left quadrant represents Φ_5 and Ψ_5 values and the data points in the bottom left quadrant represents Φ_3 and Ψ_3 values, as described in the text.

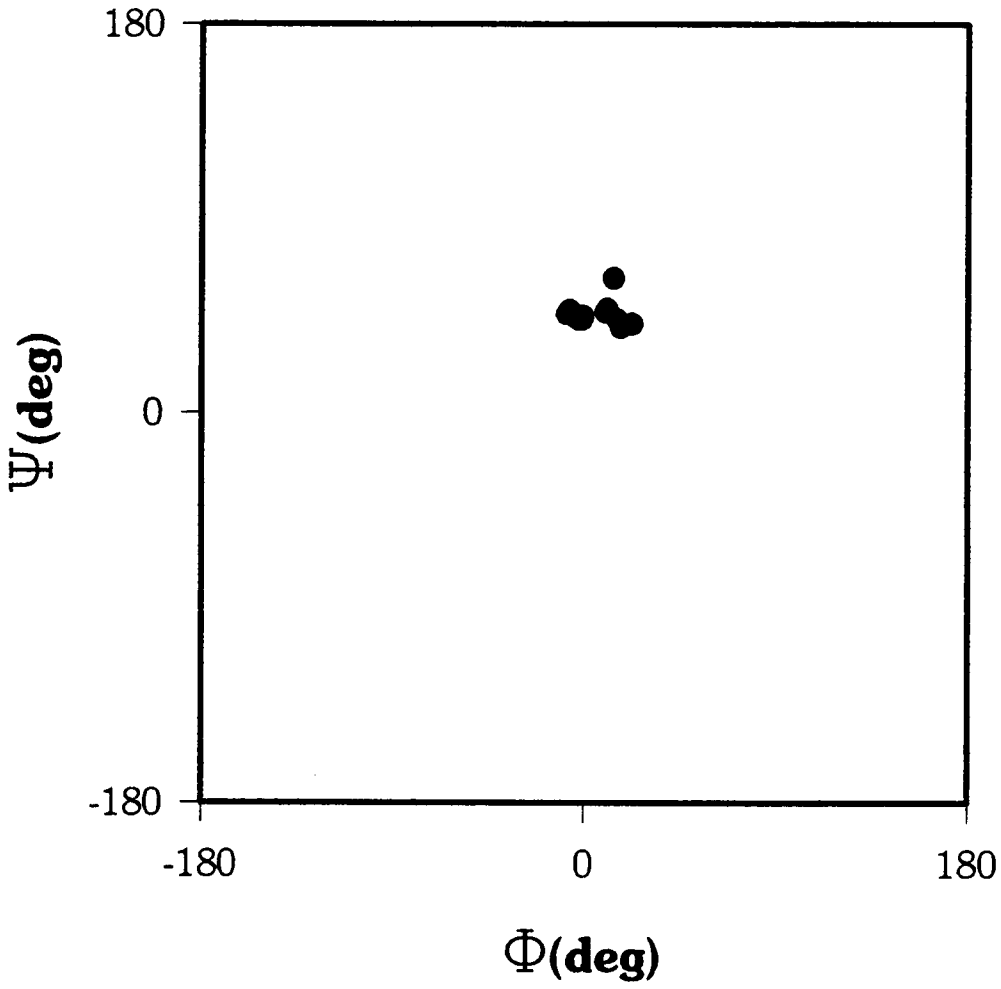

Figure V-10. A Φ vs. Ψ plot describing the nature of the β-glycosidic bond between the double-primed (ring C) and unprimed ring (ring B) in the APH(3′)-IIIa-bound ribostamycin structures.. The Φ dihedral angle is defined by H1″-C1″-O_β-C5 and the Ψ dihedral angle is defined by H5-C5-O_β-C1″. The data points represents both $\Phi_{4/6}$ and $\Psi_{4/6}$ values.

Figure V-11. Representative examples of the two major conformers (1 and 2) of ribostamycin superimposed at ring B. Part B shows only the ring atoms to demonstrate the orientation of rings A and C.

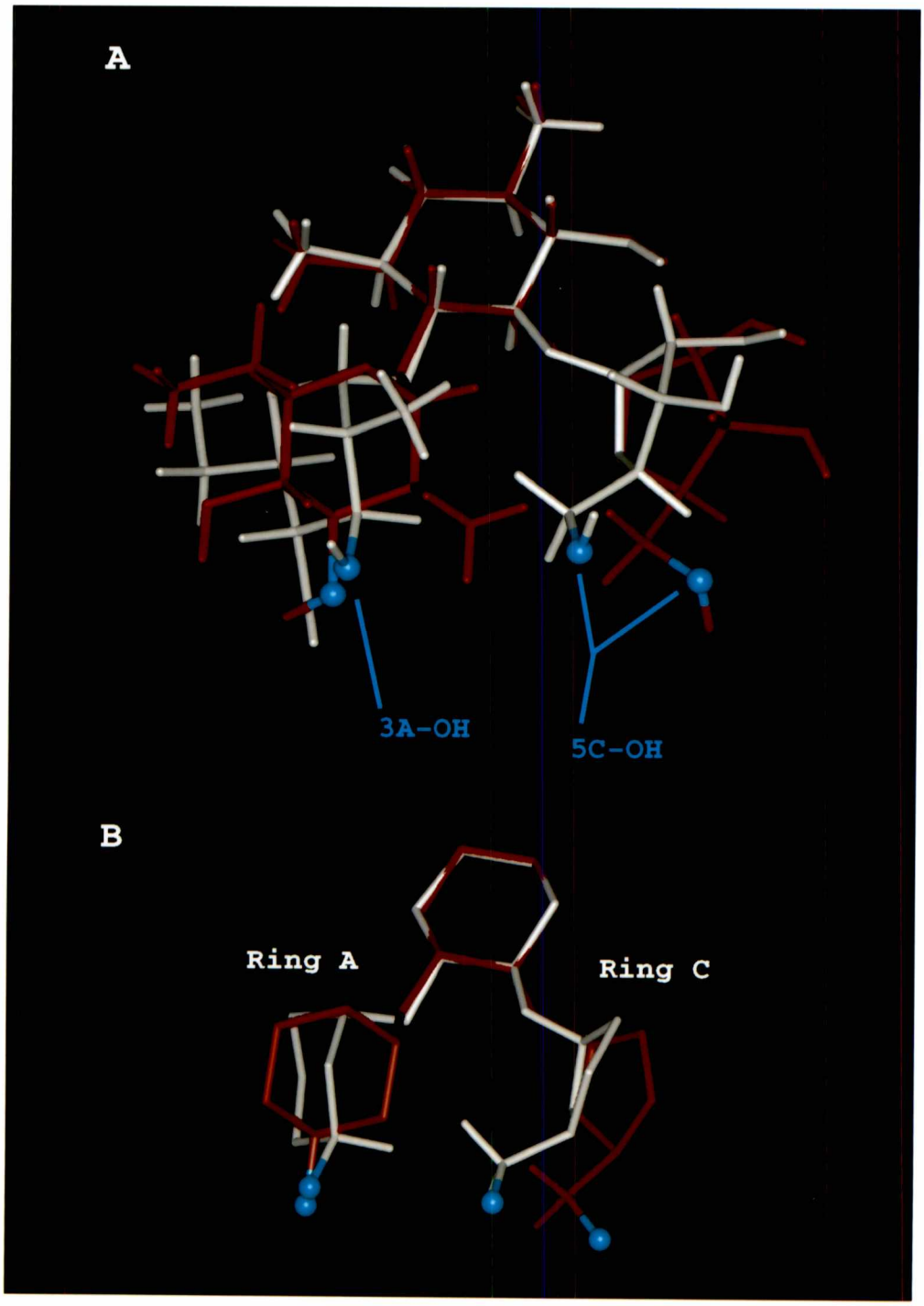
A
3A-OH
5C-OH
B
Ring A
Ring C

Figure V-12. The structures of aminoglycosides bound to APH(3′)-IIIa and rRNA. (A) The structure of a paromomycin•rRNA complex recently determined by NMR (Fourmy *et al.*, 1996). The paromomycin molecule is represented by orange balls. The coordinates were kindly provided by Dr. Joseph Puglisi. (B) Conformer 2 of ribostamycin (magenta) and paromomycin (orange), of the paromomycin•rRNA complex, are superimposed at ring B. In (B), the ball represents the position of ring D of paromomycin.

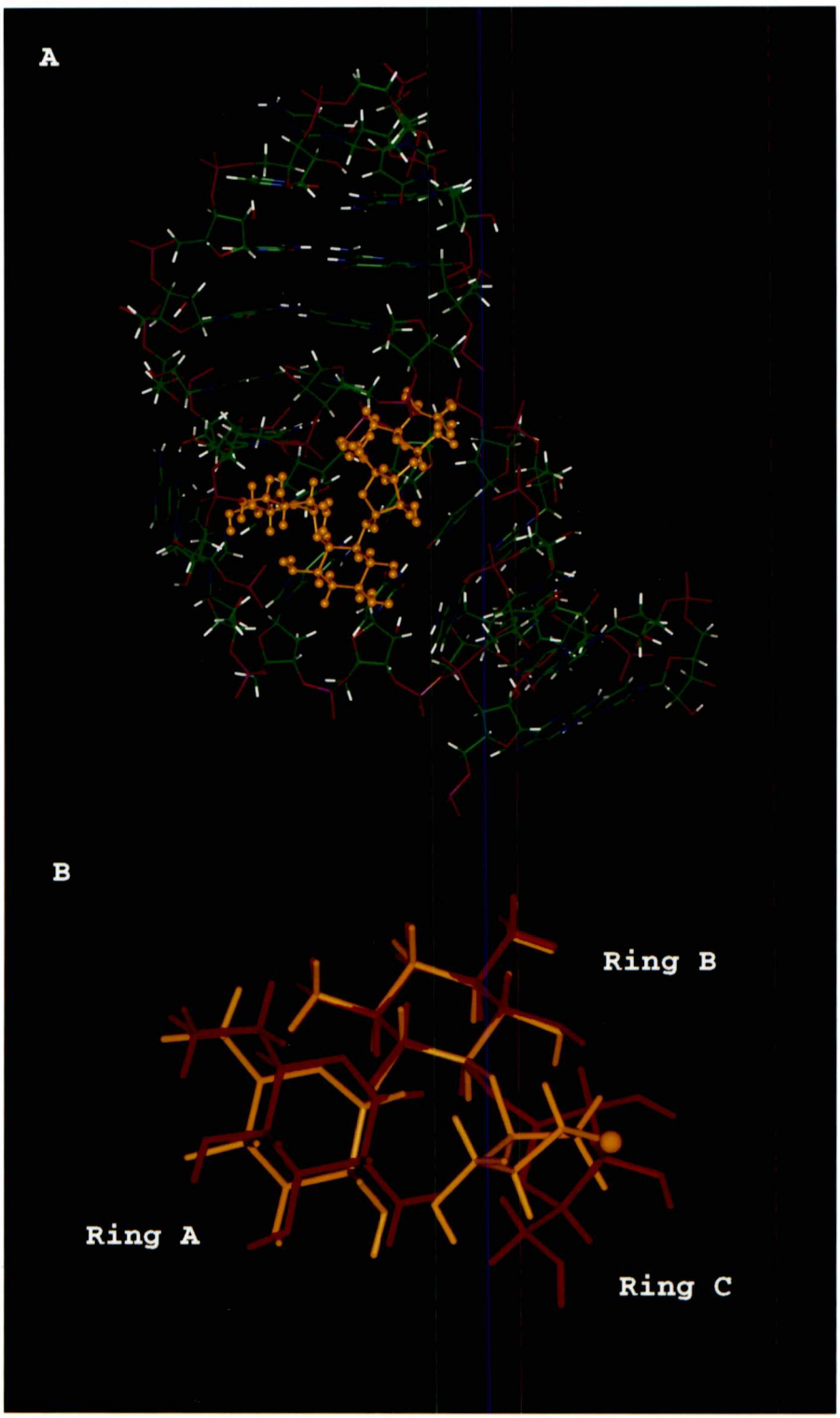
A
B
Ring B
Ring A
Ring C

Appendix B

Tables

Table II-1. ^{1}H NMR Chemical Shifts (δ values) of Kanamycin A[a,b].

Proton[c]	Ring A	Ring B	Ring C
H-1	5.49	3.16	5.04
H-2	3.59	1.43 (ax)	3.67
	----	2.18 (eq)	----
H-3	3.72	3.06	3.18
H-4	3.32	3.49	3.46
H-5	3.96	3.69	3.90
H-6	3.36	3.42	3.76
	3.10	----	----

[a] The chemical shifts are in ppm, relative to DSS.

[b] Ring A is the primed ring, ring B is the unprimed ring, and ring C is the double primed ring.

[c] Coupling constants: $^3J_{1'-2'}$ = 3.8 Hz, $^3J_{3'-4'}$ = 9.7 Hz, $^3J_{5'-6'}$ = 5.2 Hz and 3.2 Hz, $^3J_{6'-6'}$ = 8.1 Hz, $^3J_{1-2a}$ = 12.0 Hz, $^3J_{1-2e}$ = 4.1 Hz, $^3J_{1-6}$ = 9.4 Hz, $^2J_{2a-2e}$ = 12.6 Hz, $^3J_{2a-3}$ = 10.1 Hz, $^3J_{2e-3}$ = 3.6 Hz, $^3J_{4-5}$ = 9.8 Hz, $^3J_{1''-2''}$ = 3.7 Hz, $^3J_{2''-3''}$ = 10.5 Hz, $^3J_{4''-5''}$ =10.0 Hz, $^3J_{5''-6''}$ = 2.2 Hz, and $^3J_{6''-6''}$ = 9.0 Hz.

Table II-2. ^{1}H NMR Chemical Shifts (δ values) of Kanamycin B[a,b].

Proton[c]	Ring A	Ring B	Ring C
H-1	5.80	3.45	5.09
H-2	3.28	1.77 (ax)	3.86
	----	2.33 (eq)	----
H-3	3.89	3.28	3.40
H-4	3.38	3.78	3.63
H-5	3.98	3.80	3.91
H-6	3.42	3.71	3.77
	3.17	----	----

[a] The chemical shifts are in ppm, relative to DSS.

[b] Ring A is the primed ring, ring B is the unprimed ring, and ring C is the double primed ring.

[c] Coupling constants: $^3J_{1'-2'}$ = 4.2 Hz, $^3J_{3'-4'}$ = 9.3 Hz, $^3J_{6'-6'}$ = 8.6 Hz, $^3J_{1-2a}$ = 12.0 Hz, $^3J_{1-2e}$ = 4.4 Hz, $^3J_{1-6}$ = 9.2 Hz, $^2J_{2a-2e}$ = 12.8 Hz, $^3J_{2a-3}$ = 10.1 Hz, $^3J_{1''-2''}$ = 3.8 Hz, $^3J_{4''-5''}$ =10.3 Hz, $^3J_{5''-6''}$ = 4.9 Hz, and $^3J_{6''-6''}$ = 9.2 Hz.

Table II-3. ^{1}H NMR Chemical Shifts (δ values) of Butirosin A[a,b].

Proton[c]	Ring A	Ring B	Ring C	AHB chain
H-1	6.15	3.90	5.33	---
H-2	3.41	1.83 (ax)	4.27	4.31
	----	2.20 (eq)	----	
H-3	4.06	3.45	4.17	1.99
	----	----	----	2.13
H-4	3.43	4.04	4.33	3.12
H-5	3.90	3.86	3.76	----
H-6	3.47	3.60	----	----
	3.21	----	----	----

[a] The chemical shifts are in ppm, relative to DSS.

[b] Ring A is the primed ring, ring B is the unprimed ring, and ring C is the double primed ring, and the AHB chain is denoted with a triple prime.

[c] Coupling constants: $^3J_{1'\text{-}2'}$ = 3.7 Hz, $^3J_{5'\text{-}6'}$ = 8.0 Hz, $^3J_{6'\text{-}6'}$ = 13.5 Hz, $^3J_{1\text{-}2a}$ = 12.2 Hz, $^3J_{1\text{-}2e}$ = 4.4 Hz, $^3J_{1\text{-}6}$ = 9.1 Hz, $^2J_{2a\text{-}2e}$ = 13.0 Hz, $^3J_{2a\text{-}3}$ = 10.1 Hz, $^3J_{2e\text{-}3}$ = 3.6 Hz, $^3J_{4\text{-}5}$ = 9.1 Hz, $^3J_{5\text{-}6}$ = 10.5 Hz, $^3J_{1''\text{-}2''}$ = 0.0 Hz, $^3J_{4''\text{-}5''}$ = 8.2 Hz, $^3J_{5''\text{-}5''}$ = 12.0 Hz.

Table II-4. ^{15}N Assignments of Butirosin A (pH 5.90) and Ribostamycin (pH 6.30)[a].

	Butirosin A	Ribostamycin
Nitrogen	Chemical Shift (δ, ppm)	
N-1[b]	99.3	16.7
N-3	16.6	15.6
N-2′	11.3	11.9
N-6′	4.02	5.7
N-4‴	10.01	

[a]All chemical shift values have been referenced to $^{15}NH_4Cl$ in 85:15 (v/v) H_2O:^2H_2O.

[b]The assignments of N-1 and N-3 may be interchanged.

Table II-5. pK_a Values[a] of the Amino Groups of Amikacin, Butirosin A, and Ribostamycin.

	pK_a		
Amino Group Nitrogen	Amikacin	Butirosin A	Ribostamycin
N-1			6.87± 0.08
N-3	7.62 ± 0.04	7.40 ± 0.05	7.57 ± 0.13
N-2′		9.11 ± 0.08	7.80 ± 0.06
N-6′	8.92 ± 0.03	9.37 ± 0.14	8.00 ± 0.02
N-3″	9.70 ± 0.09		
N-4‴	8.13 ± 0.07	8.56 ± 0.04	

[a] Midpoints of the titration curves of ^{15}N chemical shifts vs. pH.

Table III-1. Dissociation Constants (mM) and the Enhancement Values (ε_T) of the APH(3′)-IIIa•CrATP•Antibiotic Complexes.

Constant[a,b,c]	Amikacin	Butirosin A
K_D	0.238	0.238
K_1	11.8	14.0
K_S	0.591	0.056
K_A'	0.106	0.106
K_3	0.263	0.025
K_2	0.005	0.0004
ε_T	2.78	2.23

[a]Binary dissociation constants are:

$K_D = [CrATP]_f [APH(3')\text{-}IIIa]_f / [APH(3')\text{-}IIIa \bullet CrATP]$

$K_S = [Antibiotic]_f [APH(3')\text{-}IIIa]_f / [APH(3')\text{-}IIIa \bullet Antibiotic]$

$K_1 = [CrATP]_f [Antibiotic]_f / [CrATP \bullet Antibiotic]$

[b]Ternary dissociation constants are:

$K_A' = [CrATP]_f [APH(3')\text{-}IIIa \bullet Antibiotic] / [APH(3')\text{-}IIIa \bullet CrATP \bullet Antibiotic]$

$K_2 = [APH(3')\text{-}IIIa]_f [CrATP \bullet Antibiotic] / [APH(3')\text{-}IIIa \bullet CrATP \bullet Antibiotic]$

$K_3 = [Antibiotic]_f [APH(3')\text{-}IIIa \bullet CrATP] / [APH(3')\text{-}IIIa \bullet CrATP \bullet Antibiotic]$

[c]Note that $K_1 \bullet K_2 = K_3 \bullet K_D = K_A' \bullet K_S$

Table IV-1. Correlation Time and Other Parameters That Describe the Interaction of CrATP and APH(3′)-IIIa in the Ternary APH(3′)-IIIa•CrATP•Antibiotic Complexes.

Antibiotic	τ_c (s)[a]	$f(\tau_c)$ (s)	τ_v	B (s^{-2})
Amikacin	1.09×10^{-9}	3.85×10^{-10}	1.06×10^{-12}	1.58×10^{21}
Butirosin A	0.91×10^{-9}	4.39×10^{-10}	0.71×10^{-12}	1.50×10^{21}

[a]Determined from the frequency dependence of the longitudinal relaxation rates ($1/fT_{1p}$) of water protons at 90, 250, and 400 MHz and analyzed according to the equations (Mildvan & Gupta, 1978) $1/\tau_c \sim 1/\tau_s = B(\tau_v/(1+ \omega_s^2\tau_v^2) + 4\tau_v/(1 + 4\omega_s^2\tau_v^2))$ and $f(\tau_c) = 3\tau_c/(1 + \omega_I^2\tau_c^2) + 7\tau_c/(1 + \omega_s^2\tau_c)$ where τ_c is the dipolar correlation time, τ_s is the longitudinal electron spin relaxation time, B is the zero field splitting parameter, τ_v is a time constant for ligand motion that modulates B, and ω_s and ω_I are the electron and nuclear presession frequencies, respectively,. The correlation times shown above are from the best fitted curve to the $1/fT_{1p}$ values determined at each frequency. The values for B and τ_v were obtained from the least squares fitting.

Table IV-2. Corrected Relaxation Rates and Cr^{3+}-to-^1H Distances in the APH(3′)-IIIa•CrATP•Antibiotic Complexes.

	Amikacin		Butirosin A	
Proton	$1/fT_{1p}$ (s^{-1})[a]	Distance (Å)[b]	$1/fT_{1p}$ (s^{-1})	Distance (Å)
2a	194	7.90 ± 0.58	-------[c]	>11
6			25	11.4 ± 0.84
1′	730	6.34 ± 0.47	175	8.22 ± 0.61
6′			225	7.88 ± 0.64
1″	223	7.72 ± 0.57	100	9.02 ± 0.67
3″			100	9.02 ± 0.67
2‴	421	6.95 ± 0.51		
3‴	447	6.88 ± 0.51	124	8.70 ± 0.64
4‴			112	8.85 ± 0.65

[a]The normalized reaction rates ($1/fT_{1p}$) were determined from the slope of the lines shown in Figures IV-6 and IV-7.

[b]The errors shown in the absolute distances include 10%, 8%, and 30% due to the experimental errors in the measurements of $1/fT_{1p}$, τ_c, and the dissociation constant of CrATP from the ternary complex, respectively.

[c]A correction of the relaxation rate due to the binary contribution was not possible due to the high relaxation rate of this proton in the binary CrATP•antibiotic complex.

Table V-1. Inter-ring/chain TRNOEs for Butirosin A in the 80 ms TRNOESY Spectrum and the Calculated Distance Restraints[a].

TRNOE	lower limit (Å)[b]	upper limit (Å)
H1′-H3	3.2	3.7
H1′-H4	2.5	2.8
H1′-H5″[c]	4.1	4.5
H2′-H5″	3.8	4.4
H3′-H5″	2.3	2.6
H5′-H5″	3.4	3.9
H1″-H1	3.7	4.1
H1″-H5	2.2	2.5
H1″-H6	3.1	3.6
H2‴-H1	2.7	3.1

[a] The distances were calculated from the isolated spin pair approximation with the H1′-H2′ proton pair taken as the calibration distance (r = 2.38 Å).

[b] A generous error of ±40% was used for the intensities of the TRNOEs in order to calculate the distance restraints.

[c] All restraints involving H-5″ were assigned to the *pro*-S hydrogen.

Table V-2. Inter-ring TRNOEs for Ribostamycin in the 90 ms TRNOESY Spectrum and the Calculated Distance Restraints[a].

TRNOE	lower limit (Å)[b]	upper limit (Å)
H1′-H3	3.9	4.4
H1′-H4	2.2	2.5
H1′-H5	3.7	4.3
H1′-H3″	4.3	4.9
H1′-H5″[c]	3.5	4.1
H2′-H5″	3.8	4.4
H1″-H1	3.1	3.6
H1″-H5	2.0	2.3
H1″-H6	3.4	3.9

[a] The distances were calculated from the isolated spin pair approximation with the H1′-H2′ proton pair taken as the calibration distance (r = 2.38 Å).

[b] A generous error of ±40% was used for the intensities of the NOEs in order to calculate the distance restraints.

[c] All restraints involving H-5″ were assigned to the *pro*-S hydrogen.

VITA

James Richard Cox was born on May 30th, 1968. He grew up in Paris, TN where he graduated from Henry County High School in 1986. Following high school, he attended the University of Tennessee at Martin where he obtained a B. S. degree in Chemistry in 1990 (*summa cum laude*). He then entered Murray State University and obtained a M. S. in Chemistry in 1992. He was a chemistry instructor at both the University of Tennessee at Martin and Murray State University during the 1992-1993 school year.

On August 6, 1993 he married Amy Lynne Walker and they moved to Knoxville, Tennessee where he started graduate work at The University of Tennessee, in the Department of Biochemistry. He was fortunate to have won the Hilton A. Smith Graduate Fellowship, Alexander Hollaender Graduate Fellowship, Science Alliance Award, Graduate Student Award for Excellence in Teaching and Research in the BCMB department, and an Outstanding Graduate Student Award for a Student Majoring in Biochemistry from the American Institute of Chemists Foundation. He completed his Ph.D. in Biochemistry under the direction of Dr. Engin Serpersu in August 1997. He presented his work at several meetings and published several abstracts and manuscripts (next page).

Publications

Cox, J.R. and Serpersu, E.H. (1997) "Biologically Important Conformations of Aminoglycoside Antibiotics Bound to an Aminoglycoside 3′-Phosphotransferase as Determined by Transferred Nuclear Overhauser Effect Spectroscopy" *Biochemistry* **36**, 2353-2359.

Cox, J.R., McKay, G.A., Wright, G.D., and Serpersu, E.H. (1996) "Arrangement of Substrates at the Active Site of An Aminoglycoside Antibiotic 3'-Phosphotransferase As Determined by NMR" *J. Am. Chem. Soc.* **118**, 1295-1301.

Cox, J.R. and Serpersu, E.H. (1995) "The Complete ^{1}H NMR Assignments of Aminoglycoside Antibiotics and Conformational Studies of Butirosin A Through the Use of 2D NMR Spectroscopy" *Carbohydr. Res.* **271**, 55-63.

Cox, J.R. and Serpersu, E.H. "The Conformations of Ribostamycin Bound to An Aminoglycoside Antibiotic 3′-Phosphotransferase (APH(3′)-IIIa) is Similar to Other APH(3′)-IIIa- and RNA-Bound Aminoglycosides, manuscript (Communication to the Editor) submitted to the *Journal of the American Chemical Society*.

Mohler, M.L., Cox, J.R., and Serpersu, E.H. "Conformation of Lividomycin A Bound to an Aminoglycoside-Modifying Enzyme" in press, *Carbohydrate Letters*.

Published Abstracts

Mohler, M., Cox, J.R., and Serpersu, E.H. (1996) "The Conformation of Lividomycin A at the Active Site of An Antibiotic Modifying Enzyme" *Biochemistry* **35**, 9287. Poster presented at the national meeting of the American Chemical Society in Orlando, FL (August, 1996).

Cox, J.R., McKay, G.A., Wright, G.D., and Serpersu, E.H. (1995) "Arrangement of Substrates at the Active Site of An Aminoglycoside Antibiotic 3'-Phosphotransferase (APH(3′)-IIIa)" *FASEB J.* **9**, A1340. Poster presented at the American Society for Biochemistry and Molecular Biology/Division of Biological Chemistry-American Chemical Society joint meeting in San Francisco, CA (May, 1995).

Cox, J.R. & Volp, R. F. (1993) "Liver Microsomal Lipid Peroxidation Induced by Chloropropanes" *Toxicologist* **13**, 335. Poster presented at the Society of Toxicology meeting in New Orleans, LA (March, 1993).